MODELING HEAT REJECTION IN HORIZONTAL SMOOTH ROUND TUBES AND EXPERIMENTAL VALIDATION FOR R1234ze(E), R134a AND R32

BY

RAHUL AGARWAL

THESIS

Submitted in partial fulfillment of the requirements
for the degree of Master of Science in Mechanical Engineering
in the Graduate College of the
University of Illinois at Urbana-Champaign, 2013

Urbana, Illinois

Adviser:

Professor Predrag S. Hrnjak

ABSTRACT

Heat transfer in condensers is typically divided into 3 zones: superheated, two-phase and sub cooled region. These regions, in general, are considered to be independent of each other and various correlations are available in literature to predict the heat transfer coefficient (HTC) in these regions separately. These correlations, if plotted as a function of quality for the three regions, will show discontinuity at qualities of 0 and 1. The aim of the thesis is to bridge the discontinuity by establishing the interdependency of these regions and propose a unified model to predict HTC throughout the condensers. Experimental data suggests the HTC near x=1 in de-superheating region to be significantly higher than predictions due to presence of liquid when the wall temperature drops below saturation temperature. Similarly, HTC below x=0 has been seen to decrease linearly before following Gnielinski correlation due to presence of vapor as seen in sight glass at the end of test section. The newly proposed model takes into account the presence of liquid in de-superheating and sub-cooled liquid in two-phase zone. The model has been developed independently and compared to experimental data for R134a, R1234ze(E) and R32 for mass fluxes of 100-300 $kgm^{-2}s^{-1}$, saturation temperatures of 30 ^{0}C - 50 ^{0}C and from sub-cooling of 20 ^{0}C to superheat of 50 ^{0}C in a horizontal smooth tube with 6.1 mm inner diameter. Cavallini et al. (2006) and Gnielinski correlations have been used as a baseline correlation to calculate HTC in two-phase and single phase zone respectively. The model predicts the HTC satisfactorily within an accuracy of 16 %.

Another objective of the work is to form a baseline for the heat transfer characteristics in condensation for R1234ze(E) which can be a potential replacement in automotive systems for R134a on account of low GWP. The properties of R1234ze(E) is fairly well know to be close to R134a, however, the performance data under similar operating conditions as R134a is not widely published. To enhance the performance, the use of refrigerant mixture is also a possibility. Hence, R32 which is known to have higher heat transfer coefficient for its favorable thermo physical properties is a viable option to be considered as a mixture with R1234ze with a trade-off in GWP. Experiments conducted for R134a, R1234ze(E) and R32 at various mass fluxes, saturation temperature and heat fluxes helps in analyzing the effect of various parameters on heat transfer coefficient. The work in this thesis can be used as reference to study the effect of mixtures on heat transfer coefficient.

To my parents and my brother

ACKNOWLEDGEMENTS

It gives me immense pleasure to acknowledge the individuals who made this research possible. I would like to start by expressing my gratitude towards my adviser Professor Predrag S. Hrnjak for his constant support, guidance and motivation throughout the project. His insights and flexibility for a new approach helped me evolve as a researcher. I could not have imagined a better professor or a better person to be my adviser.

I would take this opportunity to thank my colleagues Huize Li, Han Fe, Augusto Zimmerman, Aravind Ramakrishnan, Bharath Budhiraja, Yang Zou, Shenghan Jin, Neal Lawrence, Melissa Meyers and Chieko Kondou who always helped my when I got stuck and made this journey a memorable one. A special mention goes to Rahul Kolekar whose expertise in experiments was of tremendous help. I would also like to thank all the sponsors of ACRC for their support and guidance in this project.

I would like to acknowledge the moral support of my friends Dinkar Nandwana, Arpit Agarwal, Rajavasanth Rajasegar, Subhabrata Banerjee and Ashwin Bhardwaj who encouraged me in trying times and ensured that I had friends whom I can count upon in the hour of need.

Last but not the least I would like to thank my parents and my brother for their love and support throughout my life. They have made me what I am today and I owe them everything I have done and will do in my life.

TABLE OF CONTENTS

LIST OF SYMBOLS

A	Surface area	$[m^2]$	J^T	Transition gas velocity	[-]
C_p	Specific heat capacity	$[Jkg^{-1}K^{-1}]$	$\dot{m}$	Mass flow rate	$[kgs^{-1}]$
d_i	Inner diameter of test tube	[m]	Nu	Nusselt number	[-]
f_b	Friction factor	[-]	P	Pressure	[Pa]
g	Gravitational acceleration	$[ms^{-2}]$	Pr	Prandtl number	[-]
G	Mass flux	$[kgm^{-2}s^{-1}]$	$\dot{Q}$	Heat transfer rate	[W]
GWP	Global Warming Potential	[-]	q	Heat flux	$[Wm^{-2}]$
h	Specific Enthalpy	$[Jkg^{-1}]$	Re	Reynolds number	[-]
Δh_{lv}	Latent heat	$[Jkg^{-1}]$	T	Temperature	$[^0C]$
HMFR	Heat Mass Flux Ratio	[-]	X	Vapor quality	[-]
HTC	See α	$[Wm^{-2}K^{-1}]$	X	Lockhart-Martinelli parameter	[-]
J	Dimensionless gas velocity	[-]	ΔZ	Cooling length of test tube	[m]

Greek Symbols

ρ	Density	$[kgm^{-3}]$
μ	Viscosity	[Pa.s]
λ	Thermal Conductivity	$[Wm^{-1}K^{-1}]$
σ	Surface Tension	$[Nm^{-1}]$
δ	Film thickness	[m]
θ	Angle	[rad]
ε	Void fraction	[-]
α	Heat Transfer Coefficient	$[Wm^{-2}s^{-1}]$

Subscripts

Air	Evaluated for air	PC	Pre cooler
b	Evaluated at bulk temperature	R	Refrigerant
cond	Conduction heat from test section	Sat	Evaluated at saturation temperature
f	Evaluated at film temperature	SC	Sub-cool
G	Gas phase	Sensible	Sensible heat
gain	Heat gain from ambient	SH	Superheat
H2O	Water	Strat	Fully stratified flow regime
i	Inlet	Total	Toal heat transfer
L	Liquid	TP	Two phase
Latent	Latent heat	TS	Test Section
LO	Liquid phase with total flow	Tt	Turbulent-turbulent
MC	Mixing chamber	V	Vapor
O	Outlet	W	Wall

CHAPTER 1
INTRODUCTION

1.1 Background

Heat transfer in condensers is usually modeled in the two-phase zone with various correlations predicting heat transfer coefficient as a function of quality. While there are abundant correlations to predict heat transfer in two phase zone, heat transfer coefficient (HTC) in single phase is predicted with fairly high accuracy with Dittus-Boelter and Gneillinski correlations assuming single phase turbulent conditions. These correlations, if plotted as a function of enthalpy shows discontinuity between single phase and two phase zones. This discontinuity arises because the models implicitly assume thermodynamic equilibrium during condensation which indicates that the first drop of condensate would form when bulk enthalpy of vapor reaches saturation enthalpy. Experimental studies have been conducted to prove that the heat transfer coefficient starts deviating from the predictions of single phase correlations when the wall temperature drops below saturation temperature and approaches the predictions of two-phase correlations when bulk enthalpy equals saturation enthalpy. The models proposed in literature also presume the temperature of liquid in two-phase zone to be saturation temperature due to which the two phase correlations do not asymptotically satisfy the single phase heat transfer data at qualities equal to 0. It has been shown experimentally that the liquid in two-phase zone is sub-cooled and there is a smooth transition of HTC from two-phase to single phase zone. A model has been proposed which takes both these phenomena into account to explain the transition from single phase to two phase zones and vice-versa.

As per the Kyoto protocol (11 December 1997) industries are striving towards replacing R134a with new refrigerants with low GWP which can reduce the carbon-dioxide emission in atmosphere. However, it is not possible to design entirely new systems for the new refrigerants owing to enormous cost associated with it. Hence, efforts have been made towards finding a refrigerant which can be used simply as a drop-in replacement for R134a which led to the discovery of two major refrigerants, R1234yf and R1234ze with properties very close to R134a. The research work deals with establishing baseline heat transfer performance for R1234ze(E) in condensers as the data available in literature currently is limited. The heat transfer coefficients of

R1234ze(E) are also compared to R134a to see the effect of replacement on the system. In order to increase the heat transfer coefficient in condensers R1234ze(E) can be mixed with R32 which has higher heat transfer coefficients because of its favorable thermo-physical properties. Hence, a baseline data for heat transfer has also been taken for R32 which can be used as a reference when compared to the mixture of R1234ze(E) and R32.

1.2 Literature Review:

1.2.1 Condensation in Superheated Zone

Heat transfer in condensers is usually modeled in the two-phase zone with various correlations predicting heat transfer coefficient as a function of quality. These models implicitly assume thermodynamic equilibrium during condensation which indicates that the first drop of condensate would form when bulk enthalpy of vapor reaches saturation enthalpy. This assumption has been proved to be incorrect as the phenomena of condensation in superheated zone has been known and accepted in literature for many years. The effect, however, has not been quantified by many. Kondou and Hrnjak (2012) identified the presence of condensation in superheated region for CO_2. They conducted experiments near critical point which magnified the importance of condensation in superheated zone since the latent heat is very small near critical pressure where even single phase correlations predict reality a bit better than two phase correlations for lower reduced pressures. The deviation from superheat was explained using von-Karman universal temperature profile which determined the magnitude of sub-cooling based on measured wall temperature. Kondou and Hrnjak (2011b) also conducted experiments with R410A and termed the region exhibiting condensation in superheated zone (SH) as Condensing Superheated Zone (CSH). The HTC in CSH zone was shown to be much higher compared to the prediction by Gnielinski correlation. The Kondo-Hrnjak correlation was then proposed based on the argument that the heat rejection in CSH zone is a combination of sensible and latent heat. The correlation was compared to experimental data for CO_2 and R410A at mass fluxes of 100-240 $kgm^{-2}s^{-1}$ and reduced pressure of .68-1.0 in horizontal tubes which showed satisfactory agreement. The criteria for beginning of condensation (Kondou and Hrnjak, 2011a) have been identified to be the point where wall temperature drops below saturation temperature of the refrigerant at corresponding operating condition. They determined the start of condensation to be

a strong function of heat flux arguing that greater heat flux results in lower wall temperature which leads to earlier establishment of the criteria for condensation. Lee et al. (1991) experimentally investigated condensation in superheated R22 vapor and proposed a model accounting the sensible heat rejected in condensation heat transfer. Akers et al. (1959) developed an in-tube condensation model with the help of equivalent Reynolds number. They defined an all liquid flow rate that gave same heat transfer coefficient as an annular condensing flow. Webb (1998) modified this model by expressing the HTC as a function of two-phase and single phase HTC with the inclusion of the F-factor which asymptotically approaches 0 to satisfy the boundary condition at x=1. Balekjian and Katz (1958) investigated film condensation of superheated vapor on horizontal tubes for water and R114. They looked into the temperature profile of refrigerant within the tube with both superheated vapor and liquid film existing simultaneously. They defined interfacial film coefficient to be a measure of condensation at the interface which was inversely proportional to the degree of superheat. A correlation was proposed based on theory of inter-phase mass and energy transfer but it was said that more experimental measurements are needed to thoroughly understand the phenomena occurring at interface.

1.2.2 Condensation in Two Phase Zone

Condensation heat transfer in two-phase zones has been modeled using various approaches. A few intensive literature reviews have also been conducted in this field owing to the vast number of correlations and experimental studies available. Among the reviews conducted those of Cavallini et al. (2003), Dalkilic and Wongwises (2009) and Xiaoyong et al. (2012) cover the research in this field comprehensively. Dobson and Chato (1998) conducted condensation experiments with R12, R22, R134a, R32/R125 mixture and compared the data to various correlations existing in literature. They found the Travis correlation to predict the data most accurately as the underlying assumptions like symmetric annular film, no entrainment of liquid into vapor core and extrapolation of the universal velocity profile from single phase flow to model their correlation do not affect the heat transfer data significantly. They modeled the correlation based on similar assumptions following the two phase multiplier approach and found the prediction to fit the experimental data points better than other correlations. The Dobson and Chato correlation predicted the experimental data of Dalkilic et al. (2009) fairly well which was

conducted with R134a at high mass flux in vertical smooth tube. They also established the HTC to be independent of the orientation of the tube in annular regime. Jung et al. (2003) conducted experiments with R32, R134a, R123, R22, R125, R142b on horizontal plain tubes with mass flux of 100-300 $kgm^{-2}s^{-1}$ and heat flux of 7.3-7.7 kWm^{-2}. Their data was consistently under predicted by Dobson & Chato (1998) at low quality and mass flux and over predicted at high mass flux and quality. So, they modified the Dobson-Chato correlation by including HMFR (Heat Mass Flux Ratio) through data regression analysis which gave a much better prediction. More physical models have been also made by taking into account the flow regimes at various qualities. Shah formulated a simple dimensionless correlation analytically for predicting heat transfer coefficients during film condensation (Shah, 1979) with wide variety of experimental data for water, R11, R12, R22, R113, methanol, ethanol, benzene, toluene and trichloroethylene for condensation in horizontal, vertical and inclined pipes of diameter from 7 to 40 mm. The correlation worked very well and works universally for refrigerants with reasonable accuracy except for highly turbulent flows. The correlation was therefore modified again to fit into a wider range of parameters (Shah, 2009). Thome et al. (2003) proposed a flow pattern map for condensation analogous to Kattan et al. (1998) and expressed heat transfer coefficient as a function of convective and nusselt film condensation. The film thickness and wetted perimeter of the tube were calculated as a function of flow regime identified through the flow pattern map. They were able to predict 80% of the data within the accuracy of ±20%. They pointed out that HTC would have higher unpredictability at very high and very low values due to poor energy balance. At high HTC values, the value of $(T_{sat}-T_w)$ and at low HTC the temperature difference across cooling water is fairly small which increases the uncertainty of the data. Kosky and staub (1971) proposed a correlation for calculating HTC in annular regime using Martinelli analogy between heat and momentum transfer with pressure drop as an independent source of information. Cavallini et al. (2006) proposed a simplified correlation for heat exchanger design where heat transfer coefficient is predicted through two basic equations which also take the flow regime into account. The model proves to be quite successful with variety of fluid under wide range of operating conditions. Cavallini et al. (2001) reported experimental data for R134a, R32 along with 3 other refrigerants for a mass flux of 100-750 $kgm^{-2}s^{-1}$, quality of .15-.85 and saturation temperature of 30-50 ^0C. The study provided a good comparison for the experimental data shown in this work as the refrigerants and operating conditions are fairly similar. They also

established the effect of quality, mass flux and saturation pressure on HTC and compared the data with model proposed by Kosky and staub (1971). Soliman (1986) identified the discrepancies in the prediction of experimental results for condensation at high qualities as most of the correlations do not take the mist flow regime into account. As the liquid is entrained into the vapor core at high qualities the film thickness decreases which results in increase in HTC which cannot be predicted using correlations based on annular flow regime. Hence, he proposed a correlation for mist flow but cautioned against using it in any other flow regime. Since, the experiments are not conducted with visualization this correlation has not been used in this work. The pressure drop data has also been taken in the experiment which is compared to the Friedel correlation (Friedel, 1979) which was developed to fit a huge database of 25,000 pressure drop data over a wide range of conditions. The model was fairly accurate having better fit than other existing model.

1.2.3 Condensation in Sub-Cooled Zone

The presence of sub-cooled liquid in two phase zone is usually neglected in modeling of HTC. Hence, very few studies have been conducted to quantify and analyze the sub-cooling of liquid film in two phase zone. Hashizume et al. (1992) analyzed the temperature profile of refrigerants near the exit of condensers at very low quality. They measured the temperature in adiabatic section at the exit of condensers and found the sub-cooling of approximately 10 ^{0}C and proposed a numerical model for condensation at vapor condensate surface. A model with unified correlation in condensers has been proposed in this work which takes the effect of condensation in de-superheating zone and sub-cooling in two phase zone to show the smooth transition of heat transfer coefficient from single to phase zones.

1.2.4 Condensation of R1234ze(E)

Since the discovery of R1234ze(E) the refrigerant has attracted lot of interests because of similar properties to R134a and a viable option of drop in replacement. The heat transfer properties have been measured experimentally by various researchers. Park et al. (2011) conducted condensation experiments with R134a and R1234ze(E) in vertical mini-channels of 1.45 mm hydraulic diameter at wide range of mass flux (260-500 kgm^{-2}s^{-1}), saturation temperature (25-70 ^{0}C) and heat flux (1-62 kWm^{-2}). They reported that the average heat transfer

of R1234ze(E) was 15-25 % lower than R134a on account of its thermo-physical properties. The existing correlation did not predict their data accurately, so they also proposed an improved correlation which had a good agreement with all the three fluids. Hossain et al. (2012) conducted experiments with R1234ze(E), R32 and R410A in horizontal tubes for mass flux of 100-450 $kgm^{-2}s^{-1}$, saturation temperature of 35-45 ^{0}C. They reported a reduction of 20-45 % heat transfer performance of R1234ze (E) compared to R32 and compared the data to various correlations with satisfactory agreement.

1.3 Research Objectives

The research work focuses on the condensation process covering entire range from superheated to sub-cooled refrigerant. Experiments have been conducted with three refrigerants to generalize the results and make a comparison. Overall the following research objectives were perused in the thesis:

- Validate the criteria of beginning of Condensation in Superheated zone.
- Analyze the effect of various parameters viz. mass flux, heat flux, saturation pressure on HTC.
- Compare the heat transfer performance in condensation for R134a, R1234ze(E) and R32.
- Analyze the effect of sub-cooling of liquid film on two phase condensation.
- Propose a unified model without discontinuity across single phase and two phase regions for HTC in condensation.

Overall a comprehensive study of condensation process with multiple objectives is shown which not only enriches the literature with experimental data of new refrigerant but also brings forward a novel approach for modeling of condensation from the first principles to bridge the discontinuity across various regions.

CHAPTER 2

MODELING OF HEAT TRANSFER IN CONDENSERS

A model has been proposed to unify the correlations in single phase and two phase zones for heat transfer coefficient in condensation. First the phenomena of condensation in different zones have been explained followed by mathematical formulation of heat rejection principle in condensation which facilitates the explanation of the proposed heat transfer model.

2.1 Conventional Approach in Modeling of Heat Rejection

Heat transfer models in condensers usually categorize the process in de-superheating (single phase, typically turbulent), two-phase condensation and sub-cooled (single phase, laminar or turbulent) zones. The HTC in these zones are calculated independently in the design of heat exchangers as shown in Fig. 2.1.

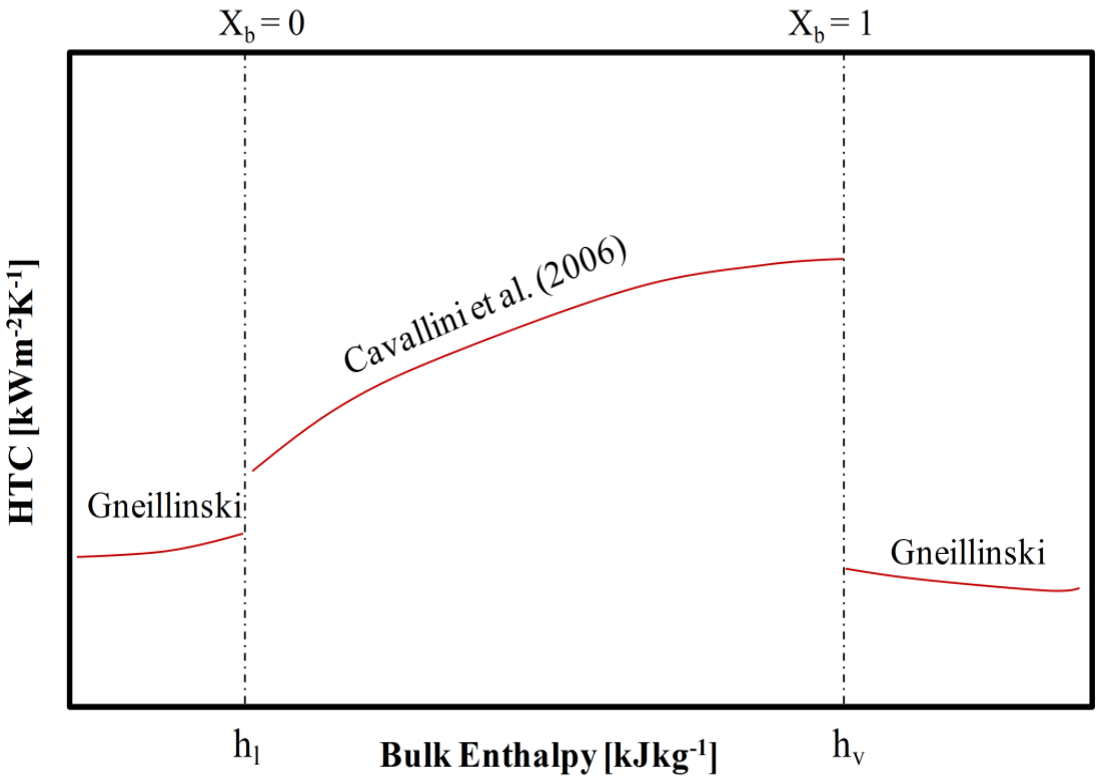

Figure 2.1: Conventional modeling of HTC

Condensation that occurs while bulk temperature is above saturation temperature is typically ignored. Kondo and Hrnjak in several publications discussed that non equilibrium process and provided data and model to account for such phenomena as shown in Fig. 2.2. Since condensation occurs at the liquid vapor interface the liquid film of refrigerant has to be sub-cooled during condensation. Existing models ignore the effect of sub-cooling which leads to discontinuity in HTC between condensing and sub-cooled zones. The proposed model re-categorizes the process of heat rejection by adding two more zones in the condensation process to take the effect of sub-cooled liquid film into account as shown in Fig. 2.3. We believe Fig. 2.4 represents the heat rejection process in condensers more realistically where condensation begins in superheated zone and vapor is present in the sub-cooled zone as well. The condensation zones have been explained in greater details below. Single phase heat rejection is treated in conventional way and is included in the model described later.

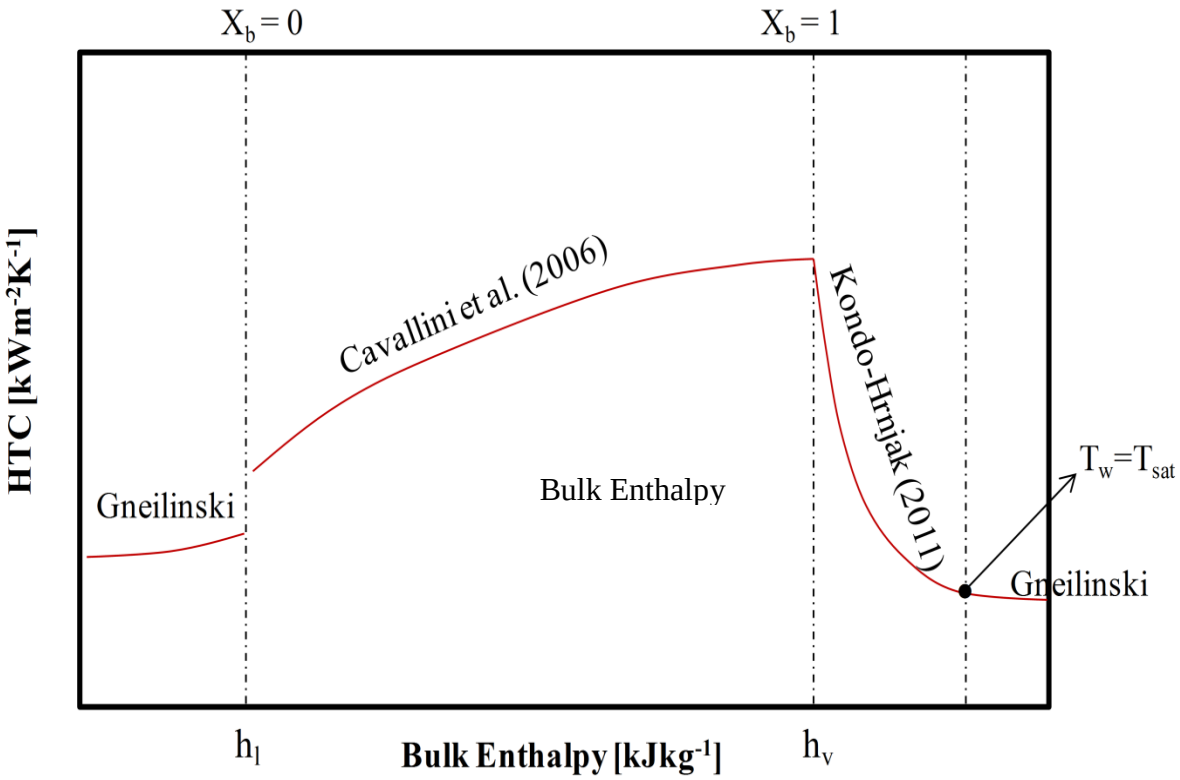

Figure 2.2: Modeling with condensation in de-superheating region

2.1.1 Condensation in Superheated (CSH) zone

It has been established and accepted in literature that HTC is significantly greater than prediction by single phase correlations near x=1 due to presence of liquid condensate in superheated region. The condensation in this region is a combination of sensible and latent heat rejection. When the wall temperature becomes equal to saturation temperature condensation at the wall can exist even if the bulk temperature of refrigerant is greater than saturation temperature. This is supported by the experimental data of Kondou and Hrnjak (2011a). Kondo-Hrnjak correlation (see Eq. 2.1) combines the single phase and two phase correlations to predict HTC in this zone as shown in Fig. 2.2.

$$\alpha\left(T_{\mathrm{rb}}-T_{\mathrm{wi}}\right)=\alpha_{\mathrm{SH}}\left(T_{\mathrm{rb}}-T_{\mathrm{sat}}\right)+\alpha_{\mathrm{TP}}\left(T_{\mathrm{sat}}-T_{\mathrm{wi}}\right) \tag{2.1}$$

2.1.2 Condensation in Two Phase Zone

Condensation in two-phase zone is fairly well understood and various correlations have been proposed to predict HTC as a function of quality. These correlations, however, neglect the effect of sub-cooling of liquid film. As a result, the two-phase correlations do not match with single phase correlations at x=0 as shown in Fig. 2.2. The model proposed in this paper deals with the latent and sensible heat rejection separately which will explain the presence of vapor in sub-cooled region.

2.1.3 Condensation in Sub-Cooled Zone

The presence of sub-cooled liquid film in condensation has been acknowledged but rarely quantified in the models proposed for heat rejection in condensers. The temperature of sub-cooled film leaving the two phase zone being lower than saturated temperature leads to the presence of vapor when the bulk enthalpy of refrigerant reaches saturated liquid enthalpy. The condensation of this vapor leads to increase in HTC near x=0. The process is analogous to condensation in superheated zone except that bulk refrigerant now is in liquid state. The model, as shown in Fig. 2.3 depicts the sub-cooling of liquid film in two-phase zone and hence calculate the HTC near x=0 to be much greater than prediction by single phase correlations.

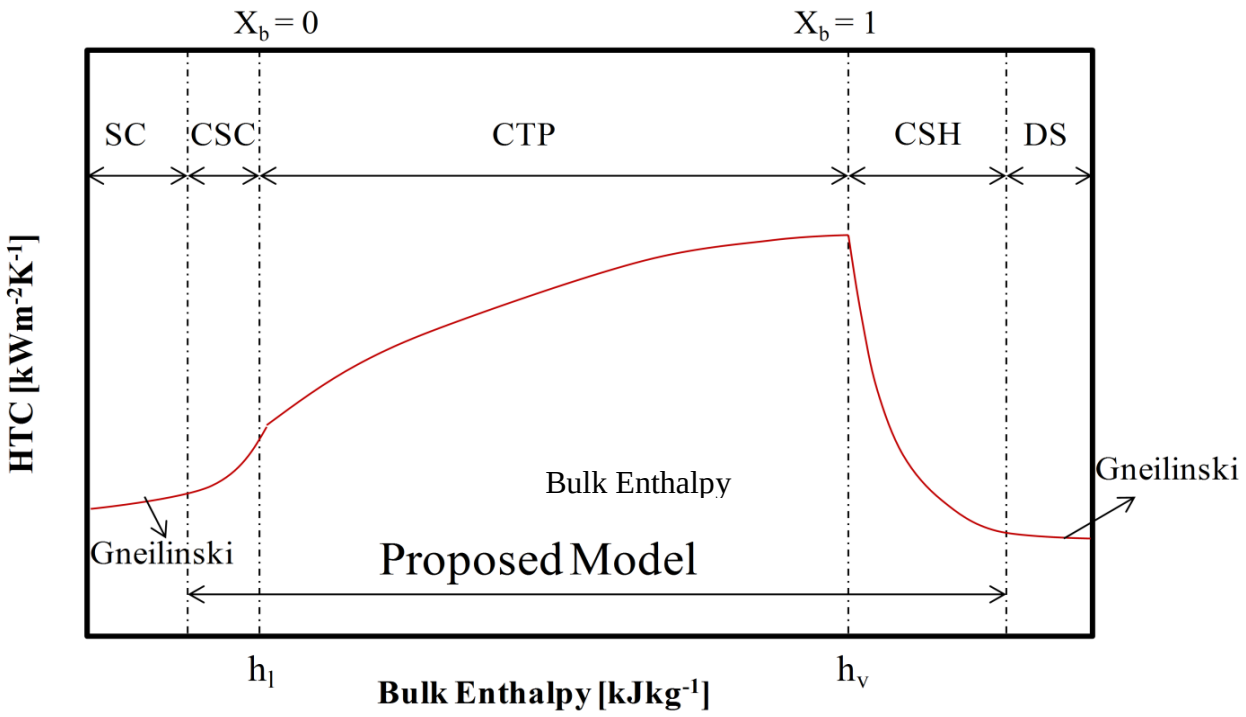

Figure 2.3: Proposed model showing smooth transition across all the zones

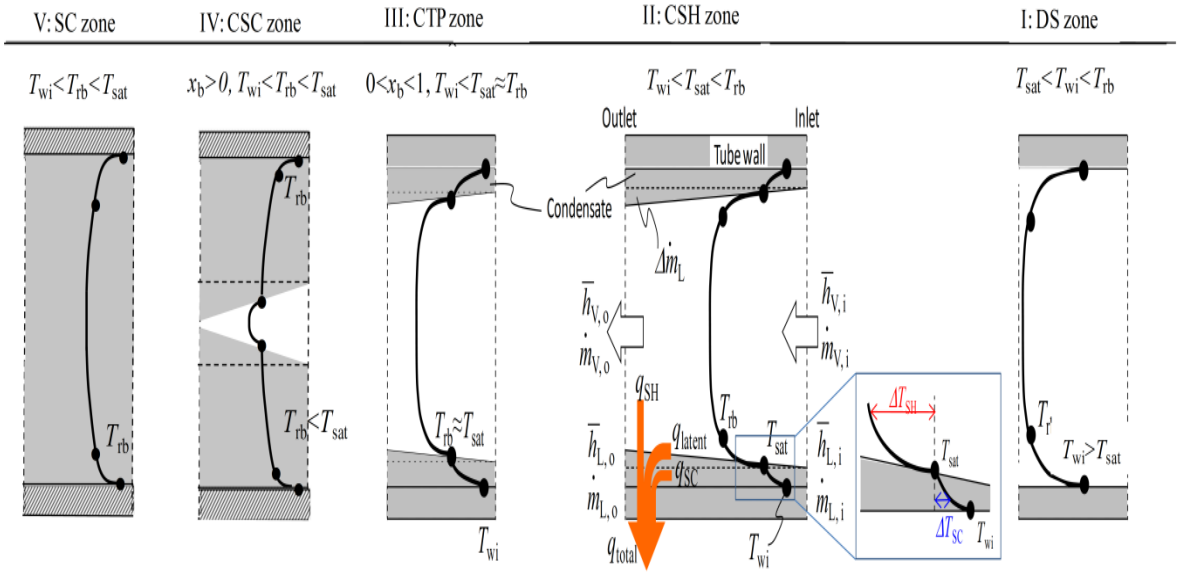

Figure 2.4: Illustration of heat flow and temperature distribution in condensers

2.2 Principle of Heat Rejection in Condensers

Figure 2.4 illustrates the heat flow and the temperature profile in condensing superheat zone, where bulk mean refrigerant temperature is above saturation point. According to Soliman's flow regime (Soliman, 1986) condensation begins as mist flow and then changes into annular flow. According to Altman et al. (1959), thin ridges or droplets flow on the interior tube surface. The authors are working on visualization of refrigerant in condensers to see the flow regime at the beginning of condensation. Figure 2.4 explains the heat exchange with annular flow model for simplification. From continuity, the total mass flow rate $\dot{m}_{\text{total}}$ of vapor and liquid refrigerant is,

$$\dot{m}_{\text{total}} = \dot{m}_{\text{V, i}} + \dot{m}_{\text{L, i}} = \dot{m}_{\text{V, o}} + \dot{m}_{\text{L, o}} \tag{2.2}$$

The amount of condensate $\Delta\dot{m}_{\text{l}}$ generated through a segment is expressed from the continuity as,

$$\Delta\dot{m}_{\text{L}} = \dot{m}_{\text{L,o}} - \dot{m}_{\text{L,i}} = \dot{m}_{\text{V,i}} - \dot{m}_{\text{V,o}} = \Delta\dot{m}_{\text{V}} \tag{2.3}$$

The average enthalpies in superheated vapor and sub-cooled liquid are represented with heat capacities and degree of superheat and sub-cool ΔT_{SH} , ΔT_{SC} as,

$$\bar{h}_V = h_{\text{Vsat}} + \overline{Cp_{\text{V}}\Delta T_{\text{SH}}} = h_{\text{Vsat}} + \overline{\Delta h_{\text{SH}}}, \quad \bar{h}_{\text{L}} = h_{\text{Lsat}} - \overline{Cp_{\text{L}}\Delta T_{\text{SC}}} = h_{\text{Vsat}} - \Delta h_{\text{LV}} - \overline{\Delta h_{\text{SC}}} \tag{2.4}$$

Total inlet heat at the entrance of a segment is,

$$h_{\text{b, i}}\dot{m}_{\text{total}} = \bar{h}_{\text{V, i}}\dot{m}_{\text{V, i}} + \bar{h}_{\text{L, i}}\dot{m}_{\text{L, i}} = \left(h_{\text{Vsat}} + \overline{\Delta h_{\text{SH,i}}}\right)\dot{m}_{\text{V,i}} + \left(h_{\text{Vsat}} - \Delta h_{\text{LV}} - \overline{\Delta h_{\text{SC,i}}}\right)\dot{m}_{\text{L,i}} \tag{2.5}$$

Similarly, the total outlet heat at the exit of a segment is,

$$\begin{aligned} h_{\text{b, o}}\dot{m}_{\text{total}} &= \bar{h}_{\text{V, o}}\dot{m}_{\text{V, o}} + \bar{h}_{\text{L, o}}\dot{m}_{\text{L, o}} \\ &= \left(h_{\text{Vsat}} + \overline{\Delta h_{\text{SH,o}}}\right)\left(\dot{m}_{\text{V,i}} - \Delta\dot{m}_{\text{L}}\right) + \left(h_{\text{Vsat}} - \Delta h_{\text{LV}} - \overline{\Delta h_{\text{SC,o}}}\right)\left(\dot{m}_{\text{L,i}} + \Delta\dot{m}_{\text{L}}\right) \end{aligned} \tag{2.6}$$

The subtraction from Eq. (5) to Eq. (4) gives the total heat exchange through a segment.

$$\left(h_{\mathrm{b,\,i}}-h_{\mathrm{b,\,o}}\right)\dot{m}_{\mathrm{total}}=\underbrace{\left(\overline{\Delta h_{\mathrm{SH,i}}}-\overline{\Delta h_{\mathrm{SH,o}}}\right)\dot{m}_{\mathrm{V,i}}+\overline{\Delta h_{\mathrm{SH,o}}}\Delta\dot{m}_{\mathrm{L}}}_{SH}+\underbrace{\Delta h_{\mathrm{LV}}\Delta\dot{m}}_{latent}+\underbrace{\left(\overline{\Delta h_{\mathrm{SC,o}}}-\overline{\Delta h_{\mathrm{SC,i}}}\right)\dot{m}_{\mathrm{L,i}}+\Delta h_{\mathrm{SC,o}}\Delta\dot{m}_{\mathrm{L}}}_{SC} \tag{2.7}$$

The Eq. (2.7) shows heat transfer rate caused by de-superheating of vapor flow (SH), latent heat rejection to generate condensate (latent) and sub-cooling of condensate (SC).

$$\dot{Q}_{\mathrm{total}}=\dot{Q}_{\mathrm{SH}}+\dot{Q}_{\mathrm{latent}}+\dot{Q}_{\mathrm{SC}} \tag{2.8}$$

This is the basic equation being used in modeling heat transfer in condensers. It has been assumed that $\dot{Q}_{\mathrm{sc}}$ in the condensing superheated zone is negligible and $\dot{Q}_{\mathrm{sh}}$ in two phase zone to be zero. In general, existing correlations do not account for $\dot{Q}_{\mathrm{sc}}$ separately in the model which is the reason for discontinuity in HTC at x=0. The model is a function of Cavallini and Kondo-Hrnjak correlations which have been proven to work successfully for the same data set. The two-phase correlation used can be changed; however, the underlying principle will remain the same.

2.3 Heat Transfer Model Proposed

The heat transfer model shown here is formed using the principle of energy balance in a small element of tube. Air is assumed to be the cooling medium for refrigerant flowing inside horizontal tube. The model can be described with the equations below:

$$\left.\begin{aligned}\dot{Q}_{Total}&=\alpha_o A_o(T_w-T_{air})\\ \dot{Q}_{Sensible,v}&=\alpha_{Sensible}A_{v,Sensible}(T_{bulk,v}-T_{sat})\\ \dot{Q}_{Sensible,l}&=\alpha_{Sensible}A_{l,Sensible}(T_{bulk,l}-T_w)\\ \dot{Q}_{TP}&=\alpha_{TP}A_i(T_{sat}-T_w)\end{aligned}\right\} \tag{2.9}$$

$$\dot{Q}_{Total}=\dot{Q}_{sensible,l}+\dot{Q}_{sensible,v}+\dot{Q}_{TP} \tag{2.10}$$

2.3.1 Assumptions

- Sensible heat rejection of liquid film in condensing superheat zone is neglected since it is insignificant
- Heat leak is neglected
- Properties of cooling medium are known.
- Nusselt film condensation on the wall in CSH zone
- Uniform HTC of cooling medium throughout the tube

2.3.2 De-Superheating Zone

The vapor is assumed to enter in superheated state such that $T_{wall}>T_{sat}$. Hence, due to absence of condensation in this region,

$$\dot{Q}_{TP} = 0 \tag{2.11}$$

Due to absence of any liquid in this zone

$$\dot{Q}_{Sensible,l} = 0 \tag{2.12}$$

Assuming turbulent flow of vapor, sensible HTC can be calculated as

$$\left.\begin{aligned} &\alpha_{\text{Sensible}} = Nu_0\left(\lambda_{\text{v}}/d_{\text{i}}\right) \\ &Nu_0 = \frac{\left(f_{\text{b}}/8\right)\left(G_v d_{\text{i}}/\mu_v - 1000\right)Pr_v}{1+12.7\left(f_{\text{b}}/8\right)^{1/2}\left(Pr_v^{2/3}-1\right)},\ f_{\text{b}} = \left[1.82\cdot\log_{10}\left(G_v d_{\text{i}}/\mu_v\right)-1.64\right]^{-2} \end{aligned}\right\} \text{ (Gneilinski)} \tag{2.13}$$

$$A_{v,Sensible} = \pi d_i \Delta Z \tag{2.14}$$

$$\alpha_r = \frac{\dot{Q}_{total}}{A_i(T_{rb}-T_w)} \tag{2.15}$$

2.3.3 Condensing Superheat Zone

The heat transfer in CSH zone is based on the same principle as Kondo-Hrnjak correlation where the total heat rejected is a combination of sensible and latent heat. Condensing superheat zone begins when the wall temperature drops below saturation temperature with liquid film forming on the inner wall of the tube. Since the sensible heat rejected by liquid film is assumed to be negligible compared to total heat rejected on account of very low mass of liquid, $Q_{sensible}$ only comes from superheated vapor. The process is analogous to Nusselt film condensation where liquid film formed on the wall is assumed to be falling film. Since the wall has to be completely wet the bulk vapor remains at the core of the tube making it annular flow (see Fig. 2.5(a)). The two-phase HTC in this region is calculated using Cavallini et al. (2006), shown in Eq. (2.16), where the quality is calculated based on the mass of condensate in the test section. The properties of liquid and vapor are taken at saturation and superheated conditions respectively.

$$
\begin{aligned}
&J_G = xG_{\mathrm{r}} \Big/ \sqrt{g d_{\mathrm{i}} \rho_{\mathrm{V}} \left(\rho_l - \rho_{\mathrm{V}}\right)}, \quad J_G{}^T = \left\{ \left(7.5 \Big/ 4.3 X_{tt}{}^{1.111} + 1 \right)^{-3} + 2.6^{-3} \right\}^{-1/3} \\
&X_{tt} = \left(\frac{1-x}{x} \right)^{.9} \left(\frac{\rho_v}{\rho_l} \right)^{.5} \left(\frac{\mu_l}{\mu_v} \right)^{.1} \\
&\alpha_{\mathrm{LO}} = 0.023 \left(G_{\mathrm{r}} d_{\mathrm{i}} / \mu_l \right)^{0.8} \mathrm{Pr}_l{}^{0.4} \left(\lambda_l / d_{\mathrm{i}} \right) \\
&\alpha_{\mathrm{strat}} = 0.725 \left[\frac{\lambda_l{}^3 \rho_l \left(\rho_l - \rho_{\mathrm{V}}\right) g \Delta h_{\mathrm{LV}}}{\mu_l d_{\mathrm{i}} (T_{\mathrm{sat}} - T_{\mathrm{w}})} \right]^{0.25} \left\{ 1 + 0.741 \left(\frac{1-x}{x} \right)^{0.3321} \right\}^{-1} + \left(1 - x^{0.087} \right) \alpha_{\mathrm{LO}} \Bigg\} \qquad (2.16) \\
&\alpha_{\mathrm{TP}} = \begin{cases} J_G > J_G{}^T : \alpha_{\mathrm{A}} = \alpha_{\mathrm{LO}} \Big[1 + 1.128 x^{0.8170} \left(\rho_l / \rho_{\mathrm{V}} \right)^{0.3685} \left(\mu_l / \mu_{\mathrm{V}} \right)^{0.2363} \\ \qquad\qquad \left(1 - \mu_{\mathrm{V}} / \mu_l \right)^{2.144} \mathrm{Pr}_l{}^{-0.1} \Big] \\ J_G \le J_G{}^T : \quad \left[\alpha_{\mathrm{A}} \left(J_G{}^T / J_G \right)^{0.8} - \alpha_{\mathrm{strat}} \right] \left(J_G / J_G{}^T \right) + \alpha_{\mathrm{strat}} \end{cases}
\end{aligned}
$$

The HTC for sensible heat rejection through superheated vapor is calculated using Eq. (2.13) with the actual mass flux and properties of superheated vapor. Since, the vapor essentially remains in the annulus core (see Fig. 2.5); the area for sensible heat rejection can be expressed as

$$A_{v,Sensible} = \pi(d_i - 2\delta)dz \tag{2.17}$$

Where, δ is calculated using Nusselt theory of film wise condensation

$$\delta = [\lambda_l \mu_l (T_{sat} - T_w) / h_{lv} \rho_l (\rho_l - \rho_v) g]^{.25} \tag{2.18}$$

2.3.4 Two-Phase Zone

Two phase zone begins when the bulk temperature of the refrigerant reaches saturation temperature. Since, the sensible heat rejected by liquid in CSH zone is neglected; the vapor and liquid will be at saturation temperature at that point. Hence the sensible heat rejected in two phase zone comes only from liquid.

$$\dot{Q}_{Sensible,v} = 0 \tag{2.19}$$

The two-phase HTC is again calculated using Eq. (2.14) with calculated quality, actual properties and mass flux as input. Since Cavallini et al. takes annular and stratified/stratified-wavy flow regime into account the area of sensible heat rejection is calculated in the following manner

$$A_{l,sensible} = \begin{Bmatrix} \pi d_i dz & (Annular) \\ \frac{d_i}{2}(2\pi - \theta_{strat}) & (Stratified / Stratified - wavy) \end{Bmatrix} \tag{2.20}$$

Where,

θ_{strat} is calculated using empirical correlation from Thome et al. (2003) (see Fig. 2.5(b)) and Smith's correlation (1969) is used to compute void fraction

$$\theta_{strat} = 2\pi - \left\{ \begin{array}{l} \pi(1-\varepsilon) + \left(\frac{3\pi}{2}\right)^{1/3} [1-2(1-\varepsilon) + (1-\varepsilon)^{1/3} - \varepsilon^{1/3}] - \\ \qquad \frac{1}{200}(1-\varepsilon)\varepsilon[1-2(1-\varepsilon)][1+4(1-\varepsilon)^2+\varepsilon^2] \end{array} \right\} \tag{2.21}$$

$$\varepsilon = \left[1 + \frac{\rho_v}{\rho_l}\left(\frac{1-x}{x}\right)\left(.4 + .6\left\{\frac{\rho_l/\rho_v + .4(1-x)/x}{1+.4(1-x)/x}\right\}^{.5}\right)\right]^{-1} \tag{2.22}$$

The sensible HTC also depends on whether the liquid flow is laminar, turbulent or transition regime. Hence, Nusselt no. is calculated using constant heat flux, Gnielinski (or Dittus-Boelter) and Churchill correlations in respective zones.

$$\left. \begin{array}{ll} Nu_l = 4.364 & (\mathrm{Re} < 2300) \\ Nu_t = \dfrac{\left(f_\mathrm{b}/8\right)\left(G_l d_\mathrm{i}/\mu_l - 1000\right)Pr_l}{1+12.7\left(f_\mathrm{b}/8\right)^{1/2}\left(\mathrm{Pr}_l^{2/3}-1\right)},\ f_\mathrm{b} = \left[1.82\cdot\log_{10}\left(G_l d_\mathrm{i}/\mu_l\right) - 1.64\right]^{-2} & (\mathrm{Re} > 4000) \\ Nu_{tr}^{10} = Nu_l^{10} + \left\{\dfrac{\exp\left[\dfrac{2200-\mathrm{Re}}{365}\right]}{Nu_l^2} + \dfrac{1}{Nu_c^2}\right\}^{-5}, & (2300 < \mathrm{Re} < 4000) \\ Nu_c = Nu_0 + \dfrac{.079*(f/2)^{.5}\,\mathrm{Re}\,\mathrm{Pr}}{(1+\mathrm{Pr}^{4/5})^{5/6}} & \\ where, Nu_0 = 6.3 & \\ \qquad \dfrac{2}{f} = \left\{\dfrac{1}{\left[(8/\mathrm{Re})^{10} + (\mathrm{Re}/36500)^{20}\right]^{1/2}} + \left[2.21\ln\left(\dfrac{\mathrm{Re}}{7}\right)\right]^{10}\right\}^{1/5} & \end{array} \right\} \tag{2.23}$$

Sensible HTC is calculated after finding the Nusselt number for the flow regime of the liquid

$$\alpha_{\mathrm{Sensible}} = Nu\left(\lambda_l/d_\mathrm{i}\right) \tag{2.24}$$

The HTC is then calculated using the following equation

$$\alpha_r = \frac{\dot{Q}_{total}}{A_i (T_{sat} - T_w)} \tag{2.25}$$

Since the effect of sub-cooling is taken into account these equations also cover the condensation in sub-cooled zone. It should be noted that in CSC zone the bulk temperature of refrigerant would be less than saturation temperature but still equation 2.25 is used to calculate HTC since the two-phase HTC is usually defined in this manner.

2.3.5 Sub-Cooled (SC) zone

Heat transfer in sub-cooled zone is calculated using the Eq. 2.23 and 2.24. The phenomena is analogous to de-superheating zone

The model uses the equations shown above to calculate HTC in different zones. The model is applied on a segment dz of a tube in an explicit manner where the outlet conditions of the segment are used as inlet conditions for the next segment. The calculation procedure for the model has been discussed below.

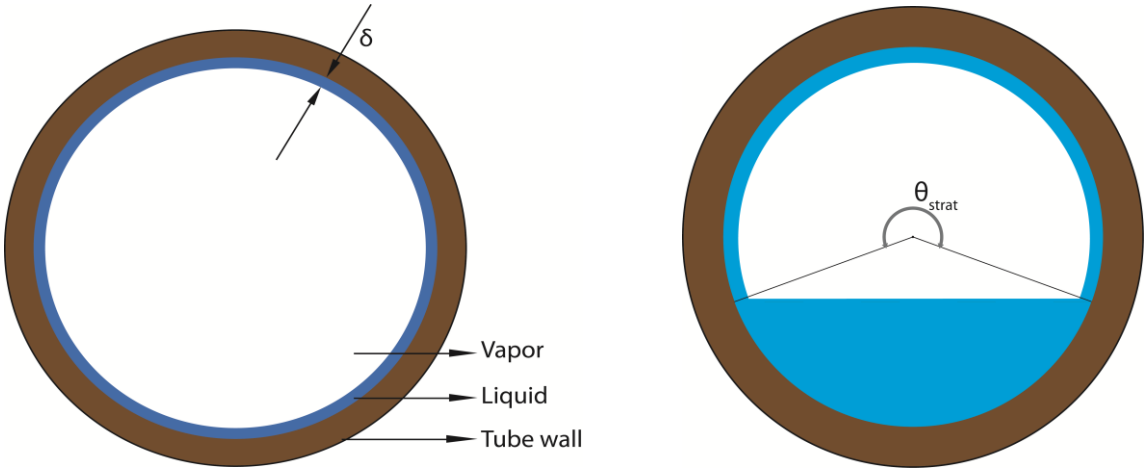

(a) Annular flow regime **(b) Stratified flow regime**

Figure 2.5: Flow regimes in heat transfer model

2.4 Calculation Procedure:

Here is a brief description of the approach taken in the model. The inlet condition of the refrigerant is superheated vapor such that the wall temperature is greater than saturation temperature. The HTC on the outer side, tube geometry, inlet mass flux, temperature of air and refrigerant at inlet are given as input. In order to cover all the zones refrigerant with high superheat (50-70 ^{0}C) at inlet is used as input

- For de-superheating zone (DS) use equations 2.9-2.15 to get the HTC using Gnielinski correlation. Using energy balance approach across each element march down the tube until wall temperature reaches saturation temperature to enter CSH zone.

- CSH zone uses equations 2.9, 2.10, 2.12, 2.13, 2.15-2.18 to get HTC with assumed inlet quality of .9999 at the beginning. Since condensation begins in this region outlet quality is calculated in each element and used as input in the next. The vapor temperature is also calculated and the CSH zone ends where the bulk temperature of vapor reaches saturation temperature to enter in two-phase zone.

- The HTC in CTP and CSC zones are calculated using equations 2.9, 2.10, 2.16, 2.19-2.24 with the inlet conditions to be the output of the last element in CSH zone. The sensible heat rejected by liquid and hence the temperature of bulk liquid is calculated to quantify the sub-cooling of liquid at the end of two-phase zone. The bulk enthalpy and temperature of refrigerant is computed separately and the two-phase zone ends when the bulk temperature of refrigerant drops below saturation temperature.

- Once the refrigerant enters sub-cooled (SC) zone, equations 2.23 and 2.24 are used to calculate HTC in each element.

The model described above is able to eliminate the discontinuity across various zones in the condensation process. The preliminary results from the model and their comparison to experimental data has been shown and analyzed in details in the next section.

CHAPTER 3

EXPERIMENTAL METHOD

3.1 Facility for Experiments

Figure 3.1 shows the schematic diagram of experimental apparatus. The refrigerant loop mainly consists of a variable speed gear pump, a coriolis-type mass flow meter, an electric pre-heater, a mixer, a pre-cooler, a test section, sight glass, two after-coolers and receiver tank. The refrigerant flow rate is regulated by the gear pump while the pressure is controlled by the refrigerant charge amount, pre-heater and flow rate of water through the after-coolers. The inlet condition at test section is adjusted by water flow rate through pre-cooler while the heat flux is controlled by the mass flow rate and inlet/outlet temperature of the cooling water in test section. The state of the refrigerant can be seen in the sight glass downstream of the test section. The cooling water in the pre-cooler and test section is again cooled in a separate loop with chilled water supply line.

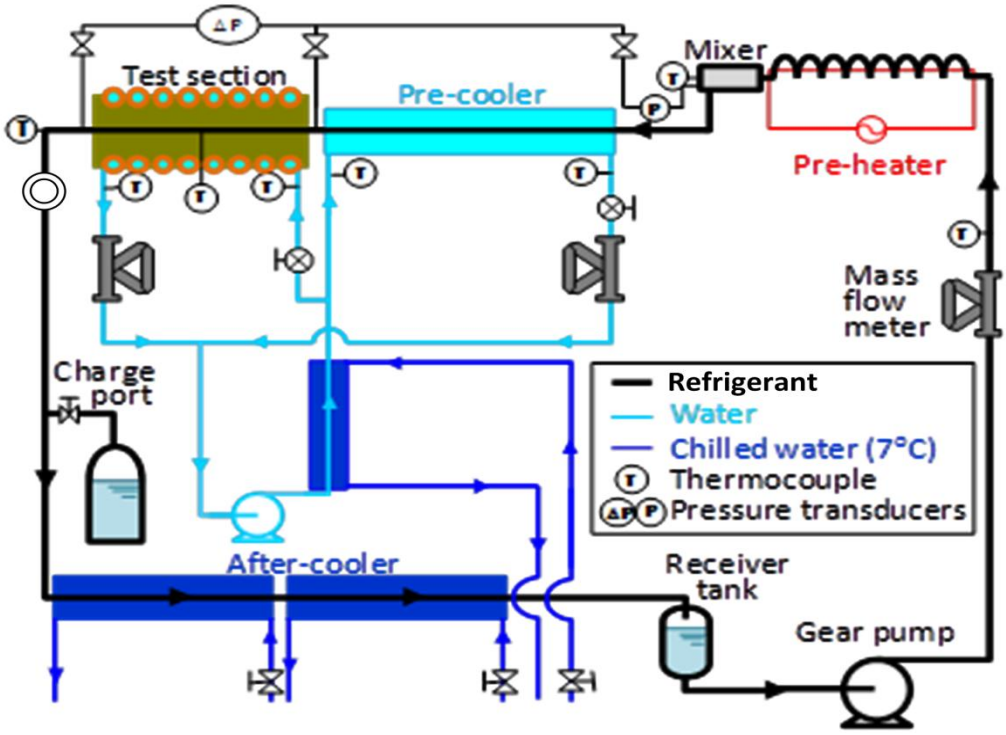

Figure 3.1: Schematic diagram of the experimental apparatus

3.2 Test Section

Figure 3.2 (a) and (b) show the schematic of the test section and arrangement of thermocouples on the test tube. The test section consists of a smooth copper tube with 6.1 mm ID and 9.53 mm OD and 150 mm length. The tube is placed horizontally and covered with a thick brass jacket which ensures uniform cooling throughout the test section. The halved brass jacket is pressed over the test tube and the small gap between them is filled with a thermal paste. The cooling water flows through copper tubes soldered to the outer surface of the brass jacket. Twelve thermocouples are embedded into the top, bottom, right, and left of the test tube wall at three positions in the axial direction. The short length of test section allows us to measure the quasi-local HTC with relatively accurate test conditions.

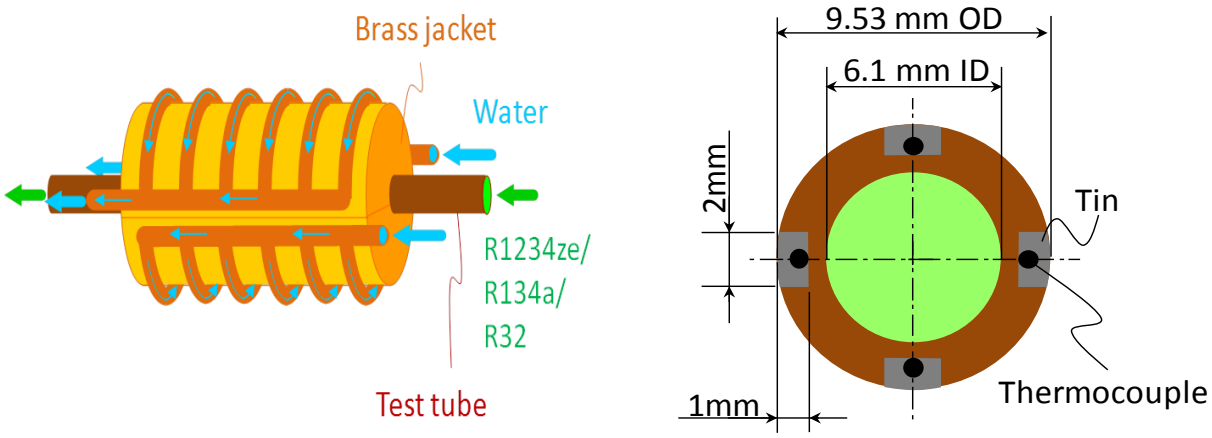

(a) Test Section (b) Dimensions of the test tube

Figure 3.2: Specifications of the test section and test tube.

3.3 Experimental Measurement and Uncertainties

During experiments the refrigerant is ensured to be in superheated state in the pre heater with a superheat of 5-50 ^{0}C. The pre cooler is in operation even for readings in superheated state. The enthalpy in pre heater is calculated by measured pressure and temperature. The inlet condition of test section is then achieved by controlling the heat rejection from pre cooler which is a function of measured mass flow rate and ΔT of cooling water. The T type thermocouples measure the wall temperature and heat flux is calculated using mass flow rate, inlet and outlet

temperature of cooling water through test section. The pressure drop in the test section and pre cooler is again measured by a differential transducer which gives the precise pressure in test section. The uncertainties of the instruments used in the experiments have been given in Table 3.1. The uncertainty propagation (Moffat, 1988) because of the instruments is shown in the form of error bars in the data shown below.

Table 3.1: Measurement uncertainties

Nomenclature	Instrument	Uncertainty
T_{rb}, T_{H2O}	Sheathed T type Thermocouple	±0.05 K
T_{wi}	Twisted T type Thermocouple	±0.16 K
P_{MC}	Diaphragm absolute pressure transducer	±4 kPa
ΔP	Diaphragm differential pressure transducer	±0.13 kPa
$\dot{m}_{H2O,\,TS}$, $\dot{m}_{r}$	Coriolis mass flow meter	±0.1 g/s
$\dot{m}_{H2O,\,PC}$	Coriolis mass flow meter	±0.5 g/s

3.4 Range of Test Conditions

The experiments have been conducted for 3 refrigerants viz. R1234ze(E), R134a and R32 for the range of operating conditions illustrated in Table 3.2. The operating conditions have been chosen to be close to condenser pressure in automotive systems. The wide range of experiments conducted allows making a comparison between the refrigerants and analyzing the effect of various parameters on HTC.

Table 3.2: Test Range for the experiments

Refrigerant	G [$kgm^{-2}s^{-1}$]	T_{sat} [^0C]	Q [kWm^{-2}]
R1234ze(E)	100-300	30-50	5-25
R134a	100,300	30,50	10
R32	100,300	30,50	10

3.5 Data Reduction Procedure

Figure 3.3 helps presenting the data reduction method. The main measured values are the refrigerant mass flow rate $\dot{m}_{\mathrm{r}}$, bulk-mean temperature $T_{\mathrm{rb,MC}}$, and absolute pressure P_{MC} in the mixer, the bulk water temperature of pre-cooler inlet $T_{\mathrm{H2O,PCi}}$ and outlet $T_{\mathrm{H2O,PCo}}$, test section inlet $T_{\mathrm{H2O,TSi}}$ and outlet $T_{\mathrm{H2O,TSo}}$, and the water mass flow rate of pre-cooler $\dot{m}_{\mathrm{H2O,\ PC}}$ and test section $\dot{m}_{\mathrm{H2O,\ TS}}$. The bulk-mean enthalpy in the mixer $h_{\mathrm{rb,MC}}$ is obtained from $T_{\mathrm{rb,MC}}$ and P_{MC} under the assumption of equilibrium by RefpropVer.8.0 (Lemmon et al., 2007). The enthalpy changes through the pre-cooler Δh_{PC} and the test section Δh_{TS} are determined by water side heat balances and as presented below.

$$\Delta h_{\mathrm{PC}} = \left[\left(T_{\mathrm{H2O,PCo}} - T_{\mathrm{H2O,PCi}}\right)\dot{m}_{\mathrm{H2O,PC}} Cp_{\mathrm{H2O}} - \dot{Q}_{\mathrm{gain,PC}}\right] \Big/ \dot{m}_{\mathrm{r}} \tag{3.1}$$

$$\Delta h_{\mathrm{TS}} = \left[\left(T_{\mathrm{H2O,TSo}} - T_{\mathrm{H2O,TSi}}\right)\dot{m}_{\mathrm{H2O,TS}} Cp_{\mathrm{H2O}} - \dot{Q}_{\mathrm{gain,TS}}\right] \Big/ \dot{m}_{\mathrm{r}} \tag{3.2}$$

Where $\dot{Q}_{\mathrm{gain,PC}}$ and $\dot{Q}_{\mathrm{gain,TS}}$ are preliminarily measured heat leak from ambient air through the insulators. The bulk mean temperature at the test section T_{rb} is obtained from bulk enthalpy and pressure with the equilibrium state function of RefpropVer.8.0.

$$\begin{aligned} T_{\mathrm{rb}} &= \left(T_{\mathrm{rb,i}} + T_{\mathrm{rb,o}}\right) \Big/ 2 \\ T_{\mathrm{rb,i}} &= f_{equiblium}\left(h_{\mathrm{b,MC}} - \Delta h_{\mathrm{PC}}, P_{\mathrm{MC}} - \Delta P_{\mathrm{PC}}\right) \\ T_{\mathrm{rb,o}} &= f_{equiblium}\left(h_{\mathrm{b,MC}} - \Delta h_{\mathrm{PC}} - \Delta h_{\mathrm{TS}}, P_{\mathrm{MC}} - \Delta P_{\mathrm{PC}} - \Delta P_{\mathrm{TS}}\right) \end{aligned} \tag{3.3}$$

The average heat flux of the test section on the interior tube wall q_{wi} is,

$$q_{\mathrm{wi}} = \frac{\left(T_{\mathrm{H2O,TSo}} - T_{\mathrm{H2O,TSi}}\right)\dot{m}_{\mathrm{H2O,TS}} Cp_{\mathrm{H2O}} - \dot{Q}_{\mathrm{gain,TS}} - \dot{Q}_{\mathrm{cond}}}{\left(d_{\mathrm{i}} \cdot \pi \cdot \Delta Z\right)} \tag{3.4}$$

Where, Q_{cond} is the conduction heat from outside the cooling brass jacket estimated numerically for each condition. The definition of average heat transfer coefficient α is,

$$\alpha = q_{\mathrm{wi}} / \Delta T, \qquad \Delta T = T_{\mathrm{rb}} - T_{\mathrm{wi}} \tag{3.5}$$

Where, T_{wi} is the average temperature of the 12 points on the tube wall. The reference refrigerant temperature is defined as an arithmetic mean of inlet and outlet bulk temperatures $T_{rb,i}$ $T_{rb,o}$, which are found from each pressure P_{TSi} and P_{TSo} and enthalpies $h_{b,i}$ and $h_{b,o}$. With this method, driving temperature difference ΔT in superheat zone is defined as the difference between tube wall and bulk refrigerant temperature. Then this continuously changes into the difference between tube wall and saturation temperature at the thermodynamic vapor quality 1.0 for two-phase zone. Table 3.1 lists the measurement uncertainties obtained from the results of two standards deviation of calibration, resolution of data loggers and calibration tools, and the stability of excitation voltages. Combined measured uncertainties are calculated from those uncertainties in conformity of ASME Performance Test Codes, 1985 and Moffat (1988).

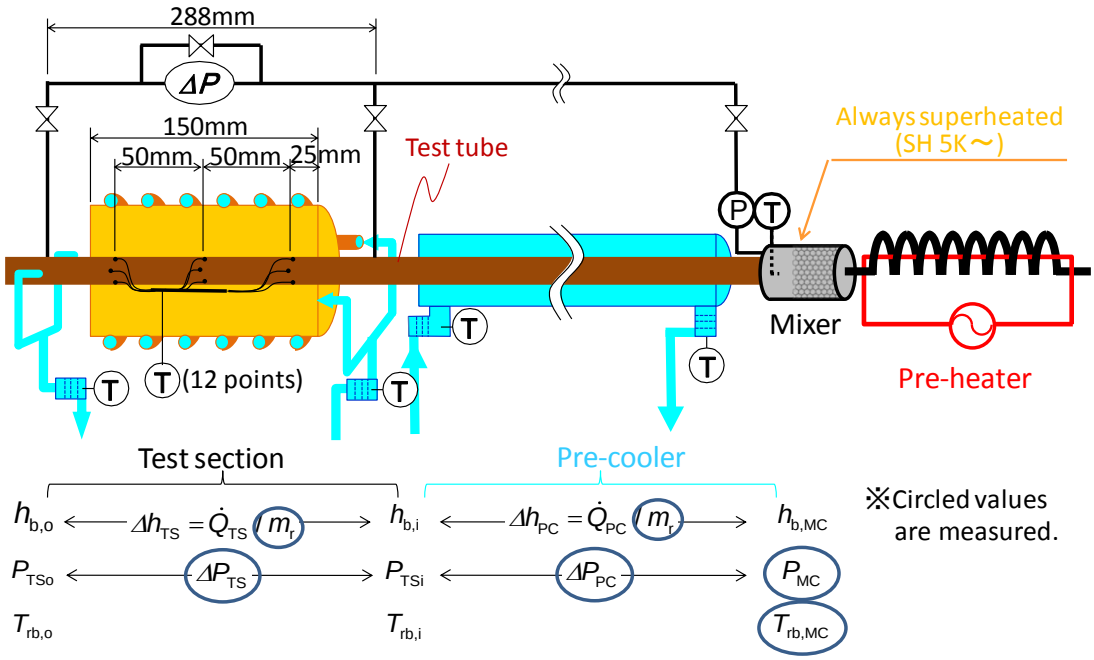

Figure 3.3: Data reduction procedure.

CHAPTER 4

RESULTS AND DISCUSSION

4.1 Smooth Transition of HTC across Superheated, Two Phase and Sub-Cooled Zone

Figure 4.1 shows the experimental results for heat transfer coefficient for three refrigerants: R1234ze (E), R134a and R32. It can be seen that all the three refrigerants exhibit similar pattern in condensation showing smooth transition from de-superheating to two-phase and two-phase to sub-cooled zone respectively. Figure 4(a) shows heat transfer data for R1234ze(E) at 100 $kgm^{-2}s^{-1}$, 10 kWm^{-2} and saturation temperature of 50^0 C which is typical operating conditions for this refrigerant. Figures 4(b) and 4(c) are the results for R134a and R32 at same operating conditions to generalize the results. The horizontal axis indicates bulk mean enthalpy of refrigerant in the test section while the vertical lines mark the saturation conditions at that condition. The enthalpy of refrigerant has been calculated under the assumption of equilibrium even during condensation in superheated zone. The upper graph shows the variation of HTC with the inlet condition in the test section. The uncertainty of the experimental measurements has been shown through error bars where the horizontal and vertical bars represent uncertainty in enthalpy and HTC respectively. The experimental data has been compared with the model developed with single phase Gnielinski correlations in de-superheating and sub-cooled zones. The heat transfer coefficient is seen to be in satisfactory agreement with the model. Since the model is developed for a flow with superheated inlet it is difficult to replicate the exact experimental conditions which were induced artificially. The center graph shows the bulk mean inlet ($T_{rb,i}$), outlet ($T_{rb,o}$) and wall temperature (T_{wi}) in the test section. It should be noted that the inlet and outlet temperatures are fairly close to each other on account of short test section length. The bottom graph shows the temperature difference between bulk refrigerant and wall which is represented by $(T_{rb,i}+T_{rb,o})/2 - T_{wi}$. It can be seen through the center figures that wall temperature is the major driving force in the transition from superheat to condensing superheat zone. The HTC in the top figure starts deviating from Gnielinski correlation when the wall temperature drops below saturation temperature indicating the start of condensation. Also, the HTC in the sub-cooled zone is much higher than single phase prediction

near x=0. This is due to the presence of vapor in the sub-cooled region on account of sub-cooled liquid film. Condensation in superheated, two phase and sub-cooled region has been explained in detail in later sections.

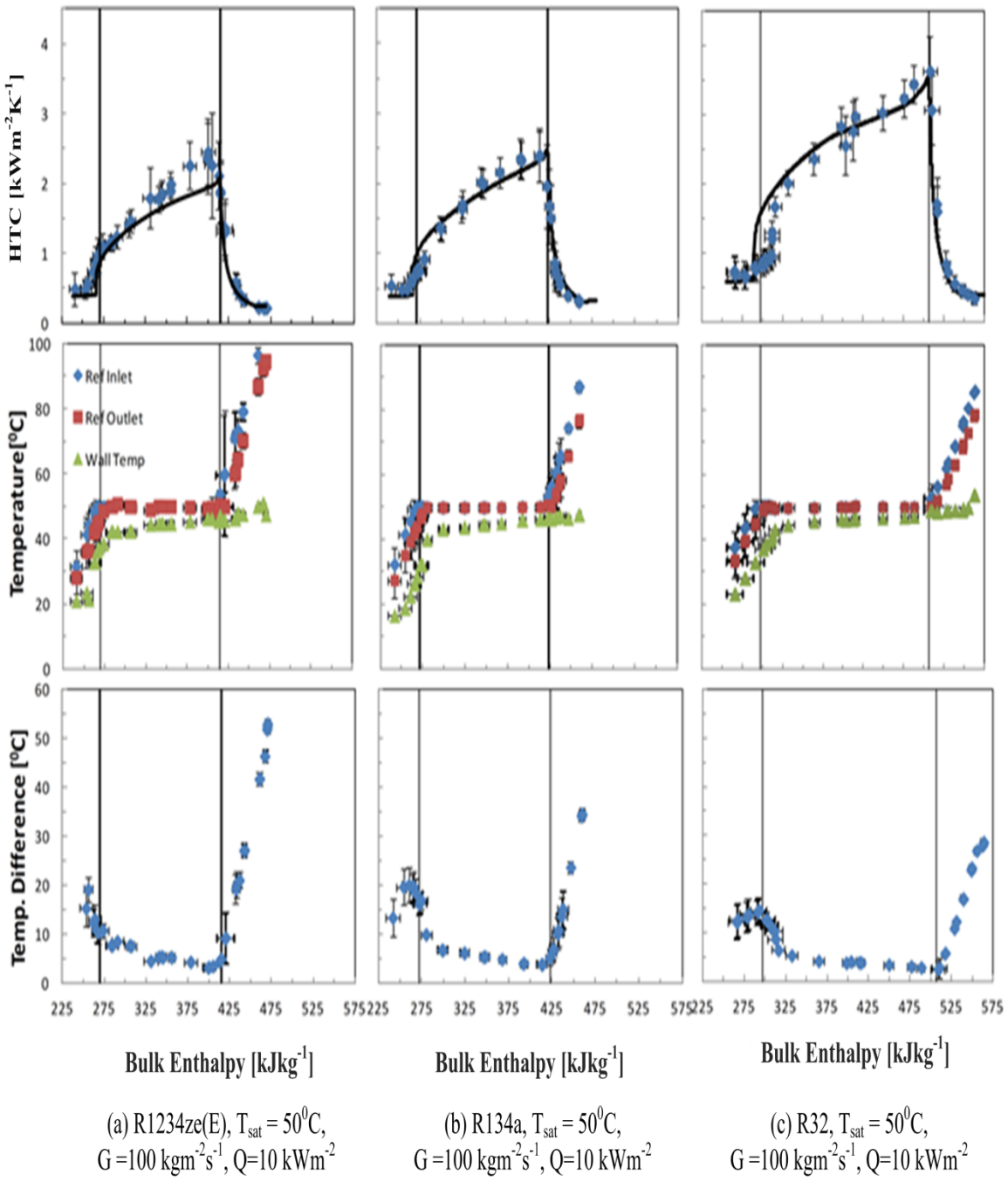

(a) R1234ze(E), T_{sat} = 50^{0}C, G =100 kgm^{-2}s^{-1}, Q=10 kWm^{-2}

(b) R134a, T_{sat} = 50^{0}C, G =100 kgm^{-2}s^{-1}, Q=10 kWm^{-2}

(c) R32, T_{sat} = 50^{0}C, G =100 kgm^{-2}s^{-1}, Q=10 kWm^{-2}

Figure 4.1: Comparison between experimental results and prediction by proposed model

4.1.1 Condensation in Superheated Zone

Figure 4.2 shows the variation of HTC in CSH zone where the vertical axis crosses horizontal axis at saturation vapor enthalpy of the refrigerant. The HTC starts deviating from single phase correlation when wall temperature reaches saturation temperature and increases until bulk refrigerant reaches saturation temperature. The increase is HTC can be attributed to increased heat rejection due to condensation. As shown in the top graph of Fig. 4.2, the component of heat transfer due to condensation increases downstream and eventually contributes to the majority of heat transfer near x=1. The presence of condensation is corroborated with increasing film thickness inside the tube. The model predicts the HTC in CSH zone within accuracy of 14.5 %.

4.1.2 Condensation in Two Phase Zone

Figure 4.3 shows the variation of HTC in TP zone where the ends of horizontal axis are marked by the saturation enthalpy of the refrigerant. The sensible heat rejected by the liquid film is negligible at the beginning but contributes approximately 15% of the total heat rejection at the end of two phase zone. As a result the liquid temperature also decreases sharply near x=0. The sub-cooling of liquid film results in the presence of vapor when the bulk enthalpy of refrigerant reaches saturation enthalpy. This leads us to the conclusion that condensation will occur even in the sub-cooled zone. The HTC in this zone is predicted within accuracy of 14.8 %.

4.1.3 Condensation in Sub-Cooled Zone

As shown in Fig. 4.4 HTC in condensing sub-cooled zone is higher than prediction by single phase correlations due to presence of vapor at the end of two phase zone. HTC decreases in CSC zone as the sensible heat rejection starts dominating two phase heat transfer. The bulk refrigerant and liquid film temperature converges at the end of this zone marking the beginning of sub-cooled zone. The jump in the model can be explained to be a result of simplified calculations for heat transfer through liquid film as only annular and stratified flow regimes are taken into account in the model. The sudden decrease in HTC occurs when the last existing vapor condenses in the element eliminating two phase heat transfer entirely. The HTC in CSC zone is not predicted extremely well by the model (accuracy of 24.8%) and the authors are working on visualization in condensers to address this issue.

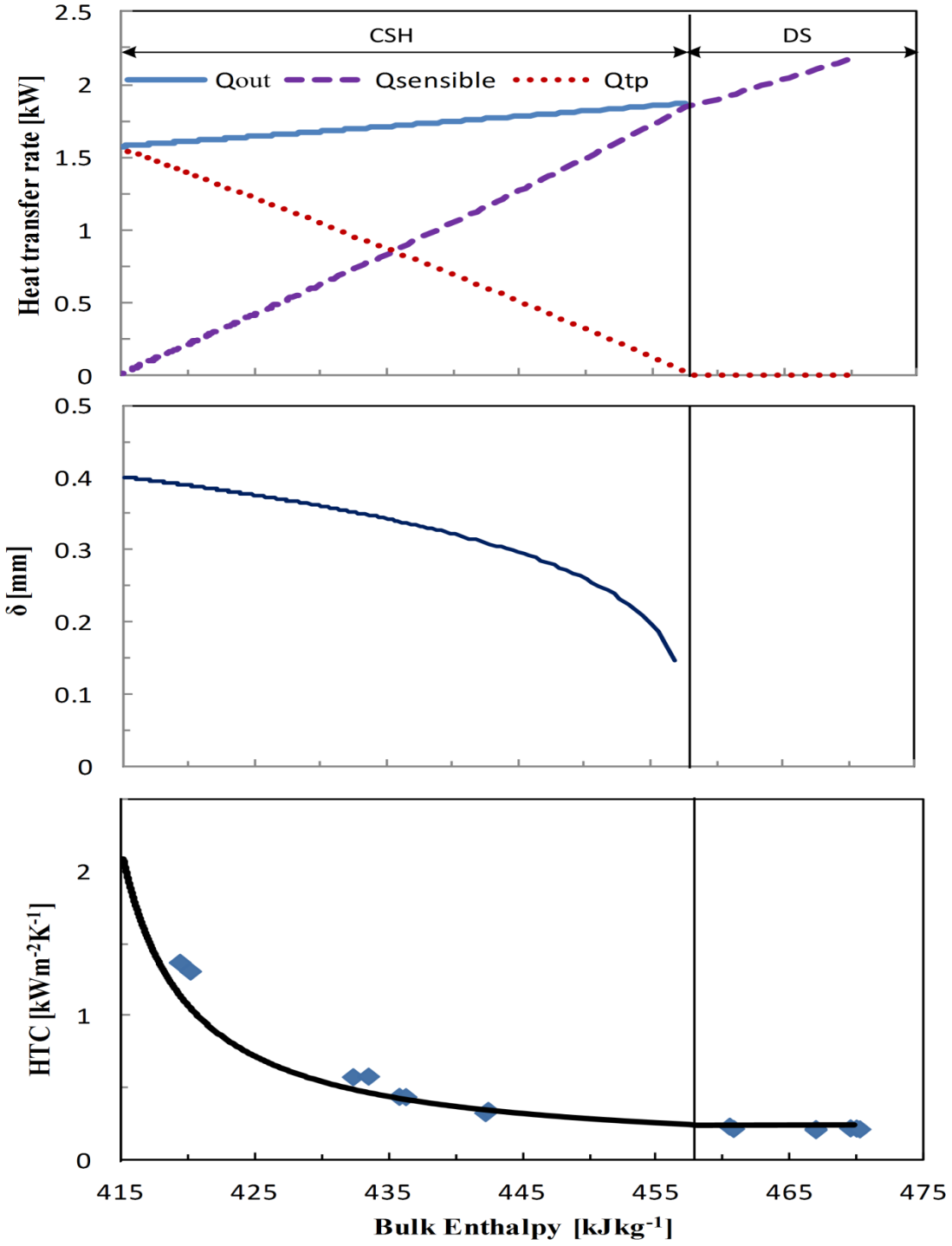

Figure 4.2: Prediction vs. results for heat rejection in superheated zone

R1234ze(E) at G= 100kgm^{-2}s^{-1}, Tsat = 50 ^{0}C, Q= 10 kWm^{-2}

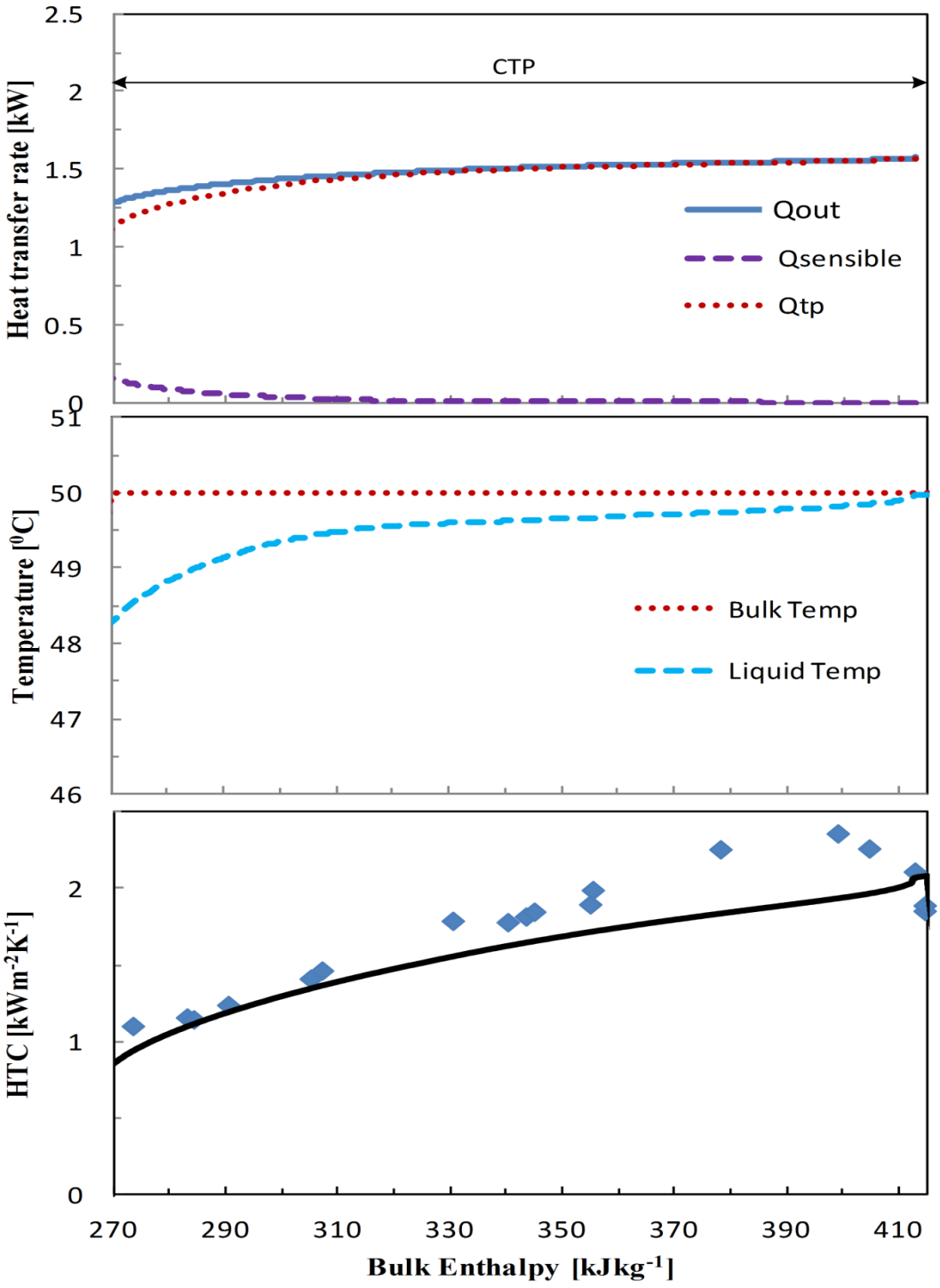

Figure 4.3: Prediction vs. results for heat rejection in two phase zone

R1234ze(E) at G= 100kgm^{-2}s^{-1}, Tsat = 50 ^{0}C, Q= 10 kWm^{-2}

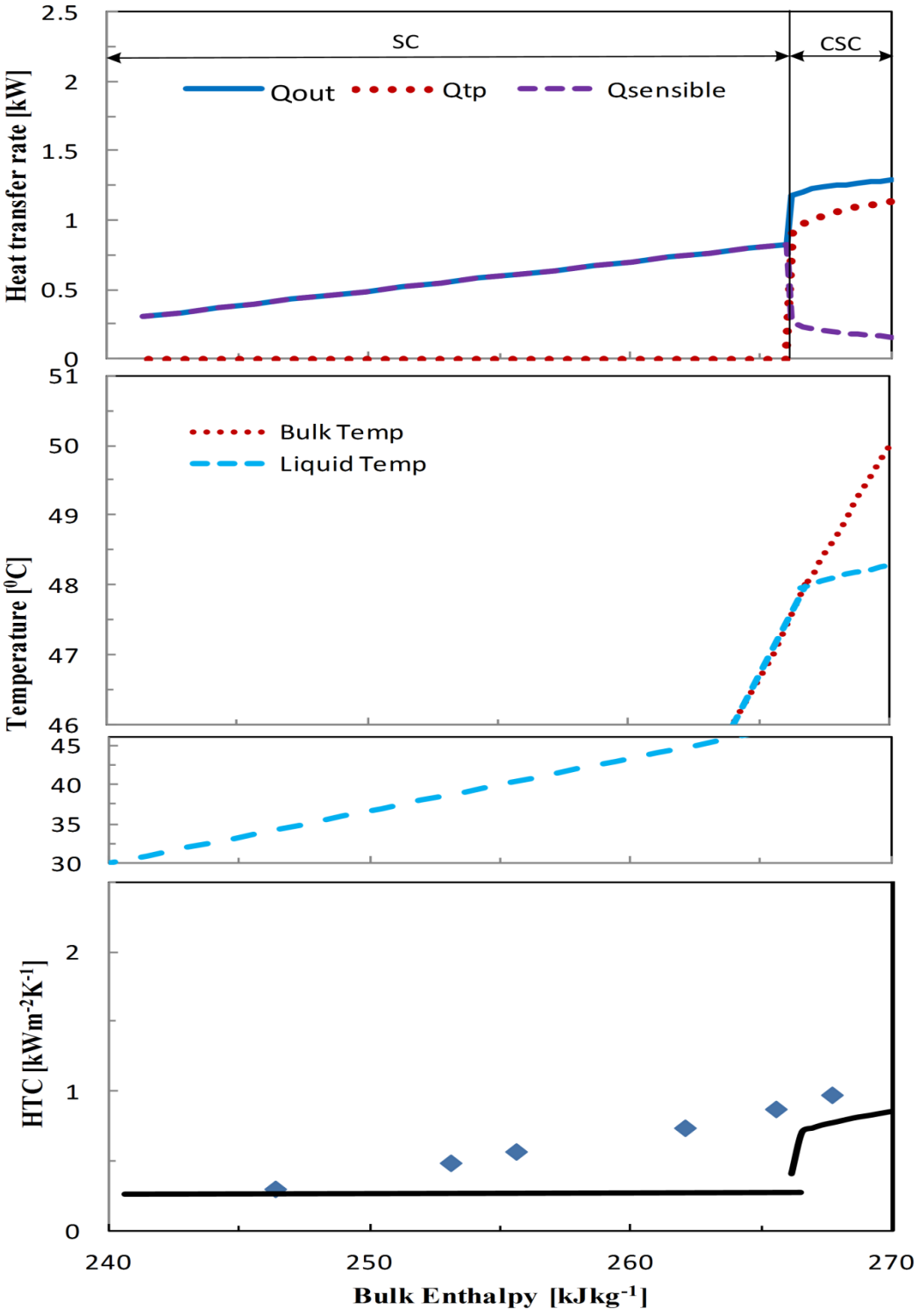

Figure 4.4: Prediction vs. results for heat rejection in sub-cooled zone

R1234ze(E) at G= 100kgm^{-2}s^{-1}, Tsat = 50 ^{0}C, Q= 10 kWm^{-2}

4.2 Effect of Parameters on Heat Transfer Coefficient

The HTC for three refrigerants have been determined under various operating conditions to have a reasonable comparison of the refrigerants and also form a conclusion regarding the effect of various parameters on HTC.

4.2.1 Effect of Mass Flux

The effect of mass flux on HTC can be seen through Figure 4.5 for R1234ze(E). The HTC decreases with vapor quality in the two-phase region. This is due to the fact that as vapor quality decreases the velocity of vapor decreases significantly to maintain the same mass flux and increased presence of liquid increases thermal resistance. This results in a less turbulent flow which decreases the HTC. Similarly, with decrease in mass flux the refrigerant moves with a lower velocity which reduces the HTC on the refrigerant side.

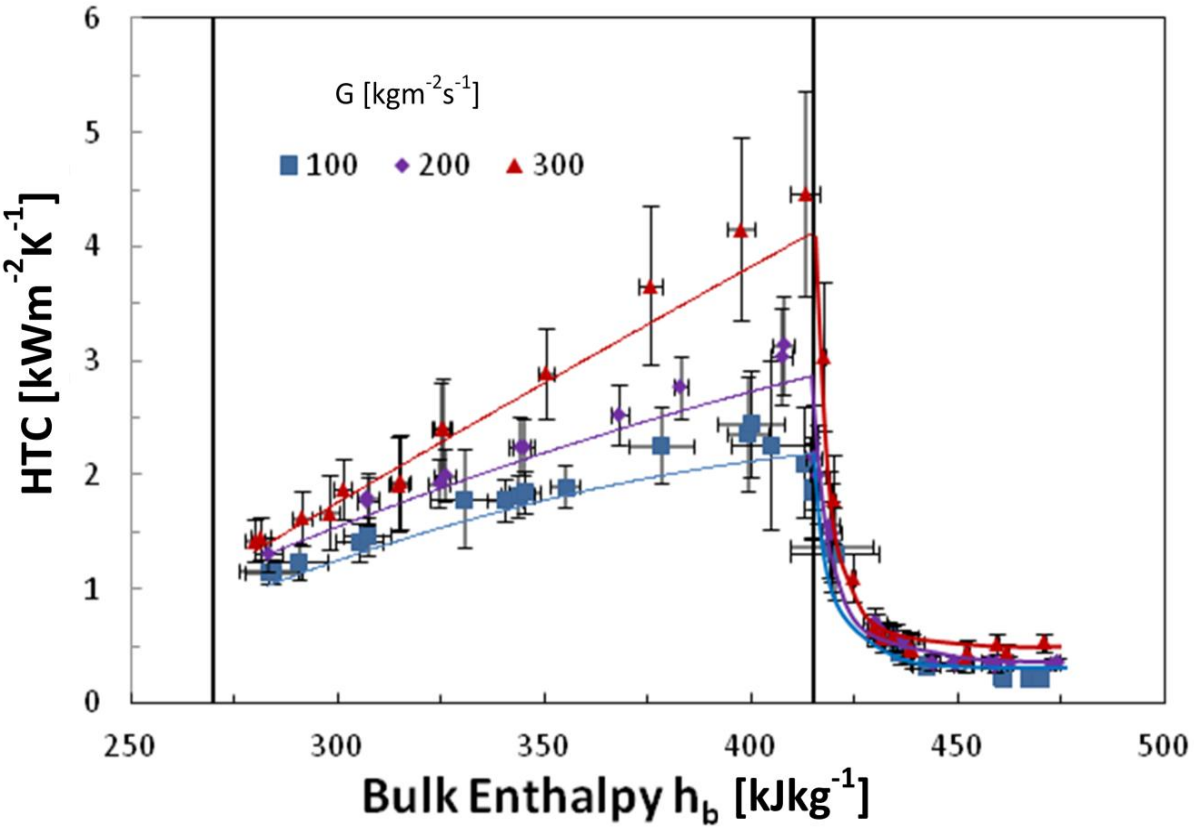

Figure 4.5: Effect of mass flux on HTC for R1234ze(E) at T_{sat} = 50 ^{0}C, Q = 10 kWm^{-2}

The effect of mass flux, however, diminishes at low qualities as higher mass flux results in greater film thickness at wall increasing the resistance from liquid. Thus the effect of high vapor velocity is diminished by greater film thickness. It can be seen that Cavallini and Kondo-Hrnjak correlations captures the effect of mass flux on HTC fairly well. The increase in experimental deviation from correlations at very high qualities can be a result of presence of mist flow regime which is not taken into account in the Cavallini correlation. Mist flow would allow liquid entrainment into vapor core which reduces film thickness resulting in higher HTC.

4.2.2 Effect of Heat Flux

Figure 4.6 shows the HTC of R1234ze(E) at 100kgm^{-2}s^{-1}, 30 ^{0}C saturation temperature at various heat fluxes. It has been observed that the HTC in two phase zone increases slightly when the heat flux is increased from 5 to 10 kWm^{-2} but it remains constant from 10 to 25 kWm^{-2}. Nusselt condensation theory, which is used in most correlations, suggests that HTC should decrease with increase in heat flux on account of larger film thickness which increases resistance on the refrigerant side. This theory, however, was proposed for laminar free convection condensation assuming quiescent vapor ignoring the effect of forced convection of the vapor. Experimental data shows that the effect of heat flux is limited and similar trend was observed for condensation of CO_2 in smooth tubes (Kondou and Hrnjak, 2012). Since the tube wall temperature decreases as heat flux increases condensation is seen to begin at higher bulk temperatures for higher heat flux operating conditions.

4.2.3 Effect of Saturation Temperature

Figure 4.7 shows the comparison of HTC for R1234ze(E) at saturation temperature of 30, 40 and 50 ^{0}C. The effect of saturation temperature is not as significant as mass flux as the HTC increases/decreases due to change in thermo physical properties of the refrigerant which do not vary drastically in these operating conditions. However, as pressure increases the vapor density of refrigerant increases lowering the vapor velocity. Also, the decrease in liquid thermal conductivity, Pr and latent heat increases the resistance in the refrigerant side. The combined effect of these thermo-physical properties reduces the HTC with increase in pressure. It is also to be noted that the HTC is well predicted by Cavallini correlation at saturation temperature of 50^{0}C but the correlation starts to deviate at lower saturation conditions.

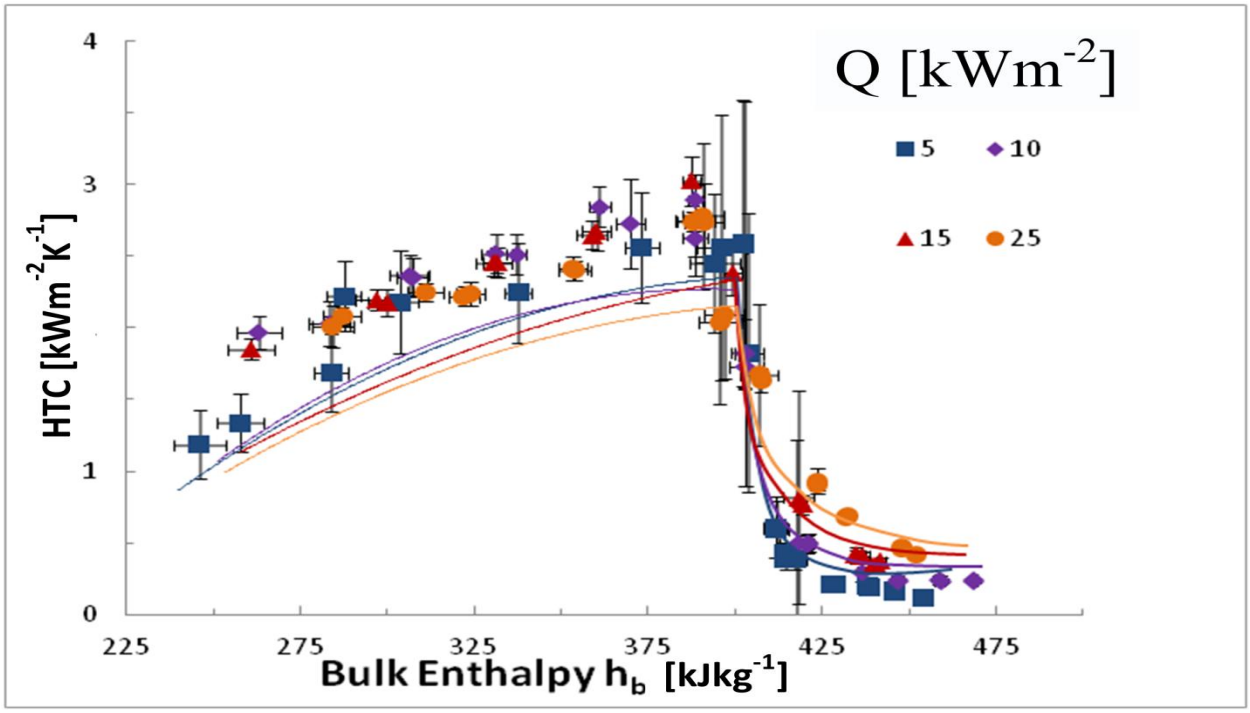

Figure 4.6: Effect of heat flux on HTC for R1234ze(E) at G= 100 kgm^{-2}s^{-1} and T_{sat} = 30 ^{0}C

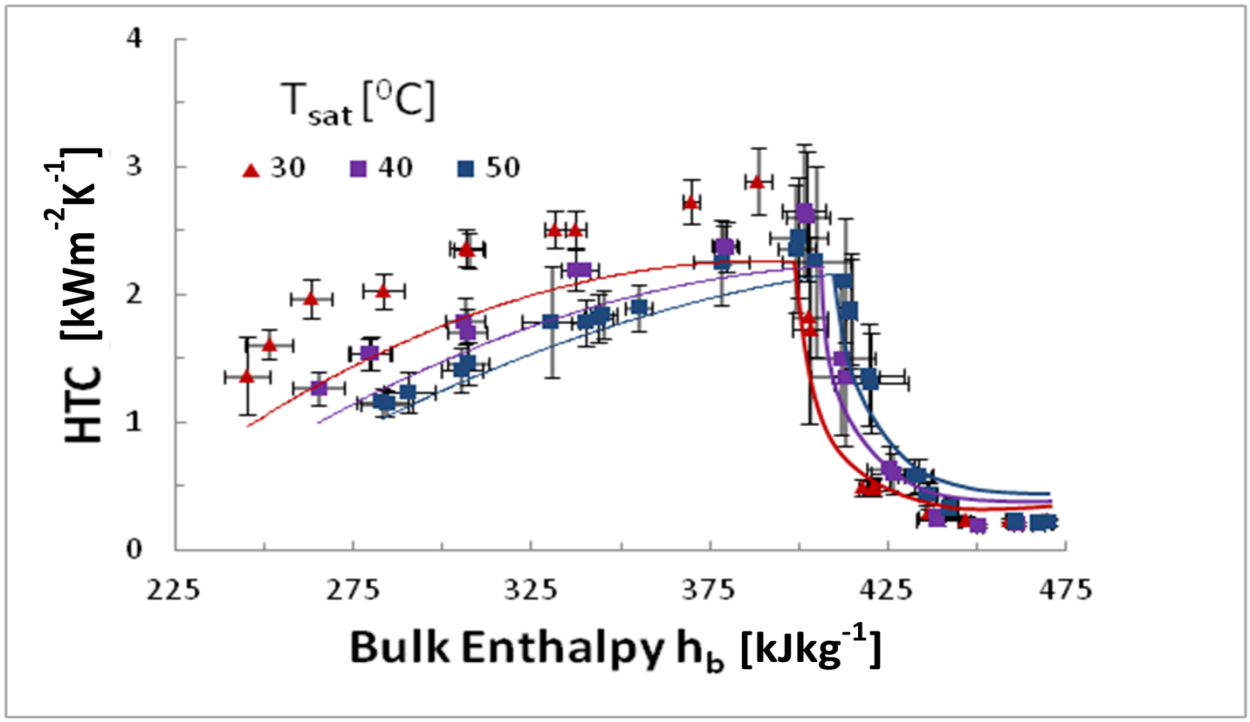

Figure 4.7: Effect of T_{sat} on HTC for R1234ze(E) at G=100 kgm^{-2}s^{-1}, Q=10 kWm^{-2}

4.3 Comparison of HTC for Different Refrigerants

R1234ze(E) is currently considered to be a potential replacement for R134a due to its similar thermo physical properties and low GWP and especially in mixtures with R32 that would bring it even closer to be almost drop in replacement. The heat transfer performance for R1234ze(E), however, has not been widely established yet. Hence, a comparative study between the two refrigerants has been done to establish a baseline. It has been known that R32 has favorable thermo physical properties like high latent heat, high liquid thermal conductivity for heat transfer in condensation. Therefore one of the potential methods to improve the performance of automotive systems is to replace R134a with a mixture of R1234ze(E) and R32. The experimental data in this paper can be used as a comparison for R1234ze(E) and R32 mixture to ascertain the degradation in HTC.

4.3.1 Heat Transfer Coefficient

Figure 4.8 shows the HTC and pressure drop for the three refrigerants at same operating conditions. The HTC of R134a is slightly higher than R1234ze(E). The refrigerants do not show much variation owing to similar thermo physical properties which determines HTC. The properties of R32, however, are better suited for condensation process due to higher latent heat, Pr and liquid thermal conductivity as shown in Table 4.1. As a result, R32 displays much higher HTC compared to R1234ze(E) and R134a. Thus a mixture of R32 and R1234ze(E) is a potential option to improve the performance in automotive and stationary systems. The HTC has been well predicted by Cavallini correlation in all three cases.

4.3.2 Pressure Drop

The pressure drop gradient for R1234ze(E) is seen to be significantly higher than R134a from Figure 4.8. The lower vapor density of R1234ze(E) results in higher velocity at same mass flux as R134a. This results in a higher slip at liquid vapor interface increasing frictional pressure drop. High vapor density of R32 results in a much lower pressure drop compared to R134a and R1234ze(E). The pressure drop data is in good agreement with Friedel (Friedel, 1979) correlation in two phase region. However, pressure drop in superheated region decreases with

increase in enthalpy indicating that condensation in superheated region effects pressure drop and a new model needs to be developed for pressure drop in CSH zone.

Thus, R32, with higher HTC and lower pressure drop gradient potentially has the benefits of being used as a component in a mixture. The flammability of the refrigerant, however, may still pose a problem.

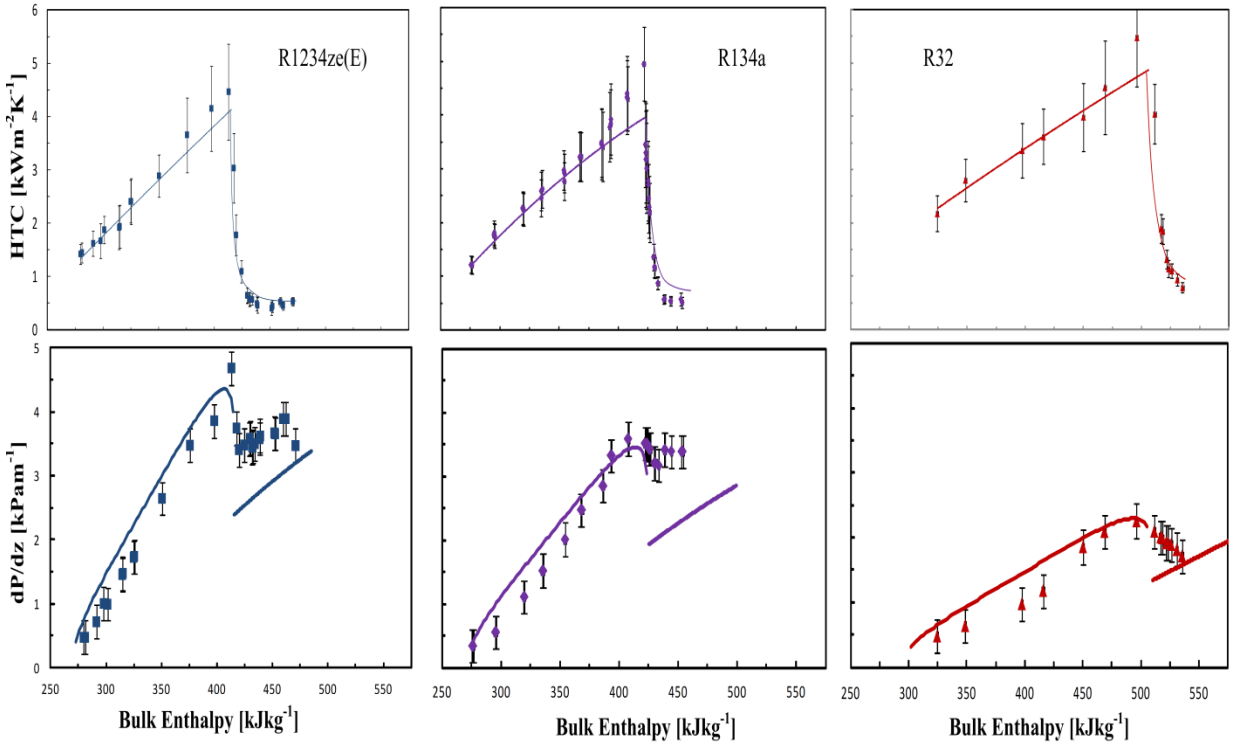

Figure 4.8: HTC and Pressure drop comparison between R1234ze(E), R134a and R32 at G=100 $kgm^{-2}s^{-1}$, T_{sat} = 50^0C, Q=10 kWm^{-2}

Table 4.1: Thermo physical properties of refrigerants of interest

T_{sat} = 40^0C	Psat (MPa)	ρ_l (kg/m^3)	ρ_v (kg/m^3)	h_{lv} (kJ/kg)	λ_l mW/(m.K)	Cp_l kJ/(kg.K)	μ_l (µPa s)	Pr_l	σ_l (mN/m)	GWP
R1234ze(E)	0.77	111.3	40.7	154.6	69.3	1.4	167	3.48	6.96	6
R134a	1.016	1146.7	50.1	163.1	74.7	1.5	161.5	3.24	6.12	1300
R32	2.49	893.4	73.3	237.1	114.6	2.16	95	1.79	4.47	550

4.4 Comparison of Experimental Data to Prediction

The experimental data obtained in the study has been compared to well known correlations and the proposed model. Since the correlations available in literature are proposed for two phase flows, Kondo-Hrnjak correlation is combined with two-phase correlations to predict data set in condensing superheat zone and the data in the sub-cooled region is not taken into account. However, the proposed model takes into account all the data points and thus gives good overall prediction accuracy.

4.4.1 Comparison to Correlations from Literature

The HTC from the experiments have been compared to well-known correlations by Cavallini et al. (2006), Thome et al. (2003), Jung et al. (2003), Dobson & Chato (1998) and Haraguchi et al. (1994). Table 4.2 lists the deviation of correlations from experimental data. Since the correlations mentioned above were developed for two phase flows the condensation in CSH zone is predicted with Kondo-Hrnjak correlation which is a function of selected two-phase correlation.

Figure 4.9 to 4.13 compares predicted results with experimental data for all five correlations. Correlations of Cavallini and Thome predicted the data with mean deviation of 12.1% and 10.5% respectively. It is noted that correlation by Cavallini et al. (2006) doesn't capture HTC at high qualities well as it takes only annular flow regime into account at high qualities. The film thickness at high qualities could be less than assumed in annular flow which would lead to under prediction of HTC. The correlation proposed by Thome et al. (2003) is based on flow regime map and it seems to capture HTC at high qualities fairly well. Dobson and Chato (1998) developed the correlation with the assumption that ratio of HTC in single and two-phase is a function of Martinelli's parameter. Since the effect of mass flux and latent heat were not taken into account, the correlation predicted the data with a deviation of 27.2%. Jung et al. considered the effect of these parameters and modified Dobson and Chato correlation by including heat to mass flux ratio in the correlation which predicted experimental data slightly better with 17% deviation. Haraguchi et al. (1994) predicted data for R1234ze(E) and R134a reasonably well but failed to capture data for R32.

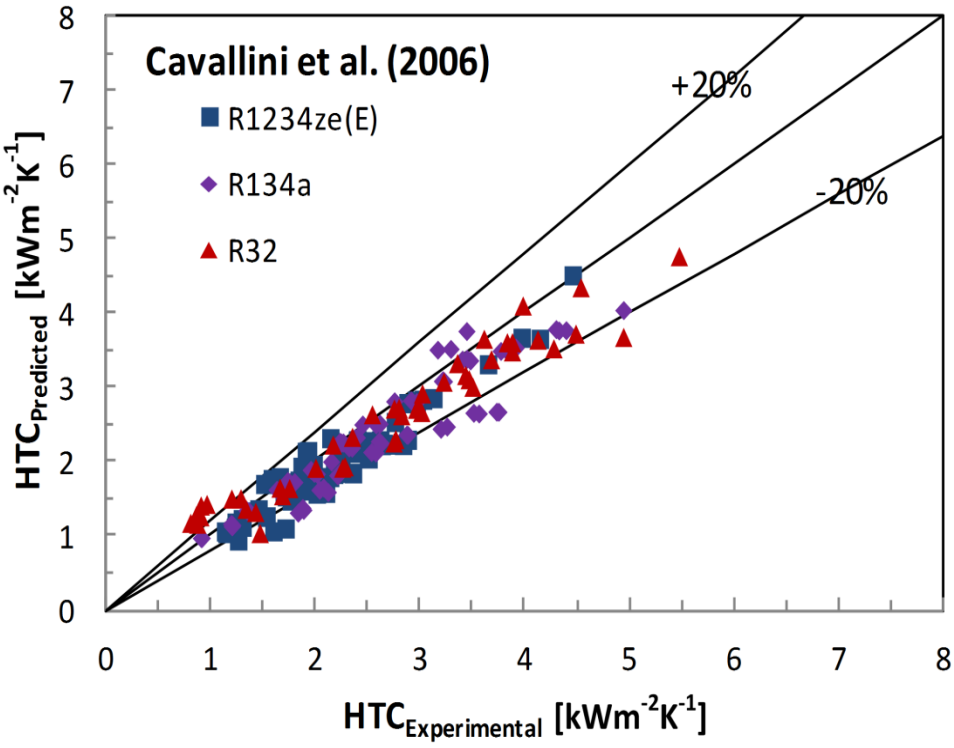

Figure 4.9: Comparison of experimental data to Cavallini et al.

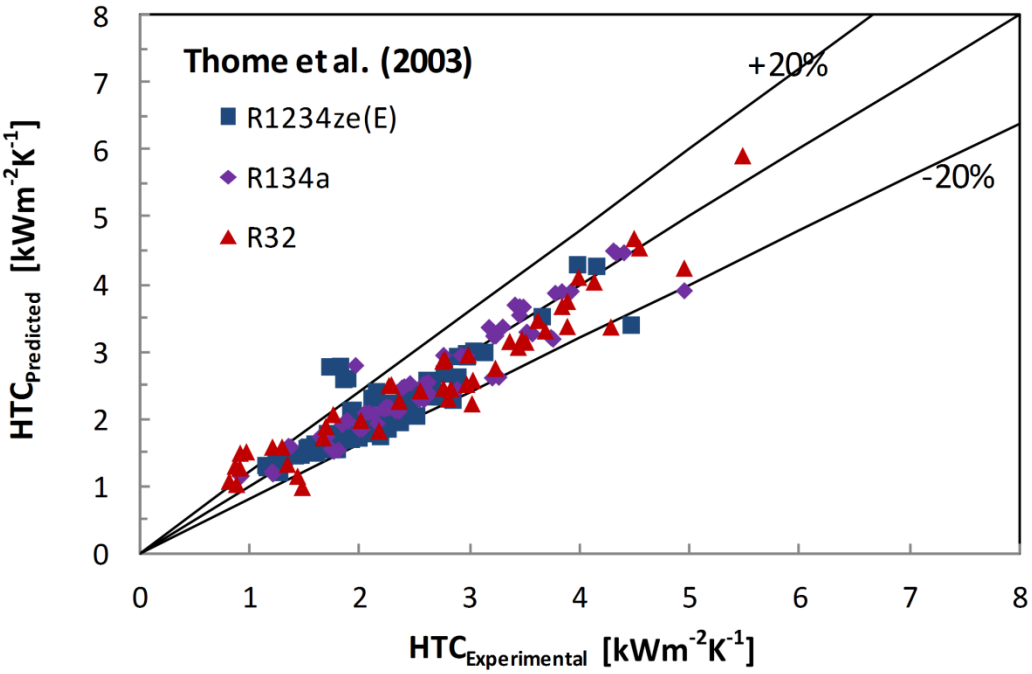

Figure 4.10: Comparison of experimental data to Thome et al.

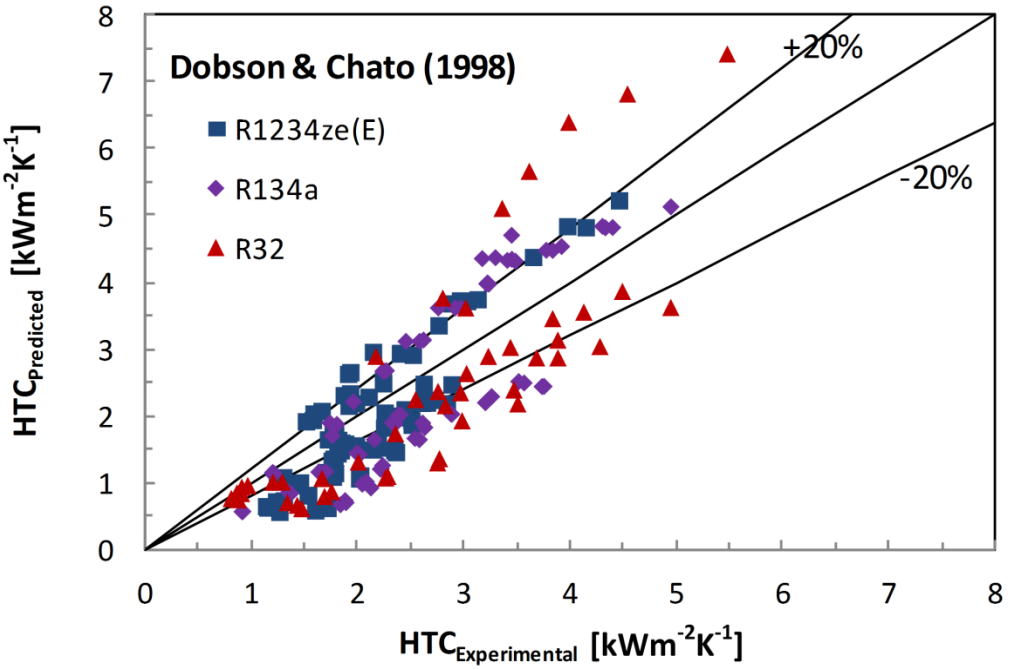

Figure 4.11: Comparison of experimental data to Dobson & Chato

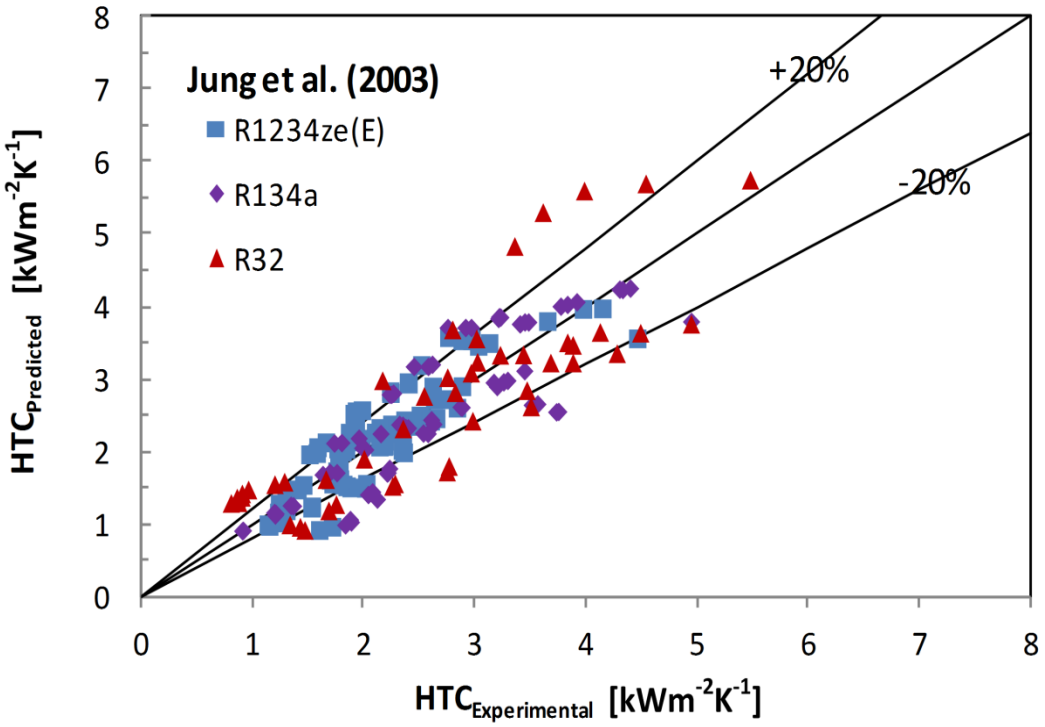

Figure 4.12: Comparison of experimental data to Jung et al.

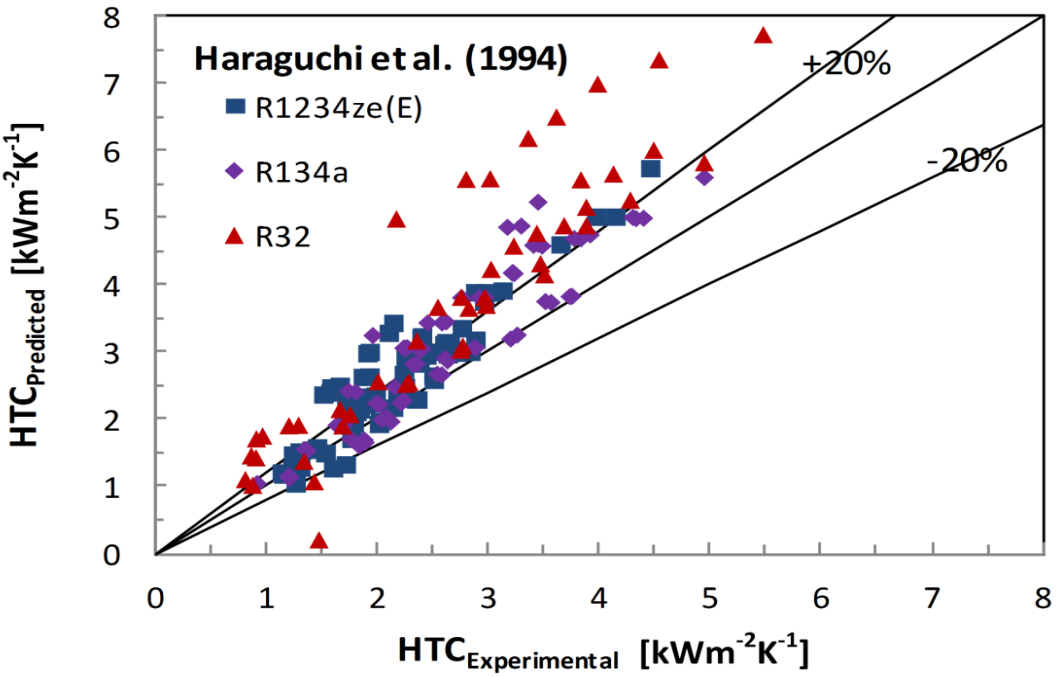

Figure 4.13: Comparison of experimental data to Haraguchi et al.

4.4.2 Comparison to the Proposed Model

The model has been compared to experimental data for R1234ze(E), R134a and R32 for condensation in superheated, two phase and sub-cooled region. Table 4.3 shows the deviation of experimental HTC from the model for 3 refrigerants. The prediction for condensation in superheated and two-phase regions is reasonably accurate. However, the model does not predict the HTC in sub-cooled region with great accuracy. This could be attributed to the fact that the sub-cooling accounted in the model is based only on flow regimes of annular and stratified/stratified wavy flows. The area associated with sub-cooling is not entirely accurate as it does not take the transition from annular to slug/plug flows into account. Hence, the simplistic approach for sub-cooling calculations leads to deviation of model from experimental data. Overall deviation of experimental data from the model has also been shown in figure 4.14. From figure 4.15 is seen that the model accurately predicts the transition point for CSH zone which strengthens the argument of wall temperature being the driving force behind the start of condensation. Also the summary of experimental results indicates that the model works well for different refrigerant at different operating conditions with accurate prediction of local HTC.

Table 4.2: Mean Absolute Deviation of various correlations against experimental data

Refrigerant	Cavallini/Kondo-Hrnjak		Thome/Kondo-Hrnjak		Jung/Kondo-Hrnjak		Dobson & Chato/Kondo-Hrnjak		Haraguchi/Kondo-Hrnjak	
	Two phase (%)	CSH (%)	Two phase (%)	CSH (%)	Two phase (%)	CSH (%)	Two phase (%)	CSH (%)	Two phase (%)	CSH (%)
R1234ze(E)	12	28	10	25	14	22	25	26	20	40
R134a	11	24	8	22	15	19	27	28	19	42
R32	14	16	15	28	25	19	30	16	42	24
Overall	12.1	22.8	10.5	24.8	16.9	20	27.2	23.7	25	36.2

Table 4.3: Mean Absolute Deviation of proposed model against experimental data

Refrigerant	Condensation Zone			Overall
	Superheated	Two-phase	Sub-cooled	
R1234ze(E)	12.9	14.5	26.6	15.7
R134a	17.6	13.9	19.3	16.3
R32	13.2	15.8	27.1	15.5
Overall	14.5	14.6	24.8	15.8

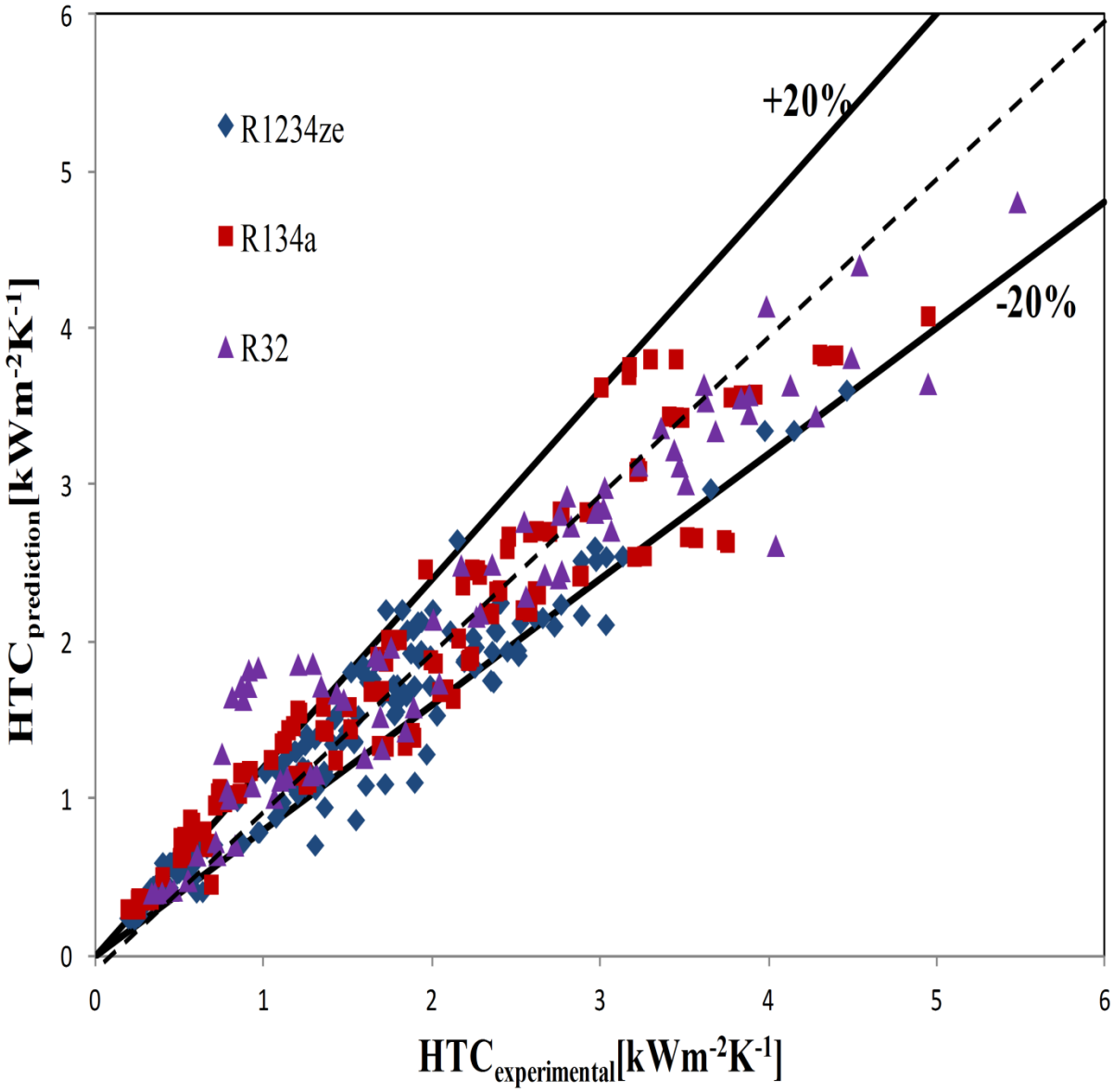

Figure 4.14: Comparison of experimental HTC with proposed model

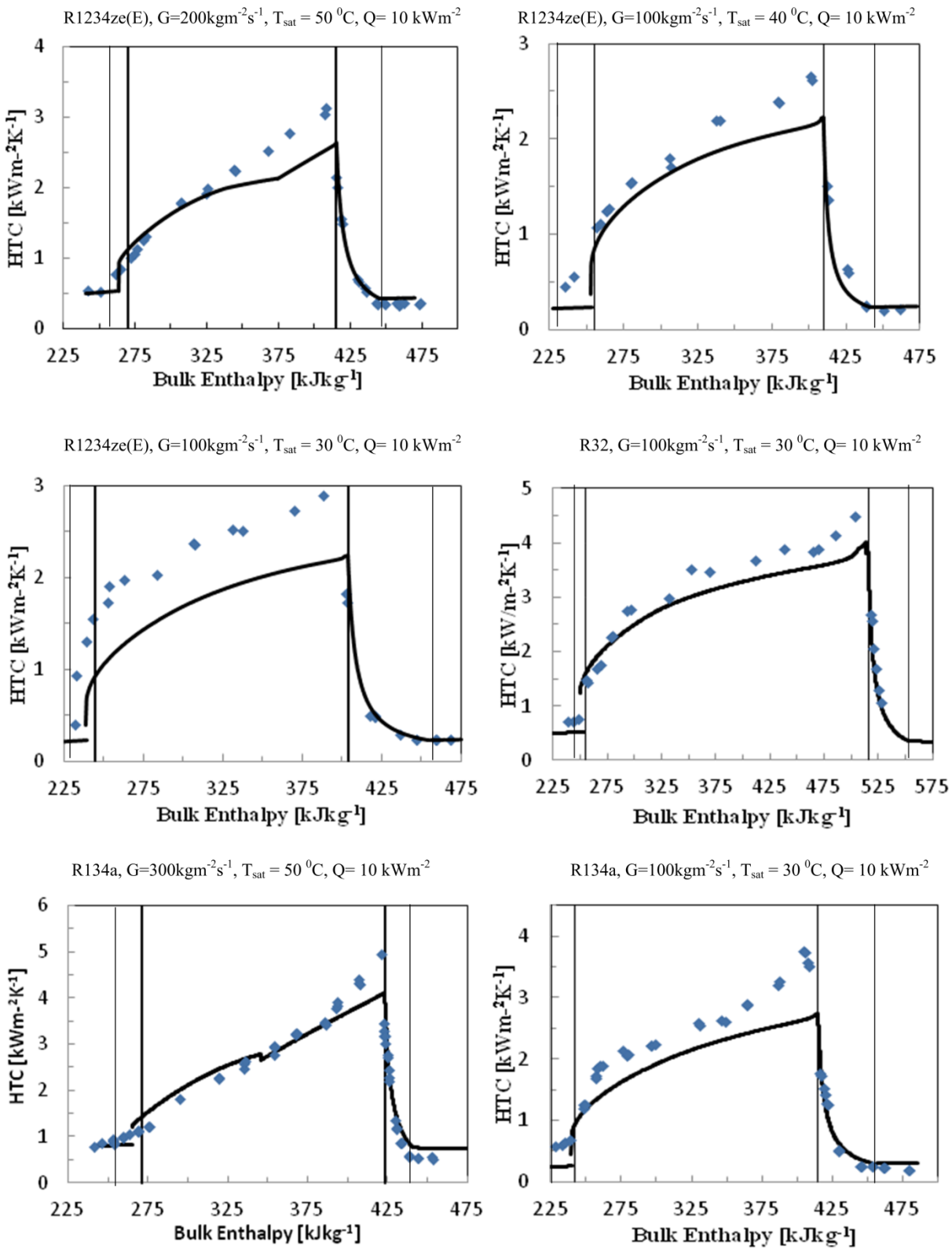

Figure 4.15: Summary of experimental data and comparison with proposed model

4.5 Summary of Experimental Results

Figure 4.18 to 4.20 shows experimental and predicted HTC of the three refrigerants where the lines show the prediction by Cavallini and Kondo-Hrnjak correlation in two-phase and superheated condensing zone respectively. The predicted HTC agrees with experimental data for all the refrigerants at given conditions.

The HTC has been plotted in P-h diagram to gain a better understanding of the condensation process in condensers at various pressures and analyze the importance of condensing superheated zone. As the latent heat of the refrigerant reduces with increase in pressure the capacity of condensers is more affected by heat transfer in condensing superheated zone. This becomes extremely important for refrigerants operating near critical point where latent heat is very small. The effect has been quantified with CO_2 by Kondo & Hrnjak (2012)

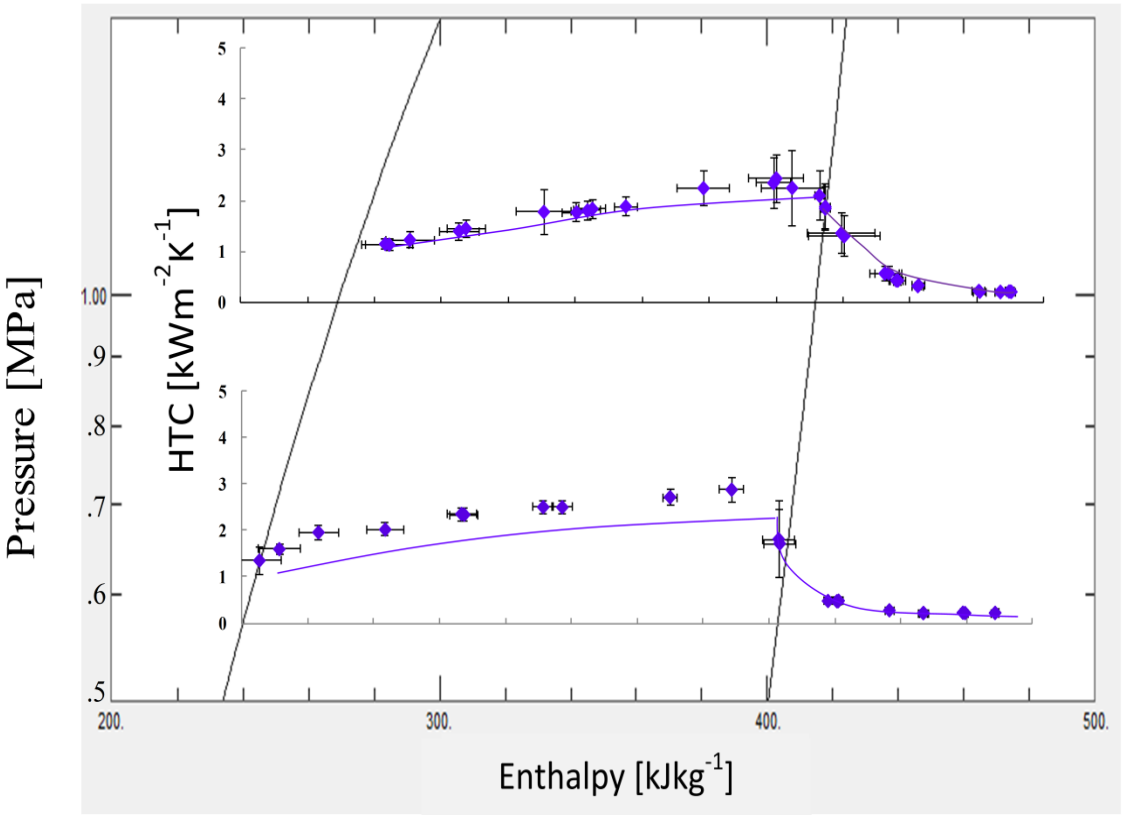

Figure 4.16: Variation of HTC with pressure and enthalpy for R1234ze(E)

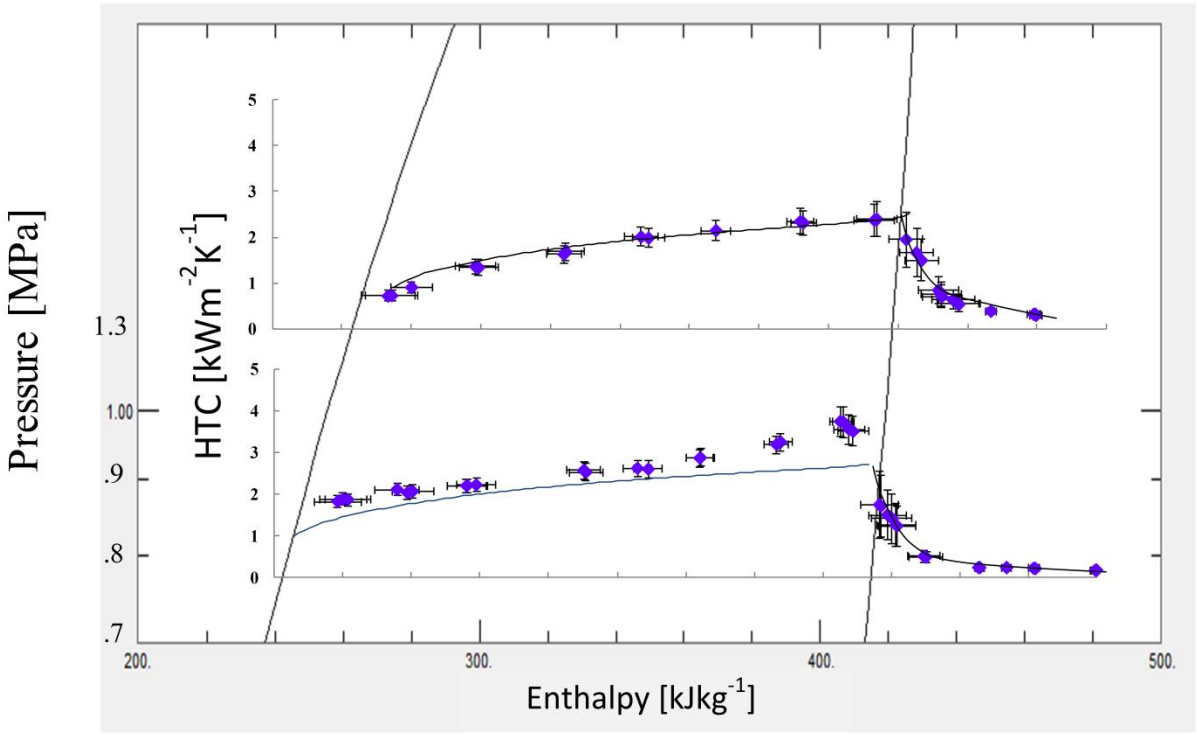

Figure 4.17: Variation of HTC with pressure and enthalpy for R134a

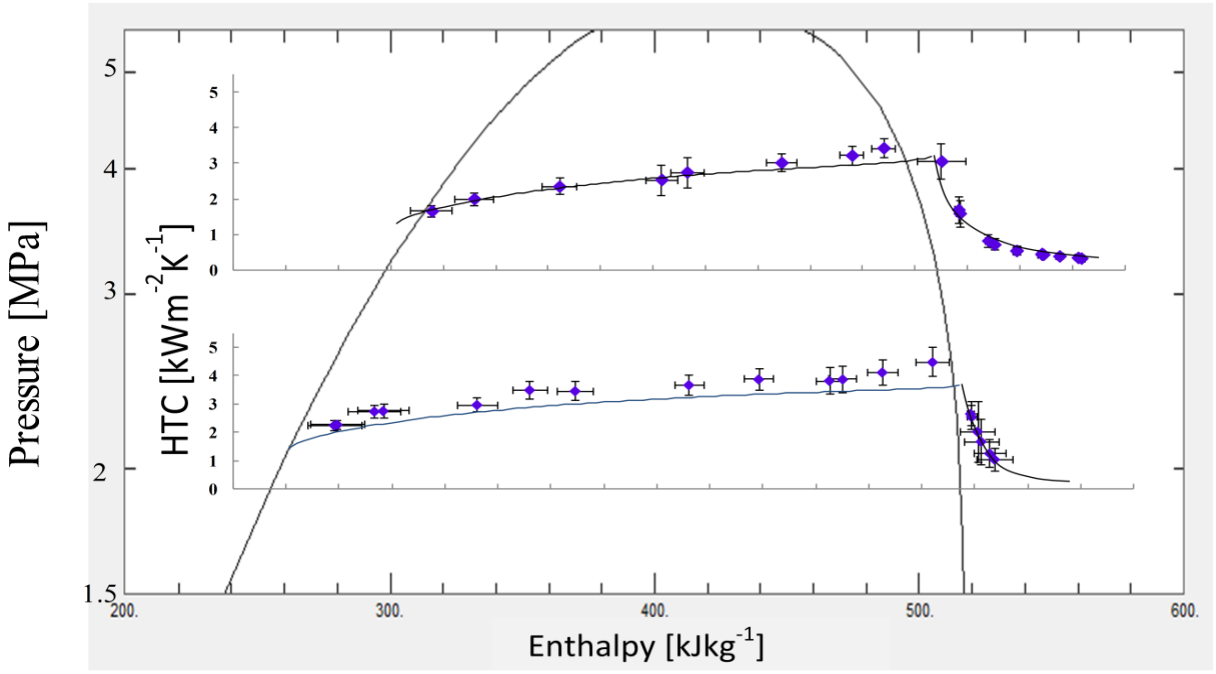

Figure 4.18: Variation of HTC with pressure and enthalpy for R32

CHAPTER 5

SUMMARY, CONCLUSIONS & RECOMMENDATIONS

5.1 Summary and Concluding Remarks

A new heat transfer model based on the principle of energy conservation in horizontal tubes has been proposed which asymptotically satisfies the single phase correlations by taking the sensible heat rejection in condensation into account. The presence of liquid in de-superheating region accounts for the discontinuity in condensing superheated zone while the presence of vapor in sub-cooled region has been seen to effect the heat transfer coefficient near x=0. Liquid sub-cooling in two-phase region is quantified which explains the smooth transition from two-phase to sub-cooled zone. Thus the model eliminates the discontinuity at very high and low qualities predicting experimental data within 16% accuracy. The model includes well known correlations of Cavallini and Gnielinski taking flow regime into consideration. This is the first attempt to include and quantify the effect of sensible heat in two phase zone and the model can be improved by taking a more detailed approach in terms of flow regime and other two-phase correlations available in literature.

The results from the model have been validated by experiments conducted with different refrigerants at various operating conditions. Experiments have been conducted for R134a, R1234ze(E) and R32 for mass fluxes of 100-300 $kgm^{-2}s^{-1}$, saturation temperatures of 30^0 C-50^0 C and from sub-cooling of 20 ^{0}C to superheat of 50 ^{0}C in a horizontal smooth tube with 6.1 mm inner diameter. The beginning of condensation in superheated zone has been proved to be the criteria $T_{wall}<T_{sat}$ by observing the wall temperature and deviation of experimental HTC from single phase correlations simultaneously. It has also been shown through experiments that HTC in sub-cooled region is much higher than single phase predictions due to presence of vapor as seen in the sight glass located at the end of the test section. The effect of various parameters on HTC has been quantified and analyzed to present a thorough study of condensation process. The results are also compared to well known correlations available in literature with satisfactory agreement.

The following points are considered to be the most important takeaways from the work presented:

- Condensation in a tube occurs not only in two phase zone but also in superheated and sub-cooled zone due to presence of liquid and vapor respectively.
- The transition from superheated to condensing superheated zone is seen when the wall temperature drops below saturation temperature of refrigerant where the HTC starts deviating from the Gnielinski correlation and approaches the HTC at x=1.
- HTC is seen to be significantly greater than single phase predictions near x=0 in sub-cooled zone due to presence of saturated vapor with sub-cooled liquid film.
- The model proposed in this work successfully takes into account the effect of sensible heat rejection in condensation providing a better physical explanation of the process. The model is validated by the experimental results to be within 16 % accurate.
- HTC increases significantly with mass flux, decreases slightly with increase in saturation temperature and practically not affected by heat flux. Among the correlations available in literature HTC is fairly well predicted by Thome/Cavallini and Kondo-Hrnjak correlations in two-phase and superheated-condensation zone respectively.
- Pressure drop is well captured by Friedel correlation for all the refrigerants at various operating conditions in the two phase zones and experiments suggests that pressure drop is affected due to the presence of liquid film in CSH zone.
- R1234ze(E) has very similar heat transfer characteristics as R134a due to close thermo-physical properties. However, R1234ze(E) exhibits much higher pressure drop which should be considered while using it as a drop-in replacement.
- R32 has higher HTC and lower pressure drop than R1234ze(E) and R134a and hence is a feasible option to be considered as a mixture component to improve the heat transfer performance in automotive systems.

5.2 Recommendations for Future Study

The work presented in the thesis is an attempt to explain the process of condensation from de-superheating to sub-cooled zone from a physical point of view. The assumptions taken in the model like heat leak, uniform properties on the perimeter of tube can be refined to give more accurate results. Although the model proposed is based on first principle it still is dependent on the correlations proposed for two phase zones. The future work of this study is to conduct experiments with flow visualization which will give a better explanation of the flow regimes and the process of condensation in the transition zones. The sight glass installed in this study at the end of test section was not appropriate for visualization. Hence, a transparent tube downstream of test section will be installed and experiments can also be conducted with the test in the transparent section itself. One of the objectives to perform this test is to measure film thickness in the test section. From a practical point of view the thickness of liquid film is the key to find the exact proportion of sensible and latent heat rejection in the process. Once, the film thickness is known more physical models can be proposed for condensation in superheated zone.

It has been pointed out throughout this work that R32 can be used as a component in a mixture with R1234ze(E) to be used as a replacement in automotive systems. The experimental data taken in the thesis can be used as a baseline to analyze the effect of mixtures on HTC. Since, experiments have been conducted with R1234ze(E), R134a and R32 it would be facilitate comparison of HTC of mixtures with individual component and R134a. Previous studies with zeotropic mixtures which indicates that the concentration of individual component have a huge impact on the degradation of HTC in mixtures. The temperature glide of mixture which is also a function of concentration ratio affects the HTC as well. Hence effort should be made to find the ideal concentration ratio of R1234ze(E) and R32 which can show similar heat transfer performance as R134a. The concentration ratio, however, depends on various other factors viz. flammability, GWP etc. and caution should be taken to select a mixture with realistic concentrations acceptable in industries.

APPENDIX A

CALIBRATION RESULTS

A.1 Thermocouple Calibration

Table A.1: Thermocouples electro motive force at different temperatures (unit: ^{0}C, mV)

Temp	21.065	14.420	13.690	20.095	30.895	30.915	43.072	33.980	34.000
1T	0.840	0.579	0.546	0.797	1.234	1.232	1.722	1.355	1.354
1R	0.841	0.580	0.547	0.798	1.234	1.232	1.722	1.356	1.355
1B	0.840	0.579	0.547	0.797	1.232	1.231	1.720	1.354	1.353
1L	0.840	0.580	0.547	0.798	1.233	1.231	1.719	1.353	1.352
2T	0.840	0.578	0.546	0.796	1.234	1.232	1.722	1.354	1.353
2R	0.842	0.580	0.547	0.798	1.235	1.233	1.719	1.354	1.351
2B	0.840	0.579	0.546	0.797	1.234	1.232	1.722	1.355	1.354
2L	0.841	0.580	0.546	0.796	1.233	1.231	1.721	1.355	1.354
3T	0.840	0.579	0.547	0.798	1.234	1.233	1.720	1.340	1.341
3R	0.837	0.579	0.546	0.796	1.232	1.230	1.720	1.354	1.353
3B	0.841	0.580	0.547	0.798	1.234	1.232	1.722	1.356	1.355
3L	0.840	0.579	0.546	0.797	1.232	1.230	1.720	1.354	1.353

Temp	22.177	22.152	16.197	38.190	44.802	44.845	49.755	49.762	55.470
1T	0.890	0.887	0.647	1.518	1.787	1.786	1.989	1.991	2.234
1R	0.891	0.888	0.649	1.519	1.787	1.789	1.989	1.991	2.234
1B	0.890	0.888	0.647	1.517	1.785	1.787	1.987	1.990	2.232
1L	0.890	0.888	0.648	1.516	1.784	1.786	1.985	1.986	2.231
2T	0.888	0.886	0.645	1.519	1.789	1.792	1.993	1.995	2.235
2R	0.887	0.891	0.643	1.521	1.792	1.793	1.996	1.998	2.238
2B	0.890	0.888	0.647	1.520	1.790	1.791	1.993	1.995	2.235
2L	0.892	0.890	0.648	1.517	1.786	1.788	1.989	1.991	2.230
3T	0.872	0.876	0.634	1.520	1.791	1.793	1.996	1.998	2.236
3R	0.890	0.888	0.648	-1.552	-5.679	-5.695	-6.448	-5.240	-5.121
3B	0.890	0.889	0.649	1.518	1.790	1.792	1.995	1.997	2.235
3L	0.892	0.888	0.648	1.516	1.788	1.789	1.992	1.994	2.231

Temp	55.97	62.137	62.082	42.805	37.935	26.830	36.900	36.920	42.165
1T	2.252	2.525	2.523	1.711	1.513	1.069	1.464	1.467	1.678
1R	2.251	2.523	2.522	1.710	1.510	1.069	1.463	1.466	1.677
1B	2.250	2.523	2.522	1.709	1.509	1.066	1.461	1.464	1.677
1L	2.248	2.521	2.520	1.708	1.508	1.067	1.462	1.465	1.677
2T	2.253	2.526	2.525	1.711	1.509	1.066	1.463	1.467	1.678
2R	2.256	2.529	2.528	1.707	1.503	1.068	1.465	1.468	1.680
2B	2.253	2.527	2.525	1.711	1.510	1.066	1.463	1.466	1.679
2L	2.248	2.521	2.521	1.711	1.510	1.066	1.461	1.464	1.675
3T	2.253	2.527	2.525	1.704	1.507	1.066	1.465	1.468	1.680
3R	-4.88	-4.797	-4.907	1.708	1.509	1.065	1.461	1.464	1.676
3B	2.252	2.525	2.524	1.711	1.511	1.064	1.463	1.466	1.678
3L	2.248	2.521	2.520	1.709	1.509	1.063	1.461	1.465	1.676

Table A.2: Calibration results

	a3	a2	a1	a0	2σ
1T	-0.52125	1.71077	23.43247	0.44586	0.149
1R	-0.49007	1.56250	23.67289	0.31250	0.149
1B	-0.49586	1.55819	23.72615	0.30389	0.150
1L	-0.53664	1.74846	23.49660	0.37002	0.142
2T	-0.40298	1.16498	24.14053	0.20820	0.141
2R	-0.42176	1.20013	24.15775	0.15666	0.159
2B	-0.42499	1.25572	24.04528	0.21288	0.149
2L	-0.48931	1.56131	23.68766	0.31551	0.184
3T	-0.17860	0.11364	25.54355	-0.23631	0.226
3R	-0.89902	2.84900	22.41952	0.72722	0.180
3B	-0.35502	0.92952	24.52264	-0.00702	0.167
3L	-0.38174	1.06129	24.36817	0.06421	0.176

Standard deviation: $2\sigma = 0.16$ [K], $T = a3\,E^3 + a2\,E^2 + a1\,E + a0$ [^oC] E [mV]

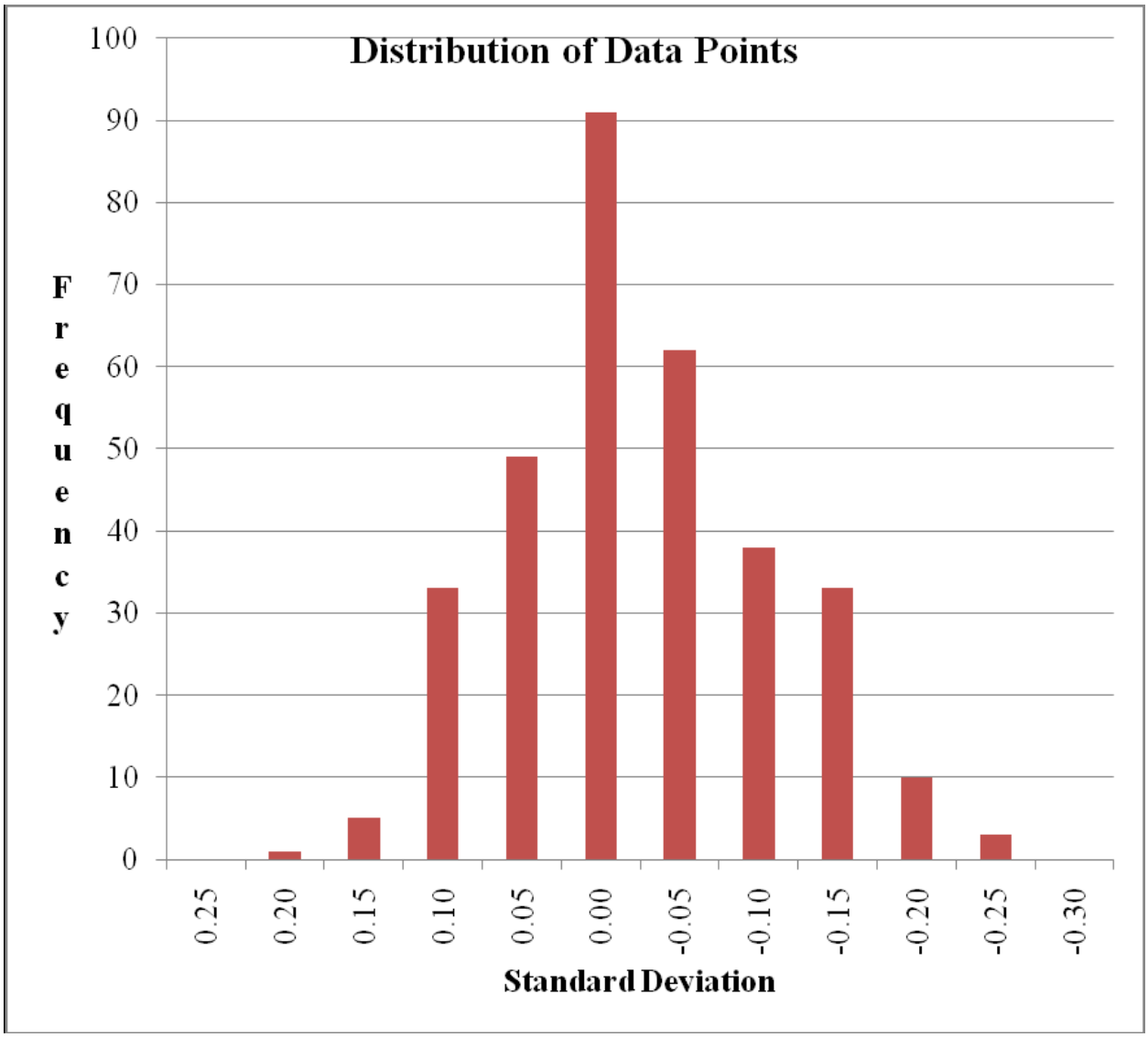

Figure A.1: Frequency Distribution of calibration data

Table A.3: Verification of Thermocouple calibration using Precision Thermocouple

Precision [^{0}C]	Thermocouple 1 [^{0}C]	Thermocouple 2 [^{0}C]	Precision [^{0}C]	Thermocouple 1 [^{0}C]	Thermocouple 2 [^{0}C]
10.274	10.2	10.23	30.213	30.01	30.16
10.277	10.2	10.25	30.218	30.01	30.16
10.283	10.2	10.28	30.213	30.08	30.18
10.278	10.13	10.23	30.216	30.03	30.16
10.275	10.18	10.25	30.213	30.03	30.18
10.278	10.1	10.23	30.215	30.03	30.16
10.278	10.18	10.23	30.214	30.03	30.13
10.28	10.18	10.23	30.213	30.01	30.16
10.277	10.18	10.23	30.215	30.01	30.13
10.276	10.2	10.23	30.212	30.01	30.13
10.276	10.18	10.17	30.214	30.03	30.16
10.28	10.18	10.23	30.212	30.03	30.16
10.281	10.23	10.23	30.215	30.03	30.16
10.281	10.18	10.17	30.212	30.01	30.16
10.282	10.18	10.23	30.215	30.01	30.13
20.249	20.13	20.16	40.18	40.01	40.13
20.252	20.15	20.16	40.18	40.01	40.1
20.251	20.1	20.16	40.176	39.99	40.1
20.253	20.13	20.16	40.178	40.01	40.1
20.252	20.13	20.16	40.177	39.94	40.06
20.252	20.13	20.16	40.179	39.94	40.08
20.255	20.1	20.16	40.18	40.01	40.1
20.249	20.1	20.16	40.181	39.99	40.1
20.251	20.1	20.16	40.181	39.99	40.18
20.25	20.13	20.21	40.181	39.94	40.1
20.252	20.13	20.16	40.18	39.99	40.18
20.248	20.13	20.16	40.181	39.92	40.13
20.251	20.13	20.16	50.146	49.9	50.04
20.249	20.13	20.21	50.147	49.9	50.09
20.251	20.1	20.16	50.148	49.9	50.02
50.15	49.9	50.07	50.149	49.9	50.07
50.145	49.95	50.07	50.138	49.95	50.07
50.147	49.88	50.07	50.142	49.97	50.07
50.144	49.95	50.02	50.144	49.95	50.07
50.149	49.9	50.09	50.14	49.95	50.07

A.2 Pressure Transducer Calibration

Table A.4: Pressure Calibration Readings

Pressure [kPa]	Voltage [V]
99.898	0.021
442.898	0.144
700.898	0.237
997.398	0.343
1288.898	0.449
1604.898	0.564
1897.898	0.67
2212.898	0.785
2424.898	0.862

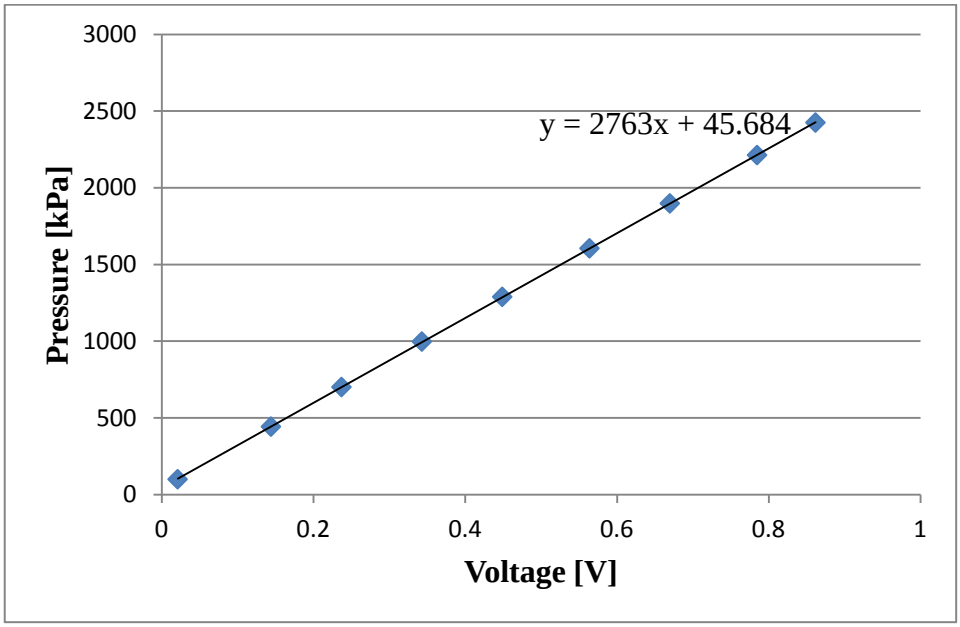

Figure A.2: Calibration of Absolute Pressure Transducer

Table A.5: Pressure Calibration Data

Voltage [V]	Pressure [Kpa]	Voltage [V]	Pressure [kPa]	Voltage [V]	Pressure [kPa]	Voltage [V]	Pressure [kPa]	Voltage [V]	Pressure [kPa]
0.151	100.3	0.474	318.8	0.967	659	1.298	885.6	1.646	1127.6
0.166	108.5	0.485	326.7	0.999	680.2	1.313	897	1.665	1140.7
0.177	117	0.503	340.9	1.01	689.8	1.327	907.7	1.692	1160
0.186	122.6	0.526	356.5	1.025	699.7	1.339	915.2	1.73	1182.9
0.198	130.6	0.549	370.7	1.041	711.6	1.368	935.6	1.766	1210.1
0.205	135.7	0.58	391.6	1.044	711.9	1.385	946.6	1.787	1226.5
0.215	143.6	0.603	409.6	1.079	735.1	1.405	960.2	1.819	1244.6
0.231	153.5	0.63	426.5	1.094	746.4	1.418	970	1.843	1262.2
0.247	164.5	0.653	443.6	1.122	764.6	1.439	984.8	1.868	1279.1
0.264	176.2	0.687	467	1.14	777.2	1.459	999.8	1.885	1291.5
0.288	192.7	0.69	467.2	1.154	788.4	1.471	1007.2	1.913	1310.7
0.299	200.8	0.715	486.7	1.165	794.3	1.495	1020.3	1.943	1329.9
0.311	209.4	0.74	502.9	1.177	804.2	1.505	1029.7	1.963	1347
0.328	220	0.78	530.9	1.19	810.4	1.526	1043.4	1.984	1359.7
0.358	240.5	0.787	536.2	1.199	819.5	1.539	1053.7	1.997	1370.2
0.369	248.3	0.861	585.3	1.205	824.7	1.553	1063.5	2.019	1385.4
0.393	264.8	0.87	592.2	1.237	843.3	1.567	1071.3	2.041	1400.3
0.415	279.4	0.9	612.4	1.249	852	1.587	1085.8	2.061	1415.5
0.439	296.7	0.938	637.9	1.263	862.6	1.602	1097.1	2.084	1428
0.458	308.8	0.947	644.8	1.276	873.1	1.63	1112.9	2.1	1442.7
2.142	1468.5	2.247	1540.3	2.357	1619	2.527	1736.5	3.522	2423.6
2.18	1496.8	2.277	1562.7	2.391	1641.2	3.217	2212.7	3.607	2480.6
2.227	1527.1	2.323	1593.5	2.495	1711.6	3.401	2335.5	3.668	2523.2

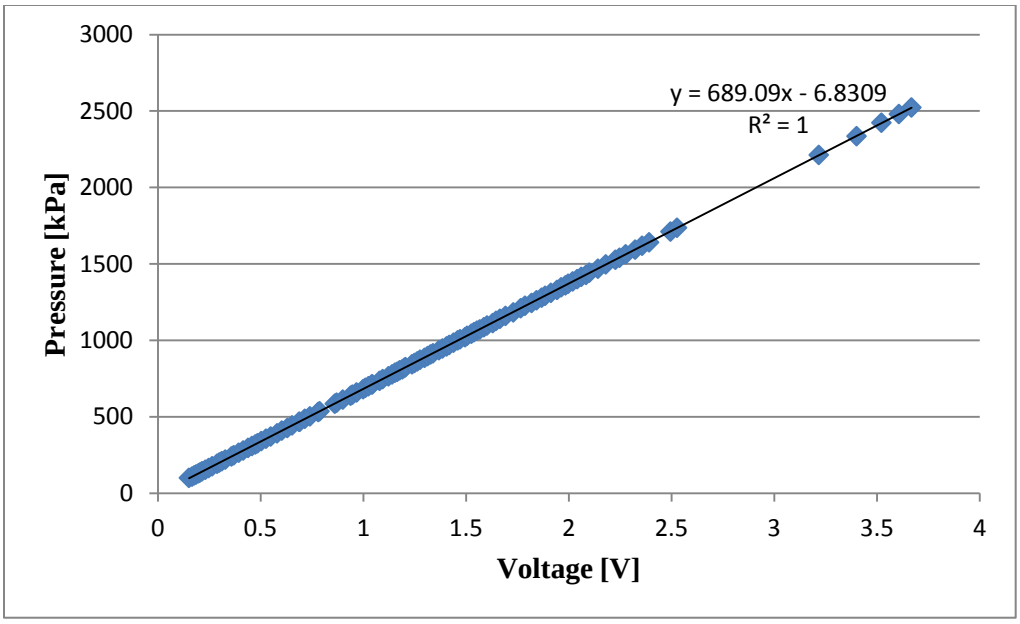

Figure A.3: Calibration of Absolute Pressure Transducer

A.3 Mass Flow Meter Calibration

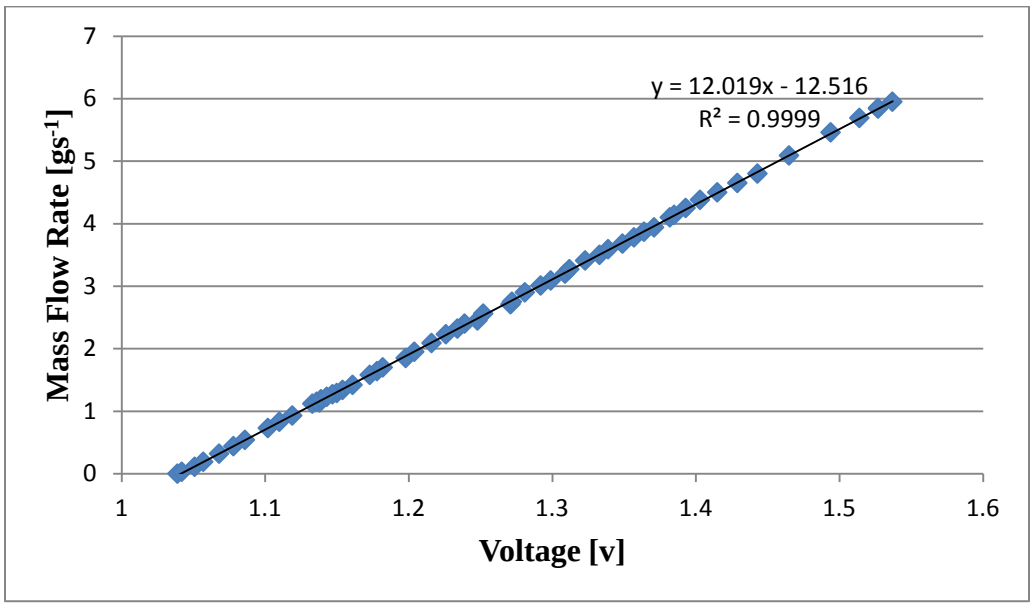

Figure A.4: Calibration of pre-cooler mass flow meter

APPENDIX B

REPEATABILITY TESTS

Repeatability tests were conducted on the experimental set up after instrument calibration, installation of sight glass and any other changes made in the systems. Figure B.1 and B.2 shows the results of repeatability tests conducted for the first time with the same instrumentation used in previous projects with R410A and CO_2. The tests were conducted at two different saturation pressures of 4.6 MPa and 3.3 MPa at mass fluxes of 200$kgm^{-2}s^{-1}$ and 100$kgm^{-2}s^{-1}$ respectively. The data were within 5% accuracy of the previous results.

The mass flow meter calibrated during the experiments was tested against another mass flow meter known to be correctly calibrated. The two mass flow meters were connected in series with water flowing through the channel. The flow rate of water was regulated with a valve and the readings shown by the two mass flow meters were compared. The results, as shown in figure B.3, indicates that the flow rates were very close to each other and hence the mass flow meter readings were repeatable. Repeatability tests for heat transfer coefficient were conducted after mass flow meter calibration with R1234ze(E) at mass flux of 100 $kgm^{-2}s^{-1}$ and saturation temperature 30 ^{0}C. The result was within an acceptable range of ±10% as shown in figure B.4.

The absolute pressure transducer in the system was replaced with a transducer of smaller range to gain better accuracy. The results of the experiments conducted to ensure repeatability of test set up is shown in figure B.5

The system was modified to install sight glass for conducting experiments with sub-cooled liquid. Hence, the section downstream of test section was replaced with a sight glass to visualize the state of the refrigerant at the end of test section to conduct sub-cooling experiments. The repeatability tests for this modification were conducted for R1234ze(E) at mass flux of 300 $kgm^{-2}s^{-1}$ and saturation temperature of 50 ^{0}C. The results are shown in figure B.6

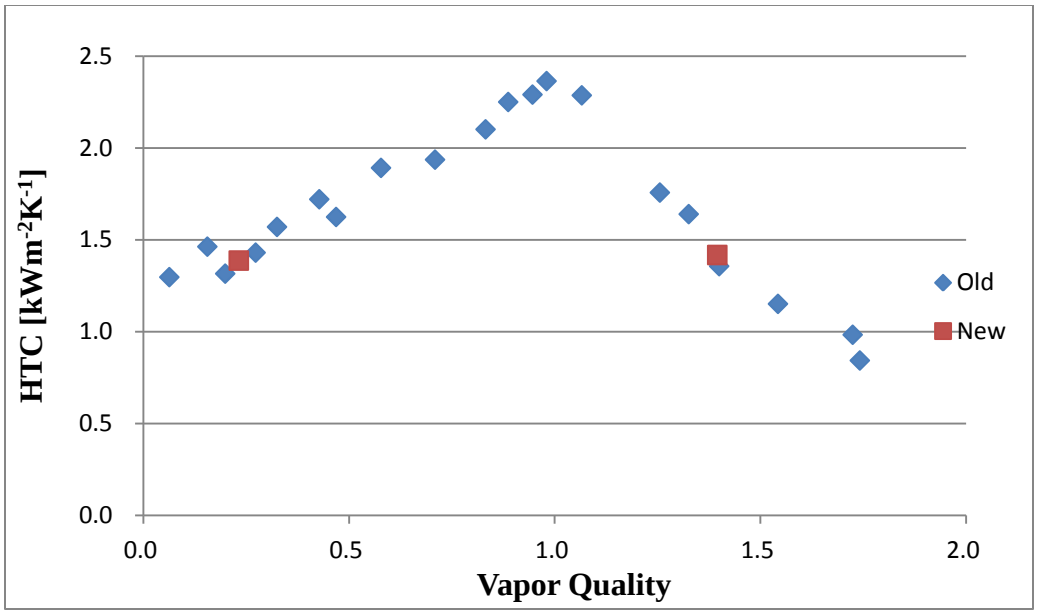

Figure B.1: R410A, 4.6 MPa, 200kgm^{-2}s^{-1}, 10kWm^{-2}

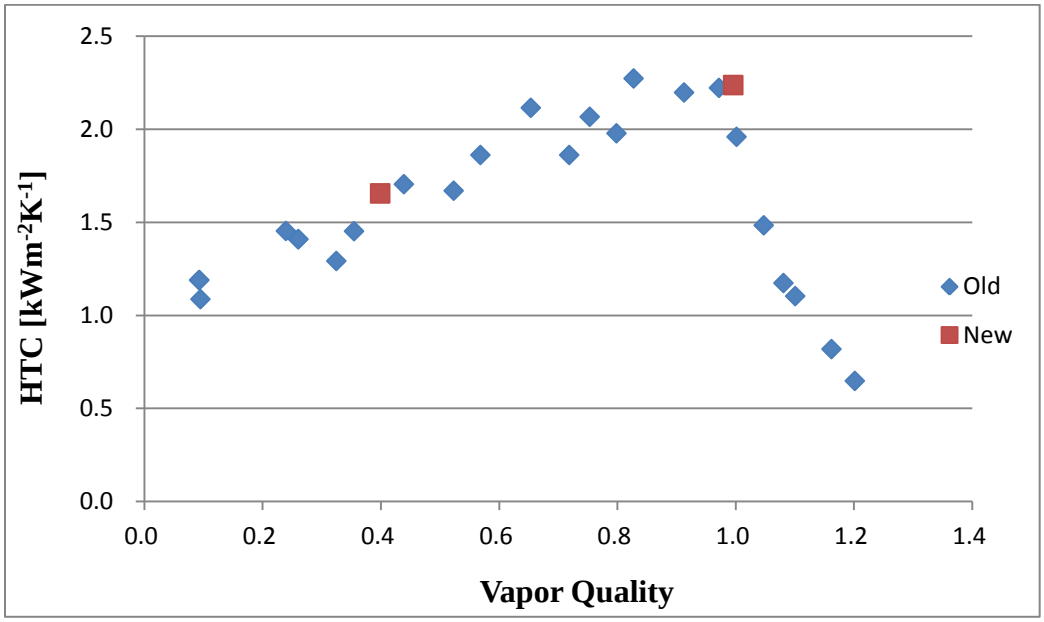

Figure B.2: R410A, 3.3 MPa, 100kgm^{-2}s^{-1}, 10kWm^{-2}

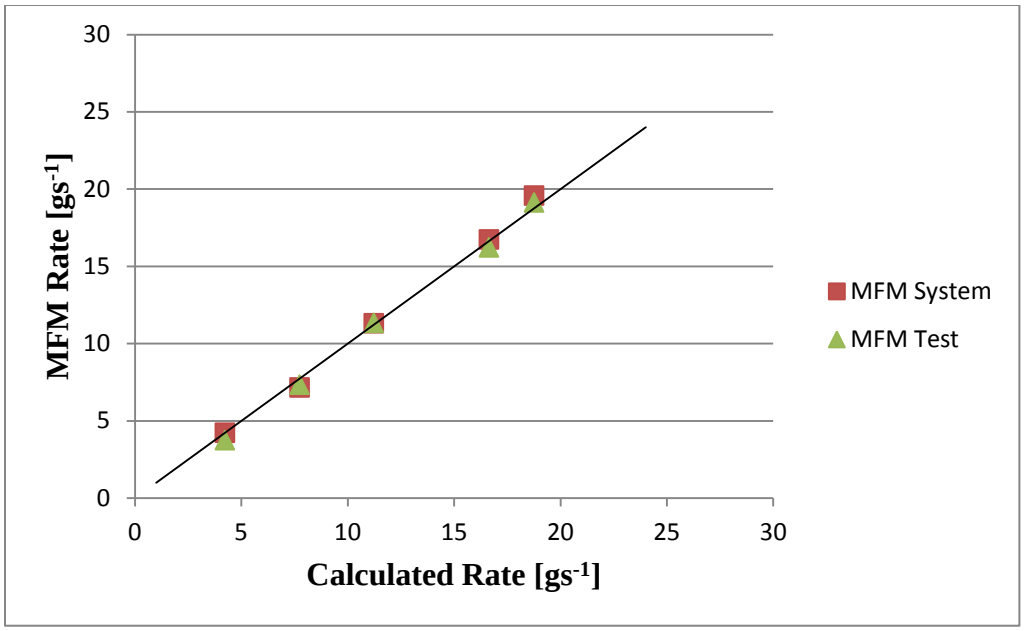

Figure B.3: Comparison of system mass flow meter with test mass flow meter and calculated mass flow rate.

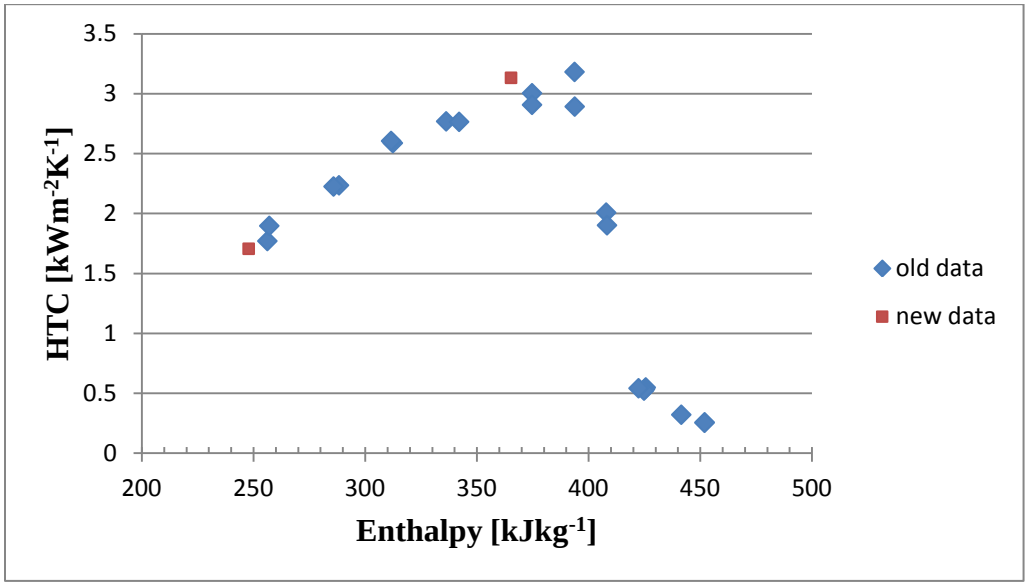

Figure B.4: R1234ze(E), .576 MPa, 100kgm^{-2}s^{-1}, 10kWm^{-2}

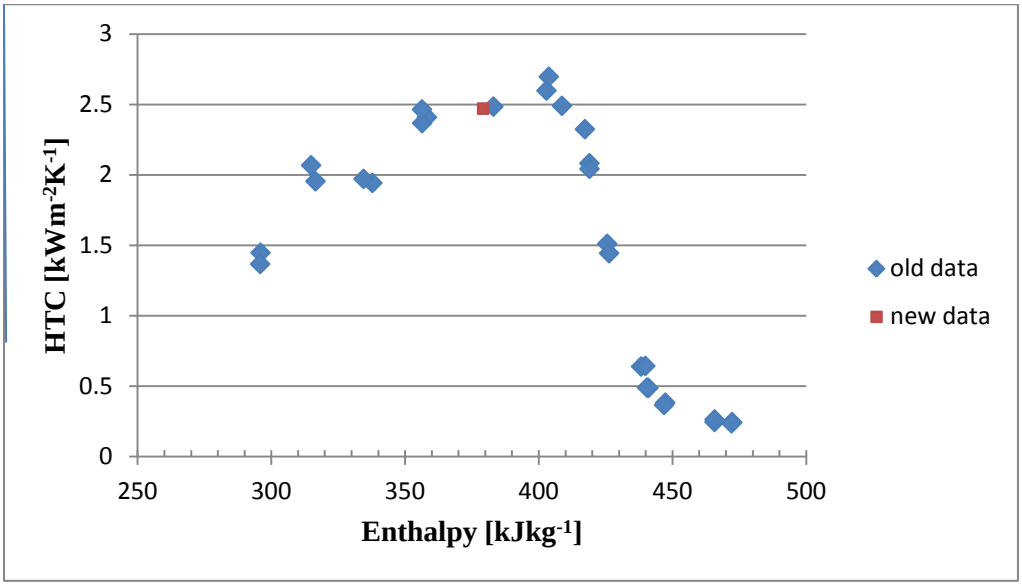

Figure B.5: R1234ze(E), .997 MPa, 100kgm^{-2}s^{-1}, 10kWm^{-2}

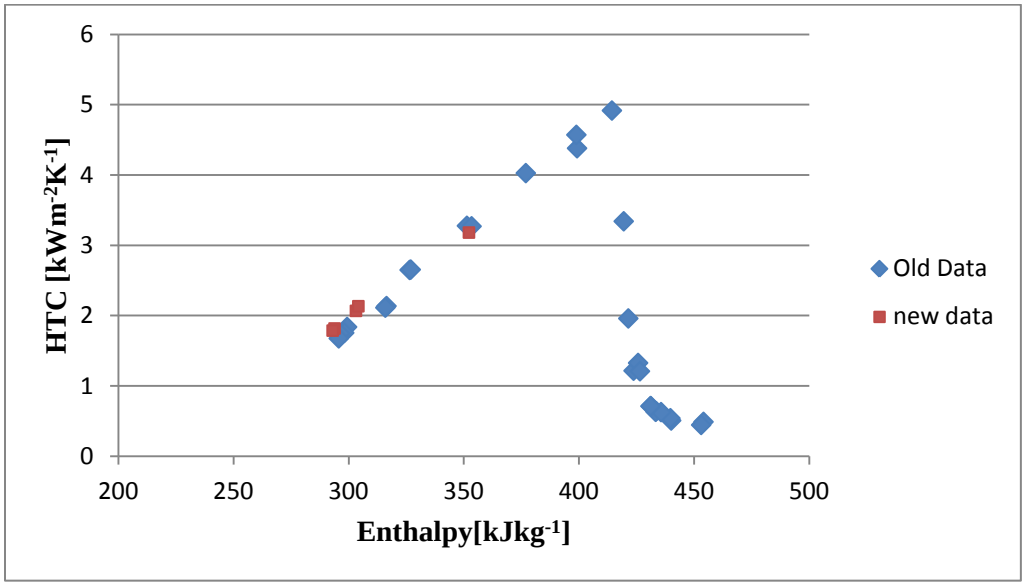

Figure B.6: R1234ze(E), .997 MPa, 300kgm^{-2}s^{-1}, 10kWm^{-2}

APPENDIX C

UNCERTAINTY ANALYSIS

When an experimental results R has a symmetric uncertainty, the range of 95 % coverage can be written as (Kondo, ACRC 264, 2012):

$$R = \hat{R} \text{ (center of experimental value or reading value) } \pm U_R \text{ (uncertainty)}$$
$$U_R = \left[\left(B_R\right)^2 + \left(tS_R\right)^2 \right]^{1/2} \tag{C.1}$$

where, B, S, and t are the degree of accuracy, accuracy degree of average value, symmetric student factor of 95%. In following uncertainty analysis, it is assumed that the effect of human error tS is negligible. Hence, the uncertainty of the measurement value R having measurement parameters $X_1 \sim X_i$ is determined as,

$$U_R \approx B_R = \left[\sum_{i=1}^{N} \left(\frac{\partial R}{\partial X_i} U_{X_i} \right)^2 \right]^{1/2} \tag{C.2}$$

$$R = f(X_1, \quad X_2, \quad \cdots, \quad X_i \quad \cdots, \quad X_N) \tag{C.3}$$

Followings are the procedure of uncertainty analysis for main measurement results of this study.

Pressure drop gradient $\Delta P/\Delta Z$

The uncertainty of pressure drop gradient at the test section is,

$$\begin{aligned} U_{\Delta P/\Delta Z}{}^2 &= \left[\frac{\partial\left(\Delta P/\Delta Z\right)}{\partial \Delta P_{TS}} U_{\Delta P_{TS}} \right]^2 + \left[\frac{\partial\left(\Delta P/\Delta Z\right)}{\partial \Delta Z_{\Delta P/\Delta Z}} U_{\Delta Z_{\Delta P/\Delta Z}} \right]^2 \\ &= U_{\Delta P_{TS}}{}^2 + \left[\frac{-1}{\Delta Z_{\Delta P/\Delta Z}{}^2} U_{\Delta Z_{\Delta P/\Delta Z}} \right]^2 = U_{\Delta P_{TS}}{}^2 + \frac{1}{\Delta Z_{\Delta P/\Delta Z}{}^4} U_{\Delta Z_{\Delta P/\Delta Z}}{}^2 \end{aligned} \tag{C.4}$$

Here,

$U_{\Delta P_{TS}} = 0.257[\text{kPa}]$

$\Delta Z_{\Delta P/\Delta Z} = 0.288[\text{m}]$

$U_{\Delta Z_{\Delta P/\Delta Z}} = \Delta Z_{\Delta P/\Delta Z} \times 5\% = 0.0144[\text{m}]$

This $\Delta Z_{\Delta P/\Delta Z}$ is the length between pressure taps.

Inlet pressure of test section P_{TSi}

The inlet pressure of test section is obtained with measured pressure of mixing chamber P_{MC} and differential pressure through the pre-cooler ΔP_{PC}.

$$P_{\mathrm{TSi}} = P_{\mathrm{MC}} - \Delta P_{\mathrm{PC}} \tag{C.5}$$

Hence, the uncertainty is determined as bellow.

$$U_{P_{\mathrm{TSi}}}{}^2 = U_{P_{\mathrm{MC}}}{}^2 + U_{\Delta P_{\mathrm{PC}}}{}^2 \approx U_{P_{\mathrm{MC}}}{}^2 \quad \because U_{P_{\mathrm{MC}}} >> U_{\Delta P_{\mathrm{PC}}} \tag{C.6}$$

Outlet pressure of test section P_{TSo}

Similarly, the outlet pressure of test section and its uncertainty are,

$$P_{\mathrm{TSo}} = P_{\mathrm{MC}} - \Delta P_{\mathrm{PC}} - \Delta P_{\mathrm{TS}} \tag{C.7}$$

$$U_{P_{\mathrm{TSi}}}{}^2 = U_{P_{\mathrm{MC}}}{}^2 + U_{\Delta P_{\mathrm{PC}}}{}^2 + U_{\Delta P_{\mathrm{TS}}}{}^2 \approx U_{P_{\mathrm{MC}}}{}^2 \quad \because U_{P_{\mathrm{MC}}} >> U_{\Delta P_{\mathrm{PC}}} \approx U_{\Delta P_{\mathrm{TS}}} \tag{C.8}$$

Enthalpy in mixing chamber h_{MC}

The specific enthalpy in the mixing chamber, located just after the pre-heater, is obtained from measured bulk mean temperature $T_{\mathrm{r,MC}}$ and pressure P_{MC} with Refprop ver.8.0. Therefore, the uncertainty of this enthalpy is the function of Refprop ver.8.0 and determined from measuring uncertainty of $T_{\mathrm{r,MC}}$ and P_{MC}.

$$U_{h_{\mathrm{MC}}} = \left[f_{\mathrm{Refprop8.0}}\left(P_{\mathrm{MC}} + U_{P_{\mathrm{MC}}}, T_{\mathrm{MC}} + U_{T_{\mathrm{MC}}}\right) - f_{\mathrm{Refprop8.0}}\left(P_{\mathrm{MC}} - U_{P_{\mathrm{MC}}}, T_{\mathrm{MC}} - U_{T_{\mathrm{MC}}}\right)\right] \Big/ 2 \tag{C.9}$$

Inlet enthalpy of the test section h_{TSi}

The inlet enthalpy of test section is obtained waterside heat-balance through the pre-cooler beginning at the mixing chamber just after the pre-heater.

$$\begin{aligned} h_{\mathrm{TSi}} &= h_{\mathrm{MC}} - \left(Q_{\mathrm{H2O}} - Q_{\mathrm{gain,PC}}\right) \Big/ m_{\mathrm{r}} \\ &= h_{\mathrm{MC}} - \left[\left(T_{\mathrm{H2O,PCo}} - T_{\mathrm{H2O,PCi}}\right) Cp_{\mathrm{H2O}} m_{\mathrm{H2O,PC}} - Q_{\mathrm{gain,PC}}\right] \Big/ m_{\mathrm{r}} \end{aligned} \tag{C.10}$$

The measured values, bulk mean temperature $T_{\mathrm{H2O,PCo}}$, $T_{\mathrm{H2O,PCi}}$ and mass flow rate $W_{\mathrm{H2O,PC}}$ and W_{r}, dominant the uncertainty of the inlet enthalpy.

$$\begin{aligned} U_{h_{\mathrm{TSi}}}{}^2 = &\left(\frac{\partial h_{\mathrm{TSi}}}{\partial h_{MC}} U_{h_{\mathrm{MC}}}\right)^2 + \left(\frac{\partial h_{\mathrm{TSi}}}{\partial T_{\mathrm{H2O,PCo}}} U_{T_{\mathrm{H2O,PCo}}}\right)^2 + \\ &\left(\frac{\partial h_{\mathrm{TSi}}}{\partial T_{\mathrm{H2O,PCi}}} U_{T_{\mathrm{H2O,PCi}}}\right)^2 + \left(\frac{\partial h_{\mathrm{TSi}}}{\partial m_{\mathrm{H2O,PC}}} U_{m_{\mathrm{H2O,PC}}}\right)^2 + \left(\frac{\partial h_{\mathrm{TSi}}}{\partial m_{\mathrm{r}}} U_{m_{\mathrm{r}}}\right)^2 \end{aligned} \tag{C.11}$$

$$\frac{\partial h_{\mathrm{TSi}}}{\partial h_{MC}} = 1.0 \tag{C.12}$$

$$\frac{\partial h_{\mathrm{TSi}}}{\partial T_{\mathrm{H2O,PCo}}} = -\frac{Cp_{\mathrm{H2O}} m_{\mathrm{H2O,PC}}}{m_{\mathrm{r}}} \tag{C.13}$$

$$\frac{\partial h_{\mathrm{TSi}}}{\partial T_{\mathrm{H2O,PCi}}} = \frac{Cp_{\mathrm{H2O}} m_{\mathrm{H2O,PC}}}{m_{\mathrm{r}}} \tag{C.14}$$

$$\frac{\partial h_{\mathrm{TSi}}}{\partial m_{\mathrm{H2O,PC}}} = -\frac{\left(T_{\mathrm{H2O,PCo}} - T_{\mathrm{H2O,PCi}}\right) Cp_{\mathrm{H2O}}}{m_{\mathrm{r}}} \tag{C.15}$$

$$\frac{\partial h_{\mathrm{TSi}}}{\partial m_{\mathrm{r}}} = \frac{\left(T_{\mathrm{H2O,PCo}} - T_{\mathrm{H2O,PCi}}\right) Cp_{\mathrm{H2O}} m_{\mathrm{H2O,PC}}}{m_{\mathrm{r}}^{\,2}} \tag{C.16}$$

Refrigerant temperature at test-section inlet $T_{\mathrm{r,TSi}}$

$$U_{T_{\mathrm{r,TSi}}} = \left[f_{\mathrm{Refprop8.0}}\left(P_{\mathrm{TSi}} + U_{P_{\mathrm{TSi}}}, h_{\mathrm{TSi}} + U_{T_{\mathrm{TSi}}}\right) - f_{\mathrm{Refprop8.0}}\left(P_{\mathrm{TSi}} - U_{P_{\mathrm{TSi}}}, h_{\mathrm{TSi}} - U_{T_{\mathrm{TSi}}}\right) \right] \Big/ 2 \tag{C.17}$$

Refrigerant temperature at test-section outlet h_{TSo}

Likewise, the outlet enthalpy of test section is obtained water-side heat-balance through the test-section.

$$\begin{aligned} h_{\mathrm{TSo}} &= h_{\mathrm{TSi}} - \left(Q_{\mathrm{H2O,TS}} - Q_{\mathrm{gain,TS}} - Q_{\mathrm{cond,TS}}\right) \Big/ m_{\mathrm{r}} \\ &= h_{\mathrm{TSi}} - \left[\left(T_{\mathrm{H2O,TSo}} - T_{\mathrm{H2O,TSi}}\right) Cp_{\mathrm{H2O}} m_{\mathrm{H2O,TS}} - Q_{\mathrm{gain,TS}} - Q_{\mathrm{cond,TS}} \right] \Big/ m_{\mathrm{r}} \end{aligned} \tag{C.18}$$

The measured values, bulk mean temperature $T_{\mathrm{H2O,TSo}}$, $T_{\mathrm{H2O,TSi}}$ and mass flow rate $W_{\mathrm{H2O,TS}}$ and W_{r}, dominant the uncertainty of the outlet enthalpy.

$$\begin{aligned} U_{h_{\mathrm{TSo}}}^{\;2} = &\left(\frac{\partial h_{\mathrm{TSo}}}{\partial h_{\mathrm{TSi}}} U_{h_{\mathrm{TSi}}} \right)^2 + \left(\frac{\partial h_{\mathrm{TSo}}}{\partial T_{\mathrm{H2O,TSo}}} U_{T_{\mathrm{H2O,TSo}}} \right)^2 \\ &+ \left(\frac{\partial h_{\mathrm{TSo}}}{\partial T_{\mathrm{H2O,TSi}}} U_{T_{\mathrm{H2O,TSi}}} \right)^2 + \left(\frac{\partial h_{\mathrm{TSo}}}{\partial m_{\mathrm{H2O,TS}}} U_{m_{\mathrm{H2O,TS}}} \right)^2 \\ &+ \left(\frac{\partial h_{\mathrm{TSo}}}{\partial Q_{\mathrm{gain,TS}}} U_{Q_{\mathrm{gain,TS}}} \right)^2 + \left(\frac{\partial h_{\mathrm{TSo}}}{\partial Q_{\mathrm{cond,TS}}} U_{Q_{\mathrm{cond,TS}}} \right)^2 + \left(\frac{\partial h_{\mathrm{TSo}}}{\partial m_{\mathrm{r}}} U_{m_{\mathrm{r}}} \right)^2 \end{aligned} \tag{C.19}$$

$$\frac{\partial h_{\mathrm{TSo}}}{\partial h_{\mathrm{TSi}}} = 1.0 \tag{C.20}$$

$$\frac{\partial h_{\mathrm{TSo}}}{\partial T_{\mathrm{H2O,TSo}}} = -\frac{Cp_{\mathrm{H2O}} m_{\mathrm{H2O,TS}}}{m_{\mathrm{r}}} \tag{C.21}$$

$$\frac{\partial h_{\mathrm{TSo}}}{\partial T_{\mathrm{H2O,TSi}}} = \frac{Cp_{\mathrm{H2O}} m_{\mathrm{H2O,TS}}}{m_{\mathrm{r}}} \tag{C.22}$$

$$\frac{\partial h_{\mathrm{TSo}}}{\partial m_{\mathrm{H2O,TS}}} = -\frac{\left(T_{\mathrm{H2O,TSo}} - T_{\mathrm{H2O,TSi}}\right) Cp_{\mathrm{H2O}}}{m_{\mathrm{r}}} \tag{C.23}$$

$$\frac{\partial h_{\mathrm{TSo}}}{\partial Q_{\mathrm{cond,TS}}} = -\frac{1}{m_{\mathrm{r}}} \tag{C.24}$$

$$\frac{\partial h_{\mathrm{TSo}}}{\partial Q_{\mathrm{gain,TS}}} \approx 0 \tag{C.25}$$

$$\frac{\partial h_{\mathrm{TSo}}}{\partial W_{\mathrm{r}}} = \frac{\left(T_{\mathrm{H2O,TSo}} - T_{\mathrm{H2O,TSi}}\right) Cp_{\mathrm{H2O}} W_{\mathrm{H2O,TS}}}{W_{\mathrm{r}}^{\,2}} \tag{C.26}$$

Refrigerant temperature at test-section inlet $T_{\mathrm{r,TSo}}$

$$U_{T_{\mathrm{r,TSo}}} = \left[f_{\mathrm{Refprop8.0}}\left(P_{\mathrm{TSo}} + U_{P_{\mathrm{TSo}}},\ h_{\mathrm{TSo}} + U_{T_{\mathrm{TSo}}}\right) - f_{\mathrm{Refprop8.0}}\left(P_{\mathrm{TSo}} - U_{P_{\mathrm{TSo}}},\ h_{\mathrm{TSo}} - U_{T_{\mathrm{TSo}}}\right) \right] \Big/ 2 \tag{C.27}$$

Bulk mean refrigerant temperature at test-section T_{rb}

The representing refrigerant temperature of test-section is as an arithmetic mean of inlet and outlet.

$$T_{\mathrm{rb}} = \left(T_{\mathrm{r,TSi}} + T_{\mathrm{r,TSo}}\right) \Big/ 2 \tag{C.28}$$

The outlet temperature $T_{\mathrm{r,TSo}}$ is dependent on inlet temperature $T_{\mathrm{r,TSi}}$, because each temperature is obtained from upstream enthalpy. For the exact solution, to know and differentiate the internal functions of Refoprop.Ver8.0 is necessary. However, these function is solved computationally and difficult to be differentiated. Alternatively, they are treated as if independent variables for solving the uncertainty of averaged refrigerant temperature.

$$U_{T_{\mathrm{rb}}}{}^{2} = \left(\frac{\partial T_{\mathrm{rb}}}{\partial T_{\mathrm{r,TSi}}} U_{T_{\mathrm{r,TSi}}} \right)^2 + \left(\frac{\partial T_{\mathrm{rb}}}{\partial T_{\mathrm{r,TSo}}} U_{T_{\mathrm{r,TSo}}} \right)^2 = \left(U_{T_{\mathrm{r,TSi}}}{}^{2} + U_{T_{\mathrm{r,TSo}}}{}^{2} \right) \Big/ 4 \tag{C.29}$$

Averaged heat flux on interior tube-wall q_{wi}

In the way of this measurement, the heat flux on interior tube-wall is non-uniform in circumferential and axial direction of the test tube. However, the heat flux is treated as an averaged value of test section overall. The averaged heat flux through test section on interior tube-wall is obtained as,

$$\begin{aligned} q_{\mathrm{wi}} &= \left(Q_{\mathrm{H2O,TS}} - Q_{\mathrm{gain}} - Q_{\mathrm{cond}}\right) \Big/ A_{\mathrm{wi}} \\ &= \left[\left(T_{\mathrm{H2O,TSo}} - T_{\mathrm{H2O,TSi}}\right) W_{\mathrm{H2O,TS}} Cp_{\mathrm{H2O}} - Q_{\mathrm{gain}} - Q_{\mathrm{cond}} \right] \Big/ A_{\mathrm{wi}} \end{aligned} \tag{C.30}$$

Hence, the uncertainty of the averaged heat flux is,

$$\begin{aligned} U_{q_{\mathrm{wi}}}{}^{2} = &\left(\frac{\partial q_{\mathrm{wi}}}{\partial T_{\mathrm{H2O,TSo}}} U_{T_{\mathrm{H2O,TSo}}} \right)^2 + \left(\frac{\partial q_{\mathrm{wi}}}{\partial T_{\mathrm{H2O,TSi}}} U_{T_{\mathrm{H2O,TSi}}} \right)^2 + \left(\frac{\partial q_{\mathrm{wi}}}{\partial m_{\mathrm{H2O,TS}}} U_{m_{\mathrm{H2O,TS}}} \right)^2 \\ &+ \left(\frac{\partial q_{\mathrm{wi}}}{\partial Q_{\mathrm{gainTS}}} U_{Q_{\mathrm{gain,TS}}} \right)^2 + \left(\frac{\partial q_{\mathrm{wi}}}{\partial Q_{\mathrm{cond,TS}}} U_{Q_{\mathrm{cond,TS}}} \right)^2 + \left(\frac{\partial q_{\mathrm{wi}}}{\partial A_{\mathrm{wi}}} U_{A_{wi}} \right)^2 \end{aligned} \tag{C.31}$$

$$\frac{\partial q_{\mathrm{wi}}}{\partial T_{\mathrm{H2O,TSo}}} = \frac{m_{\mathrm{H2O,TS}} Cp_{\mathrm{H2O}}}{A_{\mathrm{wi}}} \tag{C.32}$$

$$\frac{\partial q_{\mathrm{wi}}}{\partial T_{\mathrm{H2O,TSi}}} = -\frac{m_{\mathrm{H2O,TS}} Cp_{\mathrm{H2O}}}{A_{\mathrm{wi}}} \tag{C.33}$$

$$\frac{\partial q_{\mathrm{wi}}}{\partial m_{\mathrm{H2O,TS}}} = \frac{\left(T_{\mathrm{H2O,TSo}} - T_{\mathrm{H2O,TSi}}\right) Cp_{\mathrm{H2O}}}{A_{\mathrm{wi}}} \tag{C.34}$$

$$\frac{\partial q_{\mathrm{wi}}}{\partial Q_{\mathrm{gain,TS}}} \approx 0 \tag{C.35}$$

$$\frac{\partial q_{\mathrm{wi}}}{\partial Q_{\mathrm{cond,TS}}} = -\frac{1}{A_{\mathrm{wi}}} \tag{C.36}$$

$$\frac{\partial q_{\mathrm{wi}}}{\partial A_{\mathrm{wi}}} = -\frac{\left(T_{\mathrm{H2O,TSo}} - T_{\mathrm{H2O,TSi}}\right) m_{\mathrm{H2O,TS}} Cp_{\mathrm{H2O}} - Q_{\mathrm{gain}} - Q_{\mathrm{cond}}}{{A_{\mathrm{wi}}}^2} \tag{C.37}$$

Temperature difference ΔT

The temperature difference between bulk refrigerant temperature T_{rb} and averaged interior tube-wall temperature T_{wi} is,

$$\Delta T = T_{\mathrm{rb}} - T_{\mathrm{wi}} \tag{C.38}$$

Hence, the uncertainty is expressed as,

$${U_{\Delta T}}^2 = \left(\frac{\partial \Delta T}{\partial T_{\mathrm{rb}}} U_{T_{\mathrm{rb}}}\right)^2 + \left(\frac{\partial \Delta T}{\partial T_{\mathrm{wi}}} U_{T_{\mathrm{wi}}}\right)^2 = {U_{T_{\mathrm{rb}}}}^2 + {U_{T_{\mathrm{wi}}}}^2 \tag{C.39}$$

Heat transfer coefficient α

The heat transfer coefficient averaged through the test-section is defined with averaged heat flux and temperature difference as below,

$$\alpha = \frac{q_{\mathrm{wi}}}{\Delta T} \tag{C.40}$$

Hence, the uncertainty is expressed as,

$${U_{\alpha}}^2 = \left(\frac{\partial \alpha}{\partial q_{wi}} U_{q_{wi}}\right)^2 + \left(\frac{\partial \alpha}{\partial \Delta T} U_{\Delta T}\right)^2 = {U_{q_{wi}}}^2 + \left(\frac{U_{\Delta T}}{\Delta T}\right)^2 \tag{C.41}$$

APPENDIX D

EXPERIMENTAL DATA

Table D.1: R1234ze(E), G=100kgm^{-2}s^{-1}, Tsat = 30 ^{0}C

P	h_{bulk}	x	Q	$T_{r,in}$	$T_{r,out}$	T_{wall}	DT	HTC	$dPdZ^{-1}$
[MPa]	[kJkg^{-1}]	[-]	[kWm^{-2}]	[^{0}C]	[^{0}C]	[^{0}C]	[^{0}C]	[kWm^{-2}K^{-1}]	[kPam^{-1}]
0.589	232.69	-0.05	8.46	27.48	21.14	15.30	9.01	0.94	0.03
0.584	239.00	-0.01	8.28	30.33	25.82	21.75	6.33	1.31	0.08
0.589	245.17	0.02	10.35	30.60	29.56	22.50	7.58	1.37	0.01
0.580	251.20	0.06	10.21	30.11	30.11	23.76	6.34	1.61	0.03
0.586	263.09	0.13	9.54	30.43	30.43	25.59	4.84	1.97	0.05
0.571	283.35	0.27	9.57	29.55	29.55	24.85	4.71	2.03	0.09
0.565	306.50	0.41	10.10	29.22	29.21	24.95	4.26	2.37	0.19
0.568	307.34	0.41	10.23	29.38	29.38	25.03	4.35	2.35	0.22
0.566	331.30	0.56	10.45	29.28	29.27	25.13	4.15	2.52	0.45
0.560	337.09	0.60	10.35	28.92	28.91	24.80	4.12	2.51	0.43
0.574	369.80	0.79	9.87	29.75	29.74	26.14	3.61	2.73	0.54
0.588	388.49	0.91	10.83	30.57	30.56	26.82	3.75	2.89	0.57
0.574	402.76	1.00	10.20	34.33	29.72	26.44	5.59	1.83	0.52
0.577	403.08	1.00	10.30	34.77	29.91	26.38	5.96	1.73	0.52
0.580	417.74	1.09	9.31	48.90	39.55	25.34	18.89	0.49	1.17
0.584	420.42	1.10	9.06	51.79	42.15	28.39	18.58	0.49	1.21
0.593	420.80	1.10	9.14	52.03	42.98	28.78	18.73	0.49	1.72
0.590	420.95	1.10	9.45	52.29	42.92	28.68	18.93	0.50	1.15
0.588	436.36	1.20	9.83	68.00	57.70	29.26	33.59	0.29	1.07
0.590	446.64	1.26	9.76	78.22	67.76	30.84	42.15	0.23	0.92
0.584	446.73	1.26	9.88	78.22	67.79	30.90	42.11	0.23	0.92
0.568	458.67	1.34	10.70	89.89	79.08	39.98	44.51	0.24	0.41
0.573	459.34	1.34	10.50	90.49	79.91	40.12	45.08	0.23	0.41
0.572	468.42	1.40	12.03	100.10	87.89	42.67	51.33	0.23	0.43
0.572	468.48	1.40	12.17	100.17	87.93	42.87	51.18	0.24	0.43

Table D.2: R1234ze(E), G=100kgm^{-2}s^{-1}, Tsat = 40 ^{0}C

P	h_{bulk}	x	Q	$T_{r,in}$	$T_{r,out}$	T_{wall}	DT	HTC	$dPdZ^{-1}$
[MPa]	[kJkg^{-1}]	[-]	[kWm^{-2}]	[^{0}C]	[^{0}C]	[^{0}C]	[^{0}C]	[kWm^{-2}K^{-1}]	[kPam^{-1}]
0.787	235.47	-0.13	4.15	27.86	24.76	17.07	9.25	0.45	0.01
0.777	241.37	-0.09	8.56	33.75	27.32	15.35	15.18	0.56	0.01
0.766	256.36	0.01	10.10	39.99	37.53	29.37	9.39	1.08	0.01
0.772	259.05	0.02	10.74	40.27	39.18	30.09	9.63	1.12	0.01
0.771	263.16	0.05	14.15	40.19	40.19	28.87	11.31	1.25	0.01
0.771	263.23	0.05	14.14	40.21	40.21	28.87	11.34	1.25	0.01
0.769	265.22	0.07	14.41	40.10	40.10	28.77	11.33	1.27	-0.01
0.774	279.39	0.16	10.23	40.34	40.34	33.70	6.64	1.54	0.04
0.774	279.97	0.16	10.32	40.37	40.37	33.68	6.69	1.54	0.04
0.775	306.17	0.33	9.36	40.41	40.41	35.20	5.21	1.80	0.05
0.777	306.92	0.33	8.99	40.48	40.47	35.21	5.26	1.71	0.05
0.776	337.21	0.53	9.86	40.44	40.43	35.94	4.49	2.19	0.16
0.776	339.59	0.55	9.92	40.45	40.45	35.94	4.51	2.20	0.16
0.777	378.79	0.80	8.68	40.48	40.48	36.85	3.64	2.39	0.27
0.777	379.61	0.80	8.81	40.51	40.51	36.80	3.71	2.38	0.27
0.774	401.26	0.95	9.13	40.35	40.34	36.91	3.43	2.66	0.28
0.774	402.16	0.95	8.95	40.35	40.35	36.92	3.43	2.61	0.28
0.772	411.81	1.01	9.35	46.65	40.24	37.23	6.21	1.51	0.58
0.774	412.92	1.02	9.28	47.82	40.33	37.26	6.81	1.36	0.58
0.772	425.32	1.10	11.88	60.81	49.55	36.62	18.56	0.64	0.63
0.773	426.26	1.11	11.77	61.66	50.51	36.60	19.49	0.60	0.63
0.772	438.55	1.19	6.76	71.17	64.44	39.47	28.34	0.24	0.45
0.772	438.68	1.19	7.54	71.49	64.39	39.07	28.87	0.26	0.45
0.771	450.47	1.26	7.54	83.01	75.37	41.03	38.16	0.20	0.46
0.774	461.08	1.33	9.84	94.22	84.43	42.99	46.34	0.21	0.31

Table D.3: R1234ze(E), G=100kgm^{-2}s^{-1}, Tsat = 50 ^{0}C

P	h_{bulk}	x	Q	$T_{r,in}$	$T_{r,out}$	T_{wall}	DT	HTC	$dPdZ^{-1}$
[MPa]	[kJkg^{-1}]	[-]	[kWm^{-2}]	[^{0}C]	[^{0}C]	[^{0}C]	[^{0}C]	[kWm^{-2}K^{-1}]	[kPam^{-1}]
0.998	240.47	-0.20	4.84	31.60	28.19	21.00	9.85	0.49	0.04
0.999	253.08	-0.11	7.50	41.43	36.17	23.52	15.28	0.49	0.04
1.003	255.59	-0.10	10.95	44.49	36.57	21.38	19.15	0.57	0.05
0.993	262.05	-0.05	9.07	48.10	41.87	32.76	12.23	0.74	0.05
0.993	263.49	-0.04	9.35	49.15	42.77	32.85	13.12	0.71	0.03
0.992	267.68	-0.01	10.11	49.77	45.34	37.22	10.34	0.98	0.03
0.996	273.40	0.03	11.92	49.94	48.65	38.50	10.79	1.10	0.07
0.997	284.24	0.10	8.81	49.96	49.96	42.29	7.67	1.15	0.01
0.997	305.10	0.25	10.84	49.98	49.98	42.31	7.67	1.41	0.04
0.995	307.11	0.26	11.15	49.92	49.92	42.32	7.60	1.47	0.04
0.973	330.43	0.43	8.13	49.04	49.04	44.50	4.54	1.79	0.12
0.999	340.22	0.49	9.58	50.04	50.04	44.67	5.37	1.78	0.12
0.998	343.47	0.51	9.85	50.02	50.02	44.60	5.42	1.82	0.12
0.998	344.94	0.52	9.79	50.01	50.01	44.72	5.29	1.85	0.12
0.997	354.92	0.59	10.13	50.00	50.00	44.66	5.34	1.90	0.09
0.992	378.13	0.75	9.79	49.77	49.77	45.43	4.34	2.26	0.21
0.983	399.05	0.89	7.49	49.42	49.42	46.25	3.17	2.36	0.23
0.984	399.88	0.90	7.99	49.46	49.46	46.20	3.26	2.45	0.29
0.990	404.65	0.93	7.85	49.70	49.69	46.23	3.47	2.26	0.24
0.960	412.79	0.99	9.43	51.26	48.51	45.42	4.46	2.11	0.30
1.009	414.54	1.00	9.22	53.77	50.47	47.15	4.97	1.86	0.29
1.002	419.36	1.03	12.54	59.57	50.18	45.73	9.14	1.37	0.28
0.995	420.15	1.04	12.15	60.07	49.89	45.71	9.27	1.31	0.29
0.985	432.29	1.12	11.13	70.84	59.90	46.17	19.20	0.58	0.64
0.978	433.44	1.13	11.77	72.18	60.43	46.13	20.17	0.58	0.64
0.988	435.74	1.14	9.24	72.93	64.22	47.75	20.83	0.44	0.94
0.991	436.23	1.15	9.31	73.45	64.68	47.99	21.08	0.44	0.94
0.995	442.18	1.19	8.94	78.91	70.30	47.62	26.98	0.33	0.93
0.995	442.38	1.19	9.45	79.34	70.23	47.52	27.27	0.35	0.93
1.010	460.42	1.31	9.88	96.53	86.68	49.99	41.62	0.24	0.76
1.008	460.71	1.31	9.25	96.49	87.21	50.06	41.79	0.22	0.76
0.996	466.85	1.36	10.25	102.38	92.35	50.99	46.38	0.22	0.80
0.994	466.86	1.36	9.87	102.18	92.52	51.02	46.33	0.21	0.80
1.002	469.44	1.37	11.68	105.53	94.12	48.00	51.82	0.23	0.65
1.001	470.14	1.38	11.58	106.10	94.81	47.44	53.01	0.22	0.65

Table D.4: R1234ze(E), G=200kgm^{-2}s^{-1}, Tsat = 50 ^{0}C

P	h_{bulk}	x	Q	$T_{r,in}$	$T_{r,out}$	T_{wall}	DT	HTC	$dPdZ^{-1}$
[MPa]	[kJkg^{-1}]	[-]	[kWm^{-2}]	[^{0}C]	[^{0}C]	[^{0}C]	[^{0}C]	[kWm^{-2}K^{-1}]	[kPam^{-1}]
1.00	238.05	-0.22	5.59	29.17	27.15	20.76	7.40	0.76	0.20
1.00	247.19	-0.15	6.52	35.87	33.47	26.96	8.59	0.76	0.12
1.00	261.03	-0.06	8.33	45.79	42.82	33.56	10.74	0.78	0.17
1.00	264.57	-0.03	9.48	48.37	45.05	35.50	11.21	0.85	0.17
1.00	271.56	0.01	11.27	50.19	49.55	38.74	11.13	1.01	0.15
1.00	274.85	0.04	11.13	50.07	50.06	39.63	10.44	1.07	0.15
1.00	276.06	0.05	11.83	50.02	50.02	39.57	10.45	1.13	0.15
0.99	280.84	0.08	9.00	49.86	49.85	42.65	7.20	1.25	0.20
1.00	282.93	0.09	9.50	49.93	49.92	42.66	7.26	1.31	0.20
0.99	307.11	0.26	9.96	49.89	49.89	44.28	5.61	1.77	0.44
0.99	307.15	0.26	10.21	49.91	49.90	44.22	5.68	1.80	0.44
1.00	324.39	0.38	10.32	49.94	49.93	44.57	5.36	1.92	0.69
1.00	325.81	0.39	11.11	49.93	49.92	44.36	5.57	1.99	0.69
1.00	343.96	0.51	10.35	50.10	50.09	45.49	4.60	2.25	0.93
1.00	344.87	0.52	10.25	50.07	50.06	45.50	4.56	2.25	0.93
1.00	368.04	0.68	10.59	50.10	50.08	45.90	4.19	2.53	1.10
1.00	382.84	0.78	11.50	50.19	50.17	46.03	4.15	2.77	1.65
1.00	407.34	0.95	10.27	50.01	49.99	46.62	3.38	3.04	1.80
1.00	407.80	0.95	10.61	49.98	49.96	46.58	3.38	3.14	1.80
1.00	415.08	1.00	9.58	52.26	50.08	46.71	4.45	2.15	2.20
1.00	416.02	1.01	9.35	53.01	49.98	46.84	4.66	2.01	2.20
1.01	418.97	1.03	8.78	55.70	51.82	48.15	5.62	1.57	2.04
1.01	419.43	1.03	9.08	56.22	52.13	48.10	6.07	1.50	2.04
1.01	429.93	1.10	10.97	66.10	61.02	48.08	15.49	0.71	1.95
1.01	430.66	1.11	10.72	66.72	61.72	48.11	16.11	0.67	1.95
1.01	435.01	1.14	11.20	70.82	65.53	48.86	19.32	0.58	2.02
1.01	436.49	1.15	10.87	72.14	66.93	48.96	20.57	0.53	2.02
1.01	443.65	1.20	8.95	78.22	73.98	51.00	25.10	0.36	1.90
1.01	448.93	1.23	9.66	83.32	78.68	53.75	27.25	0.35	1.96
1.01	449.61	1.24	9.51	83.87	79.37	53.68	27.94	0.34	1.96
1.01	457.35	1.29	11.24	91.38	86.10	57.58	31.16	0.36	2.05
1.01	459.54	1.31	15.56	94.51	87.08	46.82	43.98	0.35	1.97
1.00	462.59	1.33	15.42	97.29	89.80	51.20	42.34	0.36	1.97
1.00	472.78	1.40	16.21	106.76	99.10	56.78	46.15	0.35	2.05
1.01	474.21	1.41	16.89	108.33	100.26	57.02	47.28	0.36	2.05

Table D.5: R1234ze(E), G=300kgm^{-2}s^{-1}, Tsat = 50 ^{0}C

P	h_{bulk}	x	Q	$T_{r,in}$	$T_{r,out}$	T_{wall}	DT	HTC	$dPdZ^{-1}$
[MPa]	[kJkg^{-1}]	[-]	[kWm^{-2}]	[^{0}C]	[^{0}C]	[^{0}C]	[^{0}C]	[kWm^{-2}K^{-1}]	[kPam^{-1}]
0.990	257.34	-0.08	8.49	42.75	40.79	34.87	6.90	1.23	0.27
0.990	257.80	-0.08	8.53	43.07	41.10	34.87	7.21	1.18	0.27
0.991	258.52	-0.07	8.55	43.57	41.59	35.54	7.04	1.22	0.31
0.989	260.65	-0.06	8.96	45.07	43.01	36.78	7.26	1.23	0.31
0.994	260.83	-0.06	8.87	45.19	43.15	36.78	7.38	1.20	0.31
0.994	261.36	-0.05	9.69	45.64	43.42	36.80	7.73	1.25	0.31
0.997	264.32	-0.03	9.62	47.65	45.44	38.71	7.83	1.23	0.29
0.993	264.59	-0.03	9.84	47.86	45.60	38.92	7.81	1.26	0.29
0.994	265.18	-0.03	10.29	48.30	45.95	38.88	8.25	1.25	0.29
0.994	266.41	-0.02	10.34	49.13	46.79	39.79	8.17	1.27	0.31
0.994	266.41	-0.02	10.33	49.14	46.78	39.61	8.35	1.24	0.29
0.995	267.08	-0.02	10.64	49.62	47.21	39.79	8.62	1.23	0.31
0.995	270.82	0.01	10.75	49.89	49.69	40.79	9.00	1.20	0.40
0.995	271.10	0.01	10.77	49.92	49.88	40.82	9.08	1.19	0.40
0.996	275.27	0.04	10.85	49.93	49.92	41.31	8.61	1.26	0.40
0.995	279.77	0.07	11.56	49.92	49.91	41.79	8.12	1.42	0.48
0.996	281.17	0.08	11.77	49.94	49.93	41.81	8.12	1.45	0.48
0.995	291.24	0.15	10.93	49.91	49.90	43.17	6.73	1.62	0.72
0.988	294.81	0.18	8.49	49.65	49.64	44.29	5.35	1.59	0.85
0.993	296.68	0.19	8.59	49.85	49.84	44.45	5.39	1.59	0.96
0.992	297.86	0.20	9.02	49.81	49.79	44.40	5.40	1.67	1.00
0.996	301.19	0.22	12.00	49.96	49.94	43.56	6.39	1.88	0.99
0.997	302.17	0.22	12.43	50.00	49.98	43.58	6.42	1.94	0.99
0.982	314.57	0.31	8.25	49.41	49.40	45.10	4.30	1.92	1.46
0.986	315.08	0.32	8.41	49.56	49.54	45.21	4.34	1.94	1.48
0.987	324.82	0.38	10.13	49.60	49.57	45.38	4.21	2.41	1.72
0.978	325.35	0.39	9.80	49.23	49.20	45.15	4.06	2.41	1.74
0.996	350.37	0.56	11.69	49.97	49.93	45.90	4.04	2.89	2.65
0.985	375.58	0.73	8.57	49.53	49.49	47.17	2.34	3.66	3.48
0.994	397.50	0.88	8.69	49.90	49.85	47.78	2.09	4.15	3.86
0.975	412.98	0.99	8.39	49.14	49.08	47.23	1.88	4.47	4.68
0.990	417.57	1.02	11.68	53.87	50.42	48.30	3.85	3.04	3.75
0.986	419.75	1.03	10.41	55.58	52.44	48.16	5.85	1.78	3.41
0.973	424.59	1.07	11.46	59.91	56.34	47.68	10.44	1.10	3.48

Continued…

Continued…

P	h_{bulk}	x	Q	$T_{r,in}$	$T_{r,out}$	T_{wall}	DT	HTC	$dPdZ^{-1}$
[MPa]	[$kJkg^{-1}$]	[-]	[kWm^{-2}]	[^0C]	[^0C]	[^0C]	[^0C]	[$kWm^{-2}K^{-1}$]	[$kPam^{-1}$]
0.977	429.59	1.10	9.01	64.18	61.33	48.78	13.97	0.65	3.58
0.978	429.67	1.10	9.12	64.28	61.40	48.76	14.08	0.65	3.59
0.992	431.82	1.12	8.79	66.43	63.64	49.68	15.36	0.57	3.44
0.989	432.01	1.12	9.04	66.60	63.73	49.62	15.55	0.58	3.46
0.973	434.09	1.13	9.20	68.30	65.31	50.65	16.16	0.57	3.50
0.977	438.35	1.16	8.16	72.11	69.49	54.16	16.64	0.49	3.58
0.977	438.88	1.17	7.06	72.42	70.15	55.94	15.34	0.46	3.62
0.984	451.61	1.25	8.61	84.55	81.72	61.78	21.36	0.40	3.67
0.982	452.37	1.26	10.12	85.46	82.15	60.96	22.84	0.44	3.65
1.000	459.41	1.31	12.44	92.51	88.59	66.83	23.72	0.52	3.89
1.000	461.89	1.32	12.18	94.81	90.88	65.82	27.03	0.45	3.89
1.000	470.63	1.38	16.66	103.68	98.12	69.46	31.44	0.53	3.47
1.000	470.80	1.38	16.74	103.84	98.26	69.47	31.59	0.53	3.47

Table D.6: R32, G=300$kgm^{-2}s^{-1}$, Tsat = 50 ^0C

P	h_{bulk}	x	Q	$T_{r,in}$	$T_{r,out}$	T_{wall}	DT	HTC	$dPdZ^{-1}$
[MPa]	[$kJkg^{-1}$]	[-]	[kWm^{-2}]	[^0C]	[^0C]	[^0C]	[^0C]	[$kWm^{-2}K^{-1}$]	[$kPam^{-1}$]
3.141	324.34	0.13	10.75	49.99	49.99	45.05	4.94	2.17	0.48
3.113	343.98	0.22	10.89	49.56	49.56	45.96	3.60	3.02	0.67
3.176	397.38	0.48	11.69	50.48	50.48	47.00	3.48	3.36	0.98
3.155	415.65	0.56	12.30	50.19	50.18	46.79	3.40	3.62	1.18
3.126	450.03	0.73	11.24	49.79	49.78	46.97	2.81	3.99	1.86
3.181	468.51	0.82	10.65	50.55	50.54	48.20	2.34	4.54	2.09
3.130	496.11	0.95	11.28	49.85	49.84	47.79	2.06	5.48	2.27
3.132	511.48	1.02	10.33	52.40	50.98	49.13	2.55	4.04	2.10
3.157	516.81	1.05	9.54	55.29	53.79	49.50	5.04	1.89	2.01
3.148	518.38	1.05	10.40	55.96	54.28	49.49	5.63	1.84	1.99
3.146	521.65	1.07	9.40	57.53	55.90	49.57	7.14	1.31	1.92
3.125	523.30	1.08	8.92	57.99	56.39	49.38	7.81	1.14	1.93
3.144	525.99	1.09	10.07	59.87	57.98	49.77	9.15	1.10	1.89
3.148	530.82	1.11	10.78	62.69	60.54	50.08	11.54	0.93	1.81
3.138	535.37	1.14	10.65	65.21	62.92	50.52	13.54	0.79	1.72

Table D.7: R32, G=100kgm^{-2}s^{-1}, Tsat = 50 ^{0}C

P	h_{bulk}	x	Q	$T_{r,in}$	$T_{r,out}$	T_{wall}	DT	HTC	$dPdZ^{-1}$
[MPa]	[kJkg^{-1}]	[-]	[kWm^{-2}]	[^{0}C]	[^{0}C]	[^{0}C]	[^{0}C]	[kWm^{-2}K^{-1}]	[kPam^{-1}]
3.146	265.27	-0.15	8.93	37.44	33.18	23.17	12.13	0.74	0.06
3.146	266.39	-0.15	8.59	37.89	33.83	23.19	12.67	0.68	0.06
3.147	277.66	-0.10	8.98	43.31	39.20	28.07	13.19	0.68	0.07
3.148	278.55	-0.09	8.86	43.68	39.67	28.01	13.67	0.65	0.07
3.148	279.04	-0.09	8.93	43.92	39.88	28.07	13.83	0.65	0.07
3.144	290.49	-0.03	11.37	49.46	44.55	32.84	14.16	0.80	0.06
3.144	291.74	-0.03	11.09	49.92	45.17	32.86	14.68	0.75	0.06
3.161	300.58	0.01	11.10	50.28	48.99	37.03	12.60	0.88	0.01
3.161	301.18	0.01	10.43	50.27	49.38	37.03	12.80	0.81	0.01
3.157	304.84	0.03	10.18	50.22	50.22	38.50	11.72	0.87	0.05
3.155	309.83	0.06	9.41	50.19	50.19	39.90	10.29	0.91	0.05
3.155	310.83	0.06	10.01	50.19	50.19	39.88	10.31	0.97	0.05
3.141	311.86	0.07	10.52	49.99	49.99	41.28	8.71	1.21	0.04
3.140	312.00	0.07	11.20	49.99	49.99	41.34	8.65	1.29	0.04
3.102	315.33	0.09	10.70	49.46	49.46	43.05	6.41	1.67	0.05
3.125	331.51	0.16	10.67	49.77	49.77	44.47	5.30	2.01	0.05
3.126	364.01	0.32	9.85	49.79	49.79	45.61	4.17	2.36	0.05
3.139	403.02	0.50	10.30	49.98	49.98	45.94	4.04	2.55	-0.01
3.140	412.75	0.55	10.68	49.99	49.99	46.12	3.87	2.76	-0.01
3.146	448.81	0.72	10.31	50.06	50.06	46.66	3.40	3.03	0.03
3.140	475.71	0.85	9.90	49.99	49.98	46.92	3.06	3.23	0.04
3.139	487.79	0.91	9.76	49.96	49.96	47.13	2.84	3.44	0.05
3.154	508.13	1.01	9.06	52.56	50.18	48.87	2.50	3.63	0.08
3.151	509.87	1.01	8.54	53.21	50.14	48.89	2.78	3.07	0.24
3.141	516.33	1.04	9.69	56.34	51.87	48.43	5.68	1.71	0.57
3.130	516.87	1.05	9.29	56.34	51.98	48.36	5.80	1.60	0.57
3.117	527.76	1.10	9.04	61.96	57.02	48.64	10.85	0.83	0.27
3.151	530.04	1.11	8.94	63.79	58.77	48.97	12.31	0.73	0.36
3.123	538.50	1.15	9.26	68.57	62.89	48.89	16.83	0.55	0.41
3.143	538.56	1.15	9.45	68.95	63.21	49.07	17.01	0.56	0.41
3.116	548.13	1.19	10.69	75.25	68.08	48.85	22.81	0.47	0.41
3.177	548.72	1.20	10.38	76.42	69.42	49.58	23.34	0.44	0.45
3.157	554.90	1.23	10.70	80.50	72.91	49.86	26.85	0.40	0.40
3.159	562.00	1.26	9.96	85.25	77.94	53.68	27.92	0.36	0.42
3.145	563.23	1.27	9.65	85.84	78.68	53.67	28.59	0.34	0.42

Table D.8: R32, G=100kgm^{-2}s^{-1}, Tsat = 30 ^{0}C

P	h_{bulk}	x	Q	$T_{r,in}$	$T_{r,out}$	T_{wall}	DT	HTC	$dPdZ^{-1}$
[MPa]	[kJkg^{-1}]	[-]	[kWm^{-2}]	[^{0}C]	[^{0}C]	[^{0}C]	[^{0}C]	[kWm^{-2}K^{-1}]	[kPam^{-1}]
1.954	239.00	-0.07	3.53	22.68	20.50	17.09	4.69	0.75	0.03
1.958	242.94	-0.05	4.01	24.79	22.54	17.98	5.68	0.71	0.05
1.947	248.24	-0.03	4.61	27.64	25.18	20.36	6.05	0.76	0.05
1.939	255.81	0.00	7.55	30.23	28.42	24.22	5.11	1.48	0.02
1.940	257.04	0.00	7.69	30.26	29.01	24.28	5.36	1.44	0.02
1.942	258.27	0.01	7.72	30.30	29.63	24.22	5.74	1.34	0.03
1.952	264.87	0.03	10.23	30.49	30.49	24.45	6.04	1.69	0.02
1.951	268.08	0.05	10.59	30.47	30.47	24.46	6.02	1.76	0.02
1.952	278.09	0.08	11.40	30.49	30.48	25.46	5.03	2.27	0.05
1.953	279.26	0.09	11.61	30.51	30.51	25.44	5.07	2.29	0.05
1.954	293.22	0.14	10.31	30.52	30.52	26.78	3.74	2.76	0.26
1.956	296.54	0.15	10.53	30.57	30.57	26.77	3.80	2.77	0.26
1.924	331.96	0.29	11.15	29.93	29.93	26.19	3.73	2.99	0.02
1.924	351.83	0.37	10.35	29.93	29.93	26.98	2.95	3.51	0.16
1.929	369.00	0.44	10.57	30.04	30.04	27.00	3.04	3.47	0.06
1.925	411.96	0.60	9.95	29.95	29.95	27.25	2.70	3.69	0.15
1.920	438.32	0.70	10.23	29.85	29.85	27.22	2.63	3.89	0.20
1.927	464.99	0.81	8.89	29.99	29.99	27.67	2.31	3.84	0.25
1.931	470.06	0.82	9.27	30.06	30.06	27.68	2.38	3.89	0.25
1.930	484.96	0.88	10.00	30.06	30.05	27.63	2.42	4.13	0.22
1.928	503.96	0.95	9.94	30.02	30.01	27.80	2.21	4.49	0.23
1.940	518.32	1.01	10.45	34.97	30.24	28.70	3.91	2.67	0.59
1.932	518.71	1.01	10.67	35.15	30.10	28.46	4.17	2.56	0.58
1.917	520.94	1.02	10.09	36.24	29.78	28.08	4.93	2.05	0.47
1.924	522.29	1.03	9.85	37.21	30.79	28.19	5.81	1.70	0.47
1.933	525.50	1.04	10.27	39.72	32.82	28.25	8.02	1.28	0.44
1.945	527.35	1.05	9.84	41.12	34.34	28.50	9.23	1.07	0.45
1.932	533.22	1.07	9.02	44.76	38.12	28.87	12.57	0.72	0.68
1.941	536.00	1.08	8.81	46.89	40.26	29.08	14.50	0.61	0.68

Table D.9: R134a, G=100kgm^{-2}s^{-1}, Tsat = 50 ^{0}C

P	h_{bulk}	x	Q	$T_{r,in}$	$T_{r,out}$	T_{wall}	DT	HTC	$dPdZ^{-1}$
[MPa]	[kJkg^{-1}]	[-]	[kWm^{-2}]	[^{0}C]	[^{0}C]	[^{0}C]	[^{0}C]	[kWm^{-2}K^{-1}]	[kPam^{-1}]
1.320	241.56	-0.20	7.23	32.33	27.45	16.55	13.34	0.54	0.01
1.320	253.99	-0.12	9.58	41.57	35.21	18.76	19.63	0.49	0.01
1.320	260.19	-0.08	9.81	45.76	39.31	22.50	20.03	0.49	0.01
1.319	264.51	-0.05	10.89	48.89	41.85	26.22	19.15	0.63	0.01
1.319	265.36	-0.04	10.60	49.37	42.49	26.21	19.72	0.59	0.01
1.323	267.71	-0.03	11.24	50.15	43.86	28.57	18.43	0.67	0.01
1.323	267.91	-0.03	11.40	50.16	43.94	28.58	18.47	0.68	0.01
1.322	271.93	0.00	11.36	50.12	46.56	32.21	16.13	0.77	0.01
1.322	272.67	0.01	11.72	50.12	46.95	32.21	16.32	0.79	0.01
1.321	273.13	0.01	11.03	50.10	47.45	32.20	16.58	0.73	0.01
1.322	274.24	0.02	11.42	50.13	48.07	32.16	16.94	0.74	0.01
1.315	279.90	0.06	9.08	49.91	49.91	40.01	9.90	0.92	0.04
1.315	279.92	0.06	9.14	49.92	49.92	40.03	9.89	0.92	0.04
1.314	298.27	0.18	9.27	49.90	49.90	43.15	6.74	1.37	0.03
1.314	299.21	0.18	9.07	49.89	49.89	43.18	6.71	1.35	0.03
1.314	323.75	0.34	10.06	49.87	49.87	43.74	6.13	1.64	0.00
1.314	324.28	0.35	10.44	49.88	49.88	43.75	6.13	1.70	0.00
1.314	345.91	0.49	10.77	49.89	49.89	44.57	5.32	2.02	0.02
1.314	348.10	0.50	10.71	49.90	49.90	44.53	5.37	2.00	0.02
1.315	367.46	0.63	10.46	49.91	49.91	45.07	4.84	2.16	0.03
1.317	391.73	0.79	9.36	49.97	49.97	46.00	3.97	2.36	0.13
1.318	392.63	0.80	9.39	50.00	50.00	45.96	4.03	2.33	0.13
1.319	413.01	0.93	9.07	50.05	50.05	46.25	3.80	2.39	0.03
1.319	413.77	0.94	9.10	50.02	50.02	46.24	3.78	2.41	0.03
1.343	422.18	0.99	9.12	53.03	50.75	46.78	5.11	1.96	0.03
1.321	425.14	1.01	9.50	55.24	50.09	46.44	6.22	1.68	0.03
1.317	426.64	1.02	9.61	56.52	49.97	46.25	7.00	1.51	0.03
1.328	431.44	1.05	8.64	60.58	53.13	46.81	10.05	0.86	1.29
1.329	432.18	1.06	8.21	61.05	53.92	46.84	10.65	0.77	1.29
1.330	432.40	1.06	7.76	61.07	54.31	46.83	10.86	0.71	1.29
1.343	435.62	1.08	8.82	64.55	56.84	47.11	13.59	0.65	0.56
1.342	437.39	1.09	8.38	65.93	58.45	47.07	15.12	0.55	0.56
1.332	446.57	1.15	9.48	74.46	65.76	46.49	23.62	0.40	0.47
1.364	458.86	1.23	11.39	86.89	76.43	47.60	34.06	0.33	0.61
1.356	459.54	1.24	10.69	87.17	77.16	47.61	34.56	0.31	0.61

Table D.10: R134a, G=100kgm^{-2}s^{-1}, Tsat = 30 ^{0}C

P	h_{bulk}	x	Q	$T_{r,in}$	$T_{r,out}$	T_{wall}	DT	HTC	$dPdZ^{-1}$
[MPa]	[kJkg^{-1}]	[-]	[kWm^{-2}]	[^{0}C]	[^{0}C]	[^{0}C]	[^{0}C]	[kWm^{-2}K^{-1}]	[kPam^{-1}]
0.716	226.58	-0.07	2.02	20.10	18.61	15.66	3.70	0.60	0.01
0.716	226.65	-0.07	2.05	20.16	18.65	15.68	3.73	0.60	0.01
0.791	232.46	-0.06	6.58	25.90	21.14	12.70	10.82	0.61	0.01
0.734	234.33	-0.03	5.28	26.74	22.95	15.89	8.96	0.65	0.01
0.765	238.13	-0.02	6.52	29.75	25.24	18.06	9.43	0.69	0.01
0.772	248.11	0.04	9.39	30.10	30.10	22.22	7.88	1.19	0.01
0.769	248.58	0.04	9.65	29.93	29.93	22.22	7.72	1.25	0.01
0.769	249.14	0.04	9.66	29.96	29.96	22.22	7.74	1.25	0.01
0.782	256.39	0.08	8.76	30.54	30.54	25.48	5.06	1.73	0.01
0.785	256.76	0.08	8.74	30.65	30.65	25.48	5.18	1.69	0.01
0.774	258.24	0.09	8.90	30.18	30.18	25.35	4.83	1.84	0.01
0.773	259.81	0.10	9.00	30.12	30.12	25.37	4.75	1.90	0.01
0.773	261.23	0.11	8.99	30.14	30.14	25.37	4.77	1.89	0.01
0.771	275.60	0.20	9.92	30.06	30.05	25.39	4.66	2.13	0.06
0.776	278.63	0.21	9.96	30.26	30.26	25.39	4.86	2.05	0.06
0.773	280.11	0.22	9.92	30.14	30.14	25.38	4.76	2.09	0.06
0.772	295.88	0.31	10.37	30.09	30.08	25.41	4.68	2.22	0.13
0.771	296.07	0.31	10.33	30.04	30.04	25.40	4.64	2.23	0.13
0.772	298.67	0.33	10.45	30.08	30.08	25.41	4.67	2.24	0.13
0.774	330.06	0.51	11.11	30.16	30.14	25.85	4.30	2.58	0.77
0.775	330.75	0.51	10.93	30.21	30.20	25.91	4.30	2.54	0.77
0.774	345.76	0.60	10.26	30.16	30.15	26.26	3.89	2.64	0.76
0.774	348.92	0.62	10.27	30.16	30.15	26.23	3.93	2.62	0.76
0.766	363.99	0.71	10.84	29.80	29.79	26.03	3.76	2.88	0.91
0.767	364.13	0.71	10.86	29.88	29.86	26.11	3.76	2.89	0.91
0.772	386.34	0.84	12.97	30.08	30.06	26.03	4.05	3.21	0.99
0.769	387.56	0.84	12.94	29.93	29.92	25.96	3.96	3.26	0.99
0.765	404.94	0.94	8.44	29.79	29.78	27.54	2.25	3.76	0.99
0.766	405.86	0.95	8.55	29.84	29.82	27.54	2.29	3.74	0.99
0.778	407.50	0.96	9.65	30.34	30.33	27.63	2.70	3.57	0.69
0.778	408.71	0.96	9.68	30.37	30.37	27.62	2.75	3.52	0.69
0.779	416.38	1.01	11.30	37.26	30.39	27.42	6.41	1.76	0.71
0.778	416.81	1.01	11.27	37.53	30.37	27.43	6.52	1.73	0.71
0.779	418.73	1.02	11.23	39.24	30.39	27.42	7.40	1.52	0.71

Continued…

Continued...

P	h_{bulk}	x	Q	$T_{r,in}$	$T_{r,out}$	T_{wall}	DT	HTC	$dPdZ^{-1}$
[MPa]	[$kJkg^{-1}$]	[-]	[kWm^{-2}]	[^0C]	[^0C]	[^0C]	[^0C]	[$kWm^{-2}K^{-1}$]	[$kPam^{-1}$]
0.778	420.10	1.03	11.14	40.85	30.37	27.82	7.79	1.43	0.69
0.775	421.29	1.04	10.89	41.62	31.01	27.75	8.56	1.27	0.69
0.780	429.94	1.09	7.95	48.85	40.77	29.09	15.72	0.51	0.84
0.769	445.30	1.18	7.60	63.87	55.81	30.48	29.36	0.26	0.27
0.770	453.54	1.22	8.65	72.64	63.50	34.18	33.89	0.26	0.25
0.770	461.92	1.27	9.33	81.50	71.36	36.78	39.65	0.24	0.23
0.778	479.41	1.37	9.97	99.37	88.29	42.64	51.19	0.19	0.18

Table D.11: R134a, G=300$kgm^{-2}s^{-1}$, Tsat = 50 ^0C

P	h_{bulk}	x	Q	$T_{r,in}$	$T_{r,out}$	T_{wall}	DT	HTC	$dPdZ^{-1}$
[MPa]	[$kJkg^{-1}$]	[-]	[kWm^{-2}]	[^0C]	[^0C]	[^0C]	[^0C]	[$kWm^{-2}K^{-1}$]	[$kPam^{-1}$]
1.317	253.11	-0.12	6.40	38.59	37.04	31.11	6.70	0.96	0.22
1.313	253.20	-0.12	6.03	38.62	37.13	31.07	6.80	0.89	0.22
1.316	253.86	-0.12	6.16	39.07	37.57	31.07	7.25	0.85	0.22
1.313	254.33	-0.11	6.25	39.41	37.87	31.08	7.56	0.83	0.22
1.313	259.40	-0.08	7.44	42.89	41.18	34.36	7.67	0.97	0.25
1.315	259.83	-0.08	7.67	43.19	41.44	34.54	7.77	0.99	0.25
1.313	263.64	-0.05	8.13	45.74	43.92	37.05	7.77	1.05	0.26
1.315	268.77	-0.02	9.10	49.16	47.17	39.97	8.19	1.11	0.28
1.311	268.77	-0.02	9.10	49.15	47.17	39.97	8.19	1.11	0.28
1.316	269.22	-0.02	9.57	49.50	47.42	39.96	8.50	1.13	0.28
1.317	275.48	0.03	9.98	49.96	49.96	41.72	8.24	1.21	0.35
1.316	275.95	0.03	9.98	49.93	49.93	41.73	8.20	1.22	0.35
1.317	276.35	0.03	9.93	49.97	49.97	41.72	8.25	1.20	0.35
1.318	294.90	0.15	11.45	50.00	50.00	43.51	6.49	1.77	0.56
1.314	295.22	0.16	11.50	49.88	49.87	43.51	6.36	1.81	0.56
1.313	295.75	0.16	11.09	49.86	49.85	43.49	6.36	1.74	0.56
1.314	319.26	0.31	11.10	49.90	49.88	45.01	4.88	2.27	1.11
1.314	319.32	0.32	10.96	49.88	49.87	45.02	4.85	2.26	1.11
1.314	319.85	0.32	10.95	49.90	49.89	45.01	4.89	2.24	1.11
1.315	334.89	0.42	11.02	49.92	49.91	45.65	4.26	2.59	1.52
1.319	334.99	0.42	10.80	50.02	50.02	45.63	4.39	2.46	1.52
1.315	335.78	0.42	11.15	49.91	49.89	45.65	4.25	2.62	1.52

Continued…

Continued…

P	h_{bulk}	x	Q	$T_{r,in}$	$T_{r,out}$	T_{wall}	DT	HTC	$dPdZ^{-1}$
[MPa]	[$kJkg^{-1}$]	[-]	[kWm^{-2}]	[^0C]	[^0C]	[^0C]	[^0C]	[$kWm^{-2}K^{-1}$]	[$kPam^{-1}$]
1.315	353.96	0.54	12.33	49.94	49.92	45.78	4.15	2.97	2.01
1.320	354.38	0.54	12.48	50.05	50.05	45.78	4.27	2.92	2.01
1.320	354.43	0.55	11.85	50.06	50.06	45.77	4.29	2.76	2.01
1.316	367.51	0.63	10.99	49.97	49.94	46.54	3.42	3.22	2.48
1.318	367.77	0.63	11.17	50.01	49.98	46.54	3.45	3.24	2.48
1.317	368.53	0.64	11.11	50.00	49.97	46.54	3.44	3.23	2.48
1.313	385.75	0.75	8.92	49.86	49.83	47.29	2.56	3.49	2.85
1.312	385.83	0.75	8.81	49.85	49.82	47.28	2.55	3.46	2.85
1.312	386.76	0.76	8.69	49.84	49.81	47.28	2.55	3.41	2.85
1.314	392.80	0.80	9.94	49.89	49.86	47.24	2.63	3.78	3.33
1.314	393.64	0.80	10.14	49.90	49.87	47.24	2.64	3.84	3.33
1.313	393.77	0.81	10.19	49.85	49.82	47.24	2.60	3.92	3.33
1.313	407.30	0.89	11.03	49.87	49.84	47.31	2.54	4.33	3.59
1.313	407.38	0.89	11.16	49.88	49.84	47.33	2.53	4.40	3.59
1.314	407.85	0.90	11.02	49.89	49.85	47.31	2.56	4.31	3.59
1.314	421.62	0.99	10.59	49.88	49.85	47.73	2.14	4.95	3.52
1.313	422.81	1.00	9.00	50.56	49.85	47.34	2.87	3.45	3.51
1.308	423.16	1.00	9.65	50.85	49.69	47.35	2.92	3.30	3.51
1.309	423.23	1.00	9.43	50.89	49.71	47.33	2.97	3.18	3.51
1.306	423.80	1.00	8.99	51.27	49.64	47.34	3.11	3.17	3.51
1.312	423.96	1.00	9.13	51.53	49.83	47.34	3.34	3.01	3.51
1.307	425.23	1.01	10.10	52.59	49.86	47.22	4.00	2.78	3.43
1.308	425.36	1.01	10.15	52.73	49.99	47.23	4.13	2.70	3.43
1.307	425.71	1.02	9.81	52.96	50.28	47.22	4.40	2.45	3.43
1.313	426.12	1.02	10.05	53.46	50.72	47.25	4.84	2.29	3.43
1.308	426.38	1.02	9.89	53.56	50.84	47.22	4.98	2.19	3.43
1.308	429.72	1.04	9.08	56.27	53.69	48.29	6.69	1.36	3.21
1.308	430.61	1.05	8.78	56.99	54.47	48.28	7.45	1.18	3.21
1.308	430.78	1.05	8.69	57.12	54.62	48.31	7.56	1.15	3.21
1.310	433.48	1.07	8.39	59.45	56.96	48.60	9.61	0.87	3.18
1.308	433.51	1.07	8.30	59.43	56.96	48.60	9.60	0.86	3.18
1.310	433.51	1.07	8.43	59.49	57.00	48.61	9.63	0.88	3.18
1.311	438.52	1.10	7.58	63.72	61.49	49.23	13.37	0.57	3.42
1.312	438.97	1.10	8.01	64.19	61.83	49.24	13.77	0.58	3.42
1.311	444.22	1.14	8.89	68.99	66.30	51.33	16.32	0.54	3.40
1.310	453.91	1.20	9.53	77.88	74.87	57.67	18.70	0.51	3.39

REFERENCES

[1] Akers, W.W., Deans, H.A., Crosser, O.K., 1959. Condensing heat transfer within horizontal tubes. Chem. Eng. Prog. S. Ser. 55 (29), 171-176.

[2] Altman, M., Staub, F.W., Norris, R.H., 1959. Local heat transfer and pressure drop for refrigerant-22 condensing in horizontal tubes. Chem. Eng. Prog. S. Ser. 56 (30), 151-159.

[3] ASME Performance Test Codes, 1985. Supplement on Instrument and Apparatus, Part1. *ASNSI / ASME PTC*, 19.1-1985.

[4] Balekjian,G., Katz,D., 1958. Heat transfer from superheated vapors to a horizontal tube. AIChE. J. 4 (1), 43-48.

[5] Cavallini, A., Censi, G., Del Col, D., Doretti, L., Longo, G.A., Rossetto, L., 2001. Experimental investigation on condensation heat transfer and pressure drop of new HFC refrigerants in a horizontal smooth tube. Int. J. Refrigeration 24, 73-87.

[6] Cavallini, A., Censi, G., Del Col, D., Doretti, L., Longo, G.A., Rossetto, L., Zilio, C., 2003. Condensation inside and outside smooth and enhanced tubes – a review of recent research. Int. J. Refrigeration 26, 373-392.

[7] Cavallini, A., Del Col, D., Doretti, L., Matkovic, M., Rossetto, L., Zilio, C., Censi, G., 2006. Condensation in horizontal smooth tubes: a new heat transfer model for heat exchanger design. Heat Tran. Eng. 27 (8), 31-38.

[8] Dalkilic, A.S., Wongwises, S., 2009. Intensive literature review of condensation inside smooth and enhanced tubes. Int. J. of Heat and Mass Tran. 52, 3409-3426.

[9] Dalkilic, A.S., Laohalertdecha, S., Wongwises, S., 2009. Experimental investigation on the condensation heat transfer and pressure drop characteristics of R134a at high mass

flux conditions during annular flow regime inside a vertical smooth tube. Proc. Of ASME Heat Trans. Summer Conference, San Francisco, California,USA.

[10] Dobson, M.K., Chato, J.C., 1998. Condensation in smooth horizontal tubes. J. Heat Tran. 120, 193-213.

[11] F-Chart, 2010. Engineering Equation Solver (EES) (academic version), Madison, WI: F-Chart.

[12] Friedel, L., 1979. Improved friction pressure drop correlations for horizontal and vertical two phase pipe flow. In: Proc. European Two-Phase Flow Group Meeting, Ispra, Italy, Paper No. E2.

[13] Haraguchi, H., Koyama, S., Fujii, T., 1994. Condensation of refrigerants HCFC 22, HFC 134a and HCFC 123 in a horizontal smooth tube (2nd report, proposals for empirical expressions for local heat transfer coefficients) Trans. JSME 60 (574) 245-252 (in Japanese).

[14] Hashizume, K., Abe, N., Ozeki, T., 1992. Condensate subcooling near tube exit during horizontal in-tube condensation. Heat transfer engineering, 13:1, 19-27.

[15] Hossain, M.A., Onaka, Y., Miyara, A., 2012. Experimental study on condensation heat transfer and pressure drop in horizontal smooth tube for R1234ze(E), R32 and R410A. Int. J. Refrigeration 35 (4), 927-938.

[16] Jung, D., Song, K., Cho, Y., Kim, S., 2003. Flow condensation heat transfer coefficients of pure refrigerants. Int. J. Refrigeration 26, 4-11.

[17] Kattan, N., Thome, J.R., Favrat, D., 1998. Flow boiling in horizontal tubes: part I-development of a diabatic two phase flow pattern map. J. Heat Transfer 120, 140-147

[18] Kondou,C., Hrnjak,P., 2011a. Heat rejection from R744 flow under uniform temperature cooling in a horizontal smooth tube around the critical point. Int. J. Refrigeration 34 (3) 719-731.

[19] Kondou,C., Hrnjak,P., 2011b. Heat rejection in condensers close to critical point-Desuperheating, condensation in superheated region and condensation of two phase fluid. Int. Conf. Heat Trans. Fluid Mech. and Thermodynamics. Mauritius.

[20] Kondou,C., Hrnjak,P., 2012. Condensation from superheated vapor flow of R744 and R410A at subcritical pressures in a horizontal smooth tube. Int. J. Heat Mass Transfer 55, 2779-2791.

[21] Kondou,C., 2012. De-superheating and condensation from R744 and R410A in smooth and microfin tubes near critical point (final report). ACRC, UIUC, Project 264.

[22] Kosky, P., Staub, F., 1971. Local condensing heat transfer coefficients in annular flow regime. AIChE Journal, 17 (5), 1037-1043.

[23] Lee, C.C., Teng, Y.J., Lu, D.C., 1991. Investigation of condensation heat transfer of superheated R-22 vapor in a horizontal tube, Proc. World Conf. Exp. Heat Trans. Fluid Mech. and Thermodynamics. In: J.F. Keffer, R.K. Shah, E.N. Ganic (Eds.) 1051-1057.

[24] Lemmon, E.W., Huber, M.L., McLinden, M.O., 2007. Reference Fluid Thermodynamic and Transport Properties-REFPROP Ver.8.0. National Institute of Standards and Technology, Boulder, CO, USA.

[25] Moffat, R.J., 1988. Describing the uncertainties in experimental results. Exp. Therm, Fluid Sci. 1, 3-17.

[26] Park, J.E., Vakili-Farahani, F., Consolini, L., Thome, J.R., 2011. Experimental study on condensation heat transfer in vertical minichannels for new refrigerant R1234ze(E) versus R134a and R236fa. Exp. Therm. Fluid Sci. 35 (3), 442-454.

[27] Shah, M.M., 1979. A general correlation for heat transfer during film condensation inside pipes. Int. J. Heat and Mass Trans. 22, 547-556.

[28] Shah, M.M., 2009. An improved and extended general correlation for heat transfer during condensation in plain tubes. HVAC&R Reasearch, 15 (5), 889-913.

[29] Smith S.L., 1969. Void fractions in two-phase flow: a correlation based upon an equal velocity head model. Proc. Instn. Mech Engrs., 184 (36), 647-664.

[30] Soliman, H.M., 1986. The mist-annular transition during condensation and its influence on the heat transfer mechanism. Int. J. Multiphase Flow 12 (2) 277-288.

[31] Thome, J.R., El Hajal, J., Cavallini, A., 2003. Condensation in horizontal tubes, part 2: new heat transfer model based on flow regimes. Int. J. Heat Mass Transfer 46 (18) 3365-3387.

[32] Webb, R.L., 1998. Convective Condensation of Superheated Vapor. Trans. ASME, J. Heat Transfer 120, 418-421.

[33] Xiaoyong, W., Xiande, F., Rongrong, S., 2012. A comparative study of heat transfer coefficients for film condensation. Energy Science and Technology, 3 (1), 1-9.